Development and evaluation of CT acquisition and analysis methods of brain perfusion

Alan J. Riordan

The printing of this thesis was kindly supported by Philips healthcare

Development and evaluation of CT acquisition and analysis methods of brain perfusion

PhD thesis, Utrecht University – with a summary in Dutch

ISBN: 978-90-8891-990-9

Cover design and layout: Alan Riordan.

Printing by: Proefschriftmaken.nl || Uitgeverij BOXPress

Development and evaluation of CT acquisition and analysis methods of brain perfusion

Ontwikkeling en evaluatie van CT acquisitie- en analysemethoden voor perfusiemetingen in de hersenen

(met een samenvatting in het Nederlands)

Proefschrift

ter verkrijging van de graad van doctor aan de Universiteit Utrecht op gezag van de rector magnificus, prof.dr. G.J. van der Zwaan, ingevolge het besluit van het college voor promoties in het openbaar te verdedigen op maandag 10 november 2014 des middags te 2.30 uur

door

Alan Jermiah Riordan

geboren op *5 januari 1983* te Cork, Ierland

Promotoren: Prof.dr.ir. M. A. Viergever

Prof.dr. W. M. Prokop

Copromotor: Dr. ir. H W. A. M. de Jong

Chapter 1: Introduction 9
Motivation 10
What is stroke? 10
Introduction to CTP 11
Overview of a clinical CTP acute stroke assessment 13
Objective of this thesis 23
Outline of the thesis 24
Chapter 2: Validation of CT brain perfusion methods using a realistic dynamic head phantom 29
Abstract 30
Introduction 31
Materials and methods 32
Results 41
Discussion and conclusions 47
Chapter 3: Improvements in accuracy and dose efficiency of CTP by application of a realistic digital phantom 53
Abstract 54
Introduction: 55
Materials and methods: 56
Results. 60
Discussion 66
Chapter 4: The Effect of Head Movement on CT Perfusion Summary Maps: Simulations with CT Hybrid Phantom Data 75
Abstract 76
Introduction 76

Methods 77
Results 80
Discussion 83
Chapter 5: A CT brain perfusion protocol to eliminate the need for selecting a venous output function 89
Abstract 90
Introduction 91
Materials and methods 92
Results 96
Discussion 100
Chapter 6: Comparison of partial volume effects in arterial and venous contrast curves in CT brain perfusion imaging 105
Abstract 106
Introduction 107
Materials and methods 108
Results 114
Discussion 117
Chapter 7: Summary and general discussion 125
Chapter 2: Validation of CT brain perfusion methods using a realistic dynamic head phantom 126
Chapter 3: Improvements in accuracy and dose efficiency of CTP by application of a realistic digital phantom. 127
Chapter 4: The Effect of Head Movement on CT Perfusion Summary Maps: Simulations with CT Hybrid Phantom Data 127
Chapter 5: CT Brain Perfusion Protocol to Eliminate the Need for Selecting a Venous Output Function 128
Chapter 6 Comparison of partial volume effects in arterial and venous contrast curves in CT brain perfusion imaging 130
Definition of an optimal CTP process 133

General discussion of limitations. 135
General conclusions 137
Nederlandse Samenvatting 143
Achtergrond en motivatie 144
CT perfusie beeldvorming 144
Doel van het proefschrift 145
Algemene conclusies 148
List of publications and articles under review/submitted 149
Published: 149
Submitted for publication: 150
Acknowlegments 151
Curriculum vitae 153

CHAPTER 1: INTRODUCTION

MOTIVATION

Stroke causes 9% of all deaths globally and is the second most common cause of death after ischaemic heart disease, stroke-related disability is the sixth most common cause of reduced disability-adjusted life-years and consumes more than 4% of direct health-care costs in industrialised countries[1-3]. Strokes are either ischaemic or haemorrhagic. Because the management of the stroke is so different for different types, and extremities, of stroke the clinical distinction is important. This distinction has been revolutionised by the introduction of CT and MRI with CT being the workhorse of stroke diagnosis during the past 20 years.

Several treatment options are available, generally aimed at dissolving the obstructing blood clot (thrombolysis) or removing it (thrombectomy). Accurate diagnosis is key in treatment decision making. CT brain perfusion (CTP) is a promising tool assist physicians in treatment decision for stroke patients due to its potential to quantify various tissue perfusion parameters. However, as of yet the clinical usefulness of the methodology has to be convincingly proven. CTP still lacks proper methods of validation and consensus on scanner protocol and analysis methods.

The aim of this thesis is to examine the technical aspects of CTP, from scanner protocol to diagnostic images, proposing methods and analyses that help to improve the clinical usefulness of CTP.

WHAT IS STROKE?

There are two main types of stroke, haemorrhagic stroke (intracerebral haemorrhage), and ischaemic stroke (reduced blood supply). About 80% of all strokes are ischaemic[4], the result of an obstruction of a cerebral artery interrupting or severely reducing the blood supply to a part of the brain. Since measuring blood perfusion is the goal of CTP this is the type of stroke that this work will focus on.

The cause of the obstruction can be generally divided into several categories, large-artery atherosclerosis (embolus or thrombosis), cardioembolism or small-vessel occlusion (lacune)[5,6]. The reduction of blood supply to the brain deprives the brain tissue of oxygen. When the brain tissue is deprived of oxygen for even a short period of time the brain cells (neurons) stop functioning and eventually die[7]. The loss of function of brain cells results in neurological symptoms. Symptoms of ischemic stroke may include; weakness or paralysis, loss of sensation, visual deficits, facial droop, failure of muscle co-ordination, vertigo, aphasia, coma or death[8]. The effects of a stroke depend on several factors, including the location and severity of the obstruction and how much brain tissue is affected [7]. The duration the tissue is shut off from blood is crucial. Earlier restoration of blood flow results in less brain cells dying.

After stroke, the circulatory system of the brain itself attempts to restore blood supply to affected regions by collateral circulation. This so called collateral blood flow may reduce the severity of the stroke by returning blood supply to the affected tissue [9]. Identifying regions of the brain that are being fed by collateral flow is also valuable information in the decision making of stroke treatment.

INTRODUCTION TO CTP

Computed tomography perfusion imaging of the brain is a technique used to assess cerebral blood perfusion in acute stroke patients. First proposed by Leon Axel in 1979, throughout the 80's perfusion imaging was largely confined to research studies of renal or myocardial blood flow using electron beam CT systems [10,11]. However, the advent of slip ring and multi-slice CT systems allowed for CTP to be carried out on conventional CT scanners and with volume imaging as opposed to single slice. The introduction of thrombolytic therapy for acute ischemic stroke raised a need for a rapid readily available technique to help identify and quantify the presence and extent of ischemia which would assist physicians in treatment decision.

Magnetic resonance perfusion, xenon CT, positron emission tomography, and single photon emission computed tomography were candidates to fulfil this role but were

hampered by limited availability, prohibitive cost for daily use, and extended procedure duration[12]. MR perfusion and diffusion weighted imaging is widely used and has several advantages and disadvantages relative to CTP. The main advantages of MRI are; the lack of ionising radiation, increased sensitivity to lacunar and posterior fossa infarcts, and differentiation between acute and chronic ischemia. The main disadvantages relative to CTP are; less availability of MRI scanners in the acute setting, slower image acquisition, patient accessibility, feasibility for patients with implants containing metals and higher cost. MR perfusion also suffers from a similar lack of consensus that is found in the field of CTP[13].

One main disadvantage of CTP, application of ionizing radiation which may damage tissue and increase risk of cancer , was offset by the wide availably of capable CT scanners, cheaper cost, short scan duration and relative ease of use. This stimulated the major CT hardware manufacturers, medical software houses, and research entities to develop CTP scanner protocols and CTP software and this research has continued at an impressive pace over the last 15 years or so.

In dedicated stroke centres CTP images are commonly acquired in addition to a non-contrast CT scan and CT Angiography. A non-contrast CT scan provides information about potential hemorrhages and early ischemic changes. CT angiography can be acquired by injecting venous contrast agent to visualize the vessel anatomy and can reveal the location of occlusions and stenosis.

CTP is similar to CT angiography, in that it contrast agent is measured, but provides information about the blood perfusion at tissue level rather highlighting vessels. Whereas angiography is based on visual assessment of contrast enhancement at a particular time point (when the contrast agent is in the arteries), for CTP it is necessary to quantify the amount of contrast enhancement in blood vessels and brain tissue over a period of time. Quantification of contrast enhancement on CT is theoretically straightforward because the iodine component of the contrast medium causes a local increase in X-ray attenuation that is linearly proportional to the iodine concentration. Thus, by measuring the changes in attenuation (in Hounsfield units, HU) over time, it is possible to estimate the temporal changes in concentration of contrast medium

within a volume element (voxel), and hence imply the blood perfusion properties of the voxel.

The concept of CTP in itself is simple, however in practice there are many elements that can adversely affect the usefulness and accuracy of the diagnostic images used by the radiologist in clinical application. It is important in the context of this work to illustrate the underlying complexity and variety of CTP imaging and I will do this by describing the steps in a typical clinical acute stroke assessment. In this way we can examine both some of the important technical aspects while appreciating how they affect, and are affected by, clinical requirements and restrictions.

OVERVIEW OF A CLINICAL CTP ACUTE STROKE ASSESSMENT

ADMISSION AND INITIAL ASSESSMENT.

When a patient presents with symptoms of acute ischemic stroke, a physician will attempt to confirm the symptoms and establish the time of stroke onset. This is important to establish the possibility of administration of recombinant tissue plasminogen activator (rtPA), the only FDA-approved treatment of stroke, and very effective if administered within 4.5 hours after stroke onset.

RtPA is, however, a risk factor for symptomatic hemorrhagic transformation which occurs in about 3.5% of all ischemic stroke patients and can cause an eleven fold increase in case fatalities[14,15]. A study carried out in 2007 showed that only 2% of patients will later receive this treatment due to delayed admission, uncertainty of the time of stroke onset or if the CT scans that follow indicate an existing hemorrage[16]. However as public awareness of stroke symptoms increases, patients are presenting earlier after onset of symptoms, increasing the number of patients receiving rtPA dramatically[17].

RtPA will likely cause worsening of an existing subarachnoid haemorrhage which occurs in about 5% of all strokes. Presence of subarachnoid haemorrhage is investigated by a non-contrast-enhanced CT (NCT) of the brain. The NCT is followed

by a CTA examination (or alternatively the CTA can follow the CTP scan) to attempt to establish the point of any occlusions in the feeding arteries and determine the presence of collateral blood supply to tissue affected by reduced perfusion.

A complete overview of the imaging protocols for patients presenting with acute stroke symptoms based on the clinical scenario and the therapeutic options can be found in a joint Statement by the American Society of Neuroradiology, the American College of Radiology, and the Society of Neuro-Interventional Surgery[13]. Within this imaging protocol the CTP is carried out to examine blood perfusion in the brain tissue with the goal of assess the extent of viable tissue, i.e. tissue that may be saved by restoration of blood flow. Determination of tissue viability based on imaging has the potential to individualize thrombolytic therapy and extend the therapeutic time window for some acute stroke patients.

The CTP process is outlined in figure 1 and can be divided in to six steps each of which is defined by several technical elements or variables. The effect and implications of each of these elements will be discussed in more detail over the following sections.

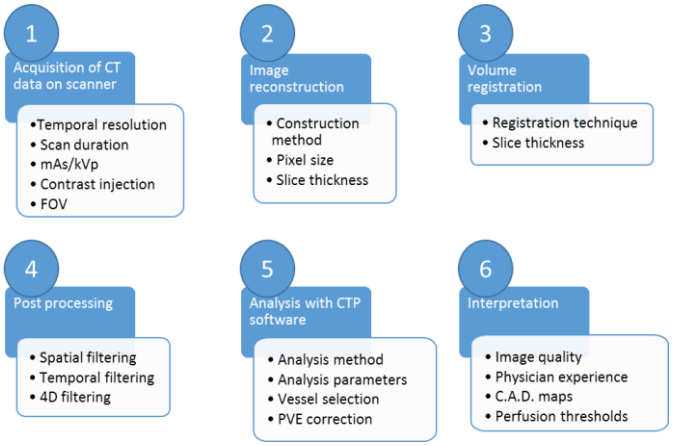

Figure 1: The CTP process denoting the main steps and the technical elements that may affect the outcome of each step.

ACQUISITION OF CT DATA

The specifics of the scan protocol, which will be discussed in this section, can vary significantly between institutes (table 1), and may be determined by the recommendations of scanner manufacturers, developers of the CTP software or clinical research groups. The range of protocol parameters detailed in this section are taken from the American Association of Physics in Medicine (AAMP) which compiled a list of “reasonable” CT scan protocols, including CTP, derived from typical scan protocols recommended by various CT scanner manufacturers. The range of these parameters in clinical/research protocols may vary even more that outlined in this section.

Following the NCT/CTA the patient remains on the scanner and the CTP scan is carried out. A bolus of non-ionic contrast agent (20 to 50ml) is injected into the cubital vein. The choice of CTP protocol is an important step as it defines the amount of information available in the CTP images that will later be used to construct diagnostic

images. For example; reduction of the temporal resolution will reduce the amount of information that can be contained in the time-attenuation curves.

Scanner protocol parameter	Typical values	Notes
X-Ray tube voltage	80 to 100 kVp	120kVP no longer widely used[18]
X-Ray tube current	100 to 300 mAs/rot	300mAs is used in arterial phase of Toshiba aquillion one scanner.
Contrast agent volume	20 to 50 ml	
Injection rate	4 to 6 ml/s	
Iodine concentration	300 to 400 ml/mg	
Field of view	20 to 25 cm	
Axial length	4 to 16 cm	
Temporal resolution	0.5 to 3 s	
CT Dose	120 to 308 CTDI-vol (mGy)	
Scan duration	40 - 200+ s	Greater than 60s are generally specialized research protocols

Table 1. Overview of reasonable setting used in CT scanner protocols for CTP.

The injection will usually have a volume between 20 to 50ml, iodine concentration of 300 to 400 mg/mL and injection rate of 4 to 6ml/s. These parameters define the temporal shape and size of the bolus. The contrast bolus will travel with the blood stream to the brain, and the CTP scan is started several seconds before the bolus arrival in the brain. The scan acquires a series of image volumes of the brain as the bolus arrives in the cerebral arteries, is distributed into the brain tissue, and then drains out via the cerebral veins. The dimensions of the frame typically have a ~20cm field of view and axial length of 4 to 16cm depending on the capabilities of the scanner. The image volumes, or frames, are usually acquired in 200-500 ms and at uniform time intervals between 0.5 to 3 seconds apart. This interval is referred to as the

temporal resolution. The length of the scan is 40 to 70s, up to several minutes in the case of special research protocols. The temporal resolution will define the amount of temporal information in the data.

The CT protocol is also defined by the amount of x-ray radiation used on each frame also referred to as the CT dose per frame. Nearly all protocols use a x-ray tube voltage of 80kVp, as this gives the best contrast enhancement for the typical iodine concentration used in the contrast agent but some current protocols use up to 120kVp to lower the image noise. The CT dose per frame is therefore defined by the tube current, again this can vary greatly between institutes, ranging from 50 to 250mAs/rot and can even vary within the scan. This value has a direct relationship with the CT noise on the images image noise is proportional to the square root of the mAs, therefore, if the mAs is reduced by half, then the noise is expected to increase by 40%.

The total dose administered to the patient is therefore a product of the CT dose per frame, defined by the mAs per frame, and the number of frames. The objective when choosing the mAs and temporal resolution is to have the lowest CT dose possible while maintaining sufficient image quality and enough temporal information to measure the passage of the contrast bolus accurately. Typical CT doses are between 120 to 308 CTDI-vol (mGy), with some even as over 450 CTDI-vol (mGy).

There are also several other variations of scan protocol that are not commonly used, but have been implemented by manufacturers for specific scanners. These protocols have unique properties and often the CTP data that they produce can only be analysed with specific software. Examples of these are Jog-mode(Philips) and shuttle-mode(Siemens), which move the table back and forth between frames to scan different positions, periodic spiral (Siemens, an adaptive 4D spiral), and Dynamic Volume Intermittent (Toshiba, where both the temporal resolution and mA and are dynamic throughout the scan).

IMAGE RECONSTRUCTION

Each frame consists of an image volume consisting of many axial slices, how thin these slices can be is physically defined by the size and number of the detector rows

on the scanner, and practically limited by the amount of time it takes to reconstruct the slices (thinner slices mean more slices for the scanner to reconstruct) and image noise (thicker slices have more averaging so less image noise.) Typical slice thicknesses are between 1 and 10mm. Again the slice thickness is an important parameter in terms of the diagnostic quality of the CTP scan, thicker slices result in more Partial Volume Effects (PVE) which can cause large errors when not accounted for or avoided and can make registration more difficult. Pixel size is also determined in during image re-construction and is typically less than 0.5mm, depending on the capability of the scanner. The pixel size and the slice thickness together define the voxel dimensions. Generally slices are reconstructed using filter back projection or in case of large axial coverage the Feldkamp algorithm. The filter that is set per protocol and applied after reconstruction, is required to control resolution and noise. Some manufacturers have also developed advanced iterative reconstruction techniques which can significantly reduce image noise. The reconstructed image volumes are then saved in dicom format.

VOLUME REGISTRATION

Patient head movement during the CTP scan means that there may be movement in multiple axis between frames requiring image registration. CTP software typically does this just before calculation of the perfusion maps. The most common type is inelastic rotational and translational registration of the slices, however this does not account for rotation in the Z-plane (such as tilting one's head back or forward) and so some software packages use full 3D registration techniques. The effectiveness of the registration depends of the degree and speed of patient head movement and the slice thickness chosen for reconstruction, thinner slices have more spatial information and so are easier to register.

PRE-PROCESSING

At this point in the CTP process the data is almost ready to be analysed by the CTP software. Reduction of the image noise is done by applying one of the many types of filters to the data both spatially and temporally. Gaussian and edge preserving filters applied both spatially and temporally are the most basic and common. In the last several years more advanced filters such as the TIPS bilateral and HYPR filter have been developed which have been shown to be effective. There is again much variability in this step of the process, not just between different filtering methods but also to "strength" at which the filters can be applied, for example using a wider Gaussian filter may reduce image noise but will result in loss of spatial resolution and PVE.

ANALYSIS WITH CTP SOFTWARE

The CTP software creates a time attenuation curve for every voxel in the volume, this is done by examining how the HU value of a voxel changes over the scan time as the contrast agent passes through the brain, and subtracting the value of the voxel before the arrival of contrast agent. This time–attenuation curve, represents the contrast enhancement over time and forms the basis for all CTP methods. Voxels that show no contrast enhancement, e.g. bone voxels, are usually excluded at this point, creating a "perfusion mask" that will ensure that computational time is not wasted on trying to determine perfusion in voxels with no blood flow.

Calculation of perfusion parameters can be simply described as measurement of an input to a system (tissue), measurement of the output of that system (tissue), and inferring the properties of that system by comparing the input to the output. The input that is measured is the Arterial Input Function (AIF), this is a measurement of the contrast enhancement due to the passage of the contrast bolus through an artery that is supplying the tissue (red curve in Figure 2 bottom right). To do this the algorithm must identify a voxel that is within an artery, some software require the user to do this manually, and some software will do this automatically based on examination of the properties of the time attenuation curves such as bolus arrival time, time to peak, and peak enhancement.

Most usefully measurable arteries will have a diameter of 0.5 to 3mm, up to 4mm if the ICA is included within the scan coverage, structures of this size will be affected by PVE effects due to the resolution limitations of the CT scanner and possibly by filtering that was applied later. This PVE manifests as a scaling down of the arterial time-attenuation curve, which means an underestimation of the input to the system. This is almost universally corrected for by measuring the time attenuation curve of the much larger diameter sagittal sinus (blue curve Figure 2) and rescaling the arterial input curve to have the same size. It is not sufficient to just use the curve of the sagittal sinus as the input function as the bolus undergoes dispersion and is delayed as it passes through the tissue and so is not an accurate representation of the input.

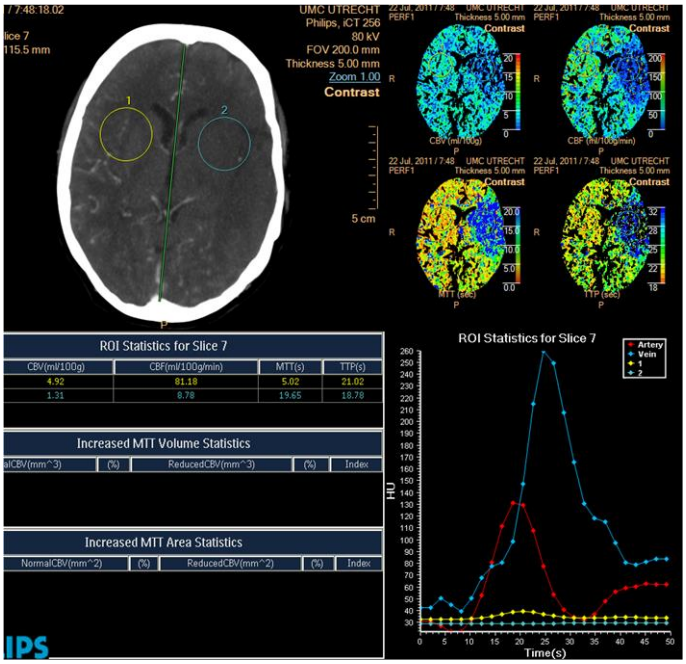

Figure 2: In the Philips healthcare perfusion package the location of and artery is designated semi-automatically by user drawn ROI. The arterial Time attenuation curve can be seen in red on the bottom right, significantly smaller than the venous output function (blue) due to partial volume effects on the smaller artery.

The output measured for each voxel is the time-attenuation curve (Yellow (healthy) and light blue (reduced perfusion) curves in figure 2) of the tissue so all voxels contained in the perfusion mask have an output measurement. The next step is to infer the properties of the system (the perfusion of blood through the tissue) by examination of the input and output together. This requires a perfusion model that describes, in terms of the perfusion parameters, how the tissue micro-vasculature alters the AIF into a locally measured tissue Time Attenuation Curve. Since often the relation between the measured AIF and tissue TAC is described by a convolution in the perfusion model, most methods to solve the parameter are based on deconvolution of the curves. There are many methods by which to do this and they can be broken into several categories: matrix based de-convolutions (sometimes referred to as Fourier based methods), fit or model based de-convolutions, maximum slope, and expectation maximization.

In each of these categories there may be several different variants, for example in the matrix based de-convolution variants are bSVD, sSVD, and dSVD , and they all will give different results for the same input CT data dependant on many factors such as the temporal resolution, image noise, filter technique and pathology and will have different computational loads. Different software vendors can even have multiple implementations of the same method in different software versions that will give different results. And many of the software suites have adjustable parameters that will drastically change the perfusion results.

All of the software will produce a set of perfusion parameter maps, showing the characteristics of each voxel in terms of cerebral blood flow (CBF), cerebral blood volume (CBV), mean transit time (MTT), time to peak (TTP) and several more dependent on the method used. These maps will have a colour scale which can be manually adjusted to make differences in perfusion apparent.

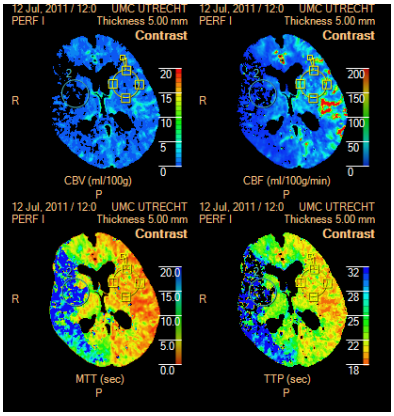

Figure 3: Typical cerebral blood volume (top left), cerebral blood flow (top right), mean transit time (bottom left) and time-to-peak (bottom right) parameter maps produce by Philips healthcare EBW brain perfusion package. A perfusion defect is evident by reduced blood perfusion in the right hemi-sphere (left of images).

INTERPRETATION OF THE PERFUSION MAPS

The perfusion parameter maps are examined by a (neuro)radiologist to attempt to identify the location and extent of “ischemic core” (irreversibly damaged tissue) and “penumbra” (hypoperfused tissue at risk for infarction) that may be recoverable if revascularization interventions with intravenous thrombolysis or endovascular therapies are successful[19,20]. Analysis is often done by comparing relative values. Since reduced perfusion due to acute stroke is usually unilateral one can compare perfusion values in the healthy hemisphere the diseased hemisphere to determine affected regions.

Several software vendors have implemented computer aided diagnosis methods to assist the radiologist in identifying the infarct and penumbra. These methods combine information from multiple perfusion parameter maps, both quantitative and relative values, to produce masks that denote these two regions, these are known as summary maps, or tissue classification maps. Although these maps can be very useful, giving quick and simple visual indications of tissue viability, they are heavily dependent on consistent, reproducible, perfusion values and quantitative accuracy. This reproducibility is strongly affected by choices in temporal resolution, CT dose, filtering technique, perfusion analysis methods and software parameters.

CTP has shown to be a promising tool for selection of patients with ischemic stroke who can potentially benefit from administration of rtPA [21]. Although CTP is fast, more widely available, and cheaper compared to other imaging modalities such as MRI and PET scans, it has not yet gained widespread acceptance in this role. The clinical relevance of arterial recanalisation as shown by CTA is supported by observational data [22]. The different tissue perfusion parameter maps may indicate widely different lesion size and locations, this is the result of the larger influence of technical and biological factors on the estimation of tissue perfusion compared to the anatomical image that is provided by angiography.

There is need for establishment of a viable protocol that is proven to yield accurate results and can be used consistently by clinicians and software vendors. In 2010 and 2013 Kudo et. al. demonstrated how this lack of consensus is causing an unacceptable variability in the perfusion measurements performed by different software[23,24]. Kudo's publication compared results from different software when given the same input, even stronger variation can be found when the one particular software is used to analyse the same perfusion but with different protocols (see chapter 3 of this thesis). Attempts have been made by the CTP community to reach a consensus, but without standardization of the tools being used to assess the best protocol and analysis method it will be difficult to reach this consensus. Comparison with perfusion measurements using microsphere based measurements in animal studies and other modalities such as PET and MRI is possible, but not in the same patient. Almost simultaneous acquisition would be required to ensure the same conditions are measured for quantitative definition of accuracy of CTP measurements. Furthermore, since clinical CTP acquisitions cannot be repeated with equal or varying settings without administering excessive CT dose, effects of different noise or tube settings (mAs) cannot be determined. This hampers the dose and image quality optimization.

This thesis describes methods to evaluate the impact of technical parameters from acquisition and analysis protocol and (non-clinical) patient specifics on CTP outcome in acute stroke. To this end a new hybrid brain phantom is suggested. Subsequently, specific attention is paid to the impact of de-convolution algorithms, patient motion and

AIF location selection. This could help standardizing and optimizing CTP studies and increasing its clinical impact.

OUTLINE OF THE THESIS

Chapter two of this thesis, describes the development of digital CTP phantom which combines anatomical data from MRI images, real CT noise masks and indicator dilution theory and proposes the head phantoms as a gold standard for CTP development.

Chapter three applies the digital head phantom to investigate the performance of an array of CTP protocols, including different temporal resolutions, CT dose, software parameters, and image filter types (Including application of the TIPS filter).

Chapter four utilizes the head phantom to examine the effect of patient head movement calculation of perfusion maps, and determines the degree and type of head movement that results in unacceptable results.

Chapter five turns the focus of the thesis to PVE, using both the head phantom and clinically acquired data to quantify the effects of PVE on measurement of the arterial input function, and proposes a practical protocol that can eliminate the requirement for correction of PVE by measurement of the venous outflow.

Chapter six looks more closely at the universally used PVE correction method, using a large patient cohort to confirm indication in the previous chapter that this method may be flawed and induce an overestimation of the CBV.

In the discussion I will outline the implications of the research, what it means for CTP and discuss some of the challenges facing the field of CTP.

References

1. Murray CJ, Lopez AD. Mortality by cause for eight regions of the world: Global Burden of Disease Study. *Lancet.* May 3 1997;349(9061):1269-1276.

2. Murray CJ, Lopez AD. Global mortality, disability, and the contribution of risk factors: Global Burden of Disease Study. *Lancet.* May 17 1997;349(9063):1436-1442.

3. Lopez AD, Mathers CD, Ezzati M, Jamison DT, Murray CJ. Global and regional burden of disease and risk factors, 2001: systematic analysis of population health data. *Lancet.* May 27 2006;367(9524):1747-1757.

4. Thrift AG, Dewey HM, Sturm JW, et al. Incidence of stroke subtypes in the North East Melbourne Stroke Incidence Study (NEMESIS): differences between men and women. *Neuroepidemiology.* 2009;32(1):11-18.

5. Bogousslavsky J, Van Melle G, Regli F. The Lausanne Stroke Registry: analysis of 1,000 consecutive patients with first stroke. *Stroke; a journal of cerebral circulation.* Sep 1988;19(9):1083-1092.

6. Mohr JP, Caplan LR, Melski JW, et al. The Harvard Cooperative Stroke Registry: a prospective registry. *Neurology.* Aug 1978;28(8):754-762.

7. Hossmann KA. Neuronal survival and revival during and after cerebral ischemia. *The American journal of emergency medicine.* Sep 1983;1(2):191-197.

8. http://www.strokecenter.org.

9. Liebeskind DS. Collateral circulation. *Stroke; a journal of cerebral circulation.* Sep 2003;34(9):2279-2284.

10. Wolfkiel CJ, Ferguson JL, Chomka EV, et al. Measurement of myocardial blood flow by ultrafast computed tomography. *Circulation.* Dec 1987;76(6):1262-1273.

11. Jaschke W, Sievers RS, Lipton MJ, Cogan MG. Cine-computed tomographic assessment of regional renal blood flow. *Acta radiologica.* Jan 1990;31(1):77-81.

12. Koenig M, Klotz E, Luka B, Venderink DJ, Spittler JF, Heuser L. Perfusion CT of the brain: diagnostic approach for early detection of ischemic stroke. *Radiology.* Oct 1998;209(1):85-93.

13. Wintermark M, Sanelli PC, Albers GW, et al. Imaging recommendations for acute stroke and transient ischemic attack patients: A joint statement by the

American Society of Neuroradiology, the American College of Radiology, and the Society of NeuroInterventional Surgery. *AJNR. American journal of neuroradiology.* Nov-Dec 2013;34(11):E117-127.

14. Hacke W, Donnan G, Fieschi C, et al. Association of outcome with early stroke treatment: pooled analysis of ATLANTIS, ECASS, and NINDS rt-PA stroke trials. *Lancet.* Mar 6 2004;363(9411):768-774.

15. Berger C, Fiorelli M, Steiner T, et al. Hemorrhagic transformation of ischemic brain tissue: asymptomatic or symptomatic? *Stroke; a journal of cerebral circulation.* Jun 2001;32(6):1330-1335.

16. Albers GW, Olivot JM. Intravenous alteplase for ischaemic stroke. *Lancet.* Jan 27 2007;369(9558):249-250.

17. Schwamm LH, Ali SF, Reeves MJ, et al. Temporal trends in patient characteristics and treatment with intravenous thrombolysis among acute ischemic stroke patients at Get With The Guidelines-Stroke hospitals. *Circulation. Cardiovascular quality and outcomes.* Sep 1 2013;6(5):543-549.

18. Wintermark M, Maeder P, Verdun FR, et al. Using 80 kVp versus 120 kVp in perfusion CT measurement of regional cerebral blood flow. *AJNR. American journal of neuroradiology.* Nov-Dec 2000;21(10):1881-1884.

19. Rowley HA. Extending the time window for thrombolysis: evidence from acute stroke trials. *Neuroimaging clinics of North America.* Aug 2005;15(3):575-587, x.

20. Sims J, Schwamm LH. The evolving role of acute stroke imaging in intravenous thrombolytic therapy: patient selection and outcomes assessment. *Neuroimaging clinics of North America.* May 2005;15(2):421-440, xii.

21. Parsons M, Spratt N, Bivard A, et al. A randomized trial of tenecteplase versus alteplase for acute ischemic stroke. *The New England journal of medicine.* Mar 22 2012;366(12):1099-1107.

22. Saver JL, Warach S, Janis S, et al. Standardizing the structure of stroke clinical and epidemiologic research data: the National Institute of Neurological Disorders and Stroke (NINDS) Stroke Common Data Element (CDE) project. *Stroke; a journal of cerebral circulation.* Apr 2012;43(4):967-973.

23. Kudo K, Sasaki M, Yamada K, et al. Differences in CT perfusion maps generated by different commercial software: quantitative analysis by using identical source data of acute stroke patients. *Radiology.* Jan 2010;254(1):200-209.

24. Kudo K, Christensen S, Sasaki M, et al. Accuracy and reliability assessment of CT and MR perfusion analysis software using a digital phantom. *Radiology.* Apr 2013;267(1):201-211.

CHAPTER 2: VALIDATION OF CT BRAIN PERFUSION METHODS USING A REALISTIC DYNAMIC HEAD PHANTOM

Alan J. Riordan, Mathias Prokop, Max A. Viergever, Jan Willem Dankbaar, Ewoud J. Smit and Hugo W. A. M. de Jong.

Published in Medical Physics, June 2011.

ABSTRACT

Purpose: Development and evaluation of a realistic hybrid head phantom for the validation of quantitative CT brain perfusion methods

Materials and methods: A combination, or hybrid, of CT images of an anthropomorphic head phantom together with clinically acquired MRI brain images was used to construct a dynamic hybrid head phantom. Essential CT imaging parameters such as spatially dependent noise, effects of resolution, tube settings and reconstruction parameters were intrinsically included by scanning a skull phantom using CT perfusion (CTP) protocols with varying mAs. This data was combined with processed high resolution 7T clinical MRI images to include healthy and diseased brain parenchyma as well as the cerebral vascular system. Time attenuation curves emulating contrast bolus passage based on perfusion as observed in clinical studies were added. Using the phantom, CTP images were generated using three brain perfusion calculation methods: bcSVD, sSVD and fit-based deconvolution and the linearity and accuracy of the three calculation methods was assessed. Dependency of perfusion outcome on calculation method was compared to clinical data. Furthermore, the potential of the phantom to optimize brain perfusion packages was investigated.

Results: All perfusion calculation methods showed overestimation of low perfusion values and underestimation of high perfusion values. Good correlation in behavior between phantom and clinical data was found (R^2=0.84).

Conclusion: A dynamic hybrid head phantom constructed from CT and MRI data was demonstrated to realistically represent clinical CTP studies which is useful for assessing CT brain perfusion acquisition, reconstruction and analysis.

INTRODUCTION

Computed Tomography (CT) perfusion (CTP) measurements are used to evaluate the extent and severity of the damaged brain tissue and to aid in prediction of patient outcome after acute ischemic stroke.[1-3] Functional perfusion maps produced by brain perfusion packages generally show several brain perfusion parameters such as: Cerebral Blood Flow (CBF), Cerebral Blood Volume (CBV) and Mean Transit Time (MTT). These maps may be calculated using a variety of methods including the maximum slope algorithm[1] , deconvolution methods such as single value decomposition (SVD)[4], box modulation transfer function[5] and an analytical fit-based deconvolution (FBD)[6]. Although CTP is aimed to provide quantitative measurements, large differences were found between the different calculation methods[7] and there is little consensus on which perfusion model/protocol is most accurate. This is primarily because lack of a well-defined CTP gold standard impedes exact definition of the accuracy and limitations of the various calculation models. Comparison with perfusion measurements using microsphere based measurements in animal studies and other modalities such as, PET and MRI is possible, but not in the same patient. Almost simultaneous acquisition would be required to ensure the same conditions are measured for quantitative definition of accuracy of CTP measurements. Furthermore, since clinical CTP acquisitions cannot be repeated with equal or varying settings without raising radiation concerns, effects of noise or tube settings (mAs), cannot be determined. This hampers the dose and image quality optimization.

A phantom realistically mimicking the perfusion process observed in brain tissue and blood vessels could serve as a very useful tool brain CTP research. Ideally, such a phantom gives a realistic representation of all anatomical features, reconstruction artifacts, noise distribution, scanner limitations and the dynamic properties of CTP scans. Furthermore, it enables assessment of the performance of the brain perfusion packages across a range of CT protocols and settings including noise levels and slice thicknesses.

Previous studies have developed both engineered and biological phantoms. Engineered solutions attempt to mimic blood perfusion by passing contrast agent through tissue-like structures such as: densely packed small spheres[8], porous gels[9],

and blood dialyzers[10]. These tissue-like structures adequately simulate soft tissue, however the design of these perfusion phantoms is basic. Developing an engineered phantom for brain perfusion that could realistically emulate the complex structure of the human brain would be extremely challenging. As a biological solution one may use a preserved human brain, similar to the method using a porcine kidney as a perfusion phantom[11]. However, this would be very difficult due to the delicate nature of brain tissue and would not easily allow investigation of a range of physiological conditions.

The purpose of this work is to develop and demonstrate a head phantom which realistically emulates a brain CTP scan to assess three CTP analysis methods. To this end, we propose a flexible hybrid phantom that combines anatomy from patient data with noise measurement from phantom data. The detailed anatomy was derived from clinical MRI scans. Subsequently, dynamic information is added to this realistic hybrid head phantom by using indicator-dilution theory, assuring maximal flexibility.

MATERIALS AND METHODS

CTP ALGORITHMS

The CT brain perfusion packages we assess in this work are: two variations of SVD, as used by the Acute Stroke Imaging Standardization (ASIST) workgroup [12], and an FBD based software package, Extended Brilliance Workspace (EBW) perfusion 4.0 (Philips Medical Systems, Best, the Netherlands)[6,13]. The two SVD based algorithms; standard SVD (sSVD)[14] and block circulant SVD (bcSVD) [14,15], were assessed by using the Perfusion Mismatch Analyzer (PMA)[16] software developed by ASIST. The FBD (Philips Medical Systems, Best, the Netherlands) fits an analytical curve to the Arterial Input Function (AIF) and the tissue Time Attenuation Curve (TAC) to calculate the perfusion parameters, using the method described by Axel[6,13].

CONSTRUCTION OF THE HYBRID HEAD PHANTOM

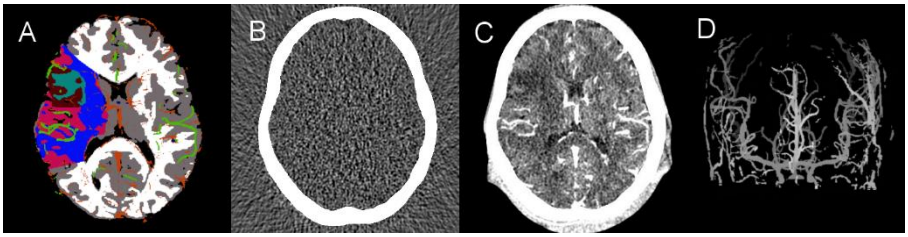

Figure 1: A: The segmentations of a 5 mm slice of the head phantom (partial volume, and resolution effects excluded to clarify the features). The vessels are shown in green (arteries) and orange (veins), colored regions define the tissue with reduced perfusion. B: An example of a 5 mm noise image used in the digital head phantom (acquired from a scan of a physical head phantom at 150 mAs) with non-uniform noise distribution inside the skull (White overlay added to noise mask here to highlight the position of the skull.) C: A frame from the head phantom with contrast enhancement beginning to appear in the arteries and veins. D: 3D cerebral artery volume seen from the front of the head.

To construct the hybrid head phantom we combined noise measurements of CT acquisitions of a physical skull phantom with clinically acquired (non-dynamic) MRI data. In addition to the noise measurements, the CT scans were also used to provide a foundation for the phantom (the skull). The MRI data provided the anatomical structure of the brain via volumetric tissue segmentation and vesselness filters. The anatomical volumes derived from MRI were registered to fit inside the skull of the CT phantom. Dynamic contrast bolus passage through vessels and tissue was emulated by using tracer kinetic theory. Details of the construction of the phantom are given next.

CT ACQUISITION AND PROCESSING

A human skull phantom filled with a tissue equivalent epoxy material was scanned using a clinical brain perfusion acquisition protocol (without contrast agent) on a 256-slice Brilliance iCT scanner (Philips Medical Systems, Best, the Netherlands). The

scan parameters were: 80 kVp, 512 x 512 matrix, 200 mm field of view, UB filter (a smoothing head image filter used by Philips), standard resolution, 65 slices, slice thickness/spacing of 1 mm. and an acquisition series of 25 time-frames at 2 second intervals (the customary frame rate widely used in the Netherlands), the rotation time of 0.33 seconds. To accurately define image noise distribution, using these settings a series of acquisitions was performed using 150 mAs (clinical dose) and a series at 305 mAs (high dose). The distribution of noise in a CT scan will vary because of effects including beam hardening and projection angle dependent attenuation and scatter. Because the physical head phantom is comprised of a real skull and a filling of brain tissue like material, it has a similar physical effect on CT image noise as a real human head. The average of a large number of acquisitions is practically noise-free, with very little variation of values due to noise. We will refer to this as being noise-free. After subtraction of this noise-free average image from a single noisy acquisition, a pure noise image with zero average results (Fig. 1B). Influence of artifacts from the skull, for example in the petrous bones or posterior fossa, will be included in any noise images generated at particular cranial level.

MRI ACQUISITION AND PROCESSING

To obtain accurate anatomical morphology, we acquired an isotropic high resolution (0.34x0.34x0.3 mm) ultrafast gradient echo sequence scan using a 7 Tesla MRI (Philips Medical Systems) with a scan length of 10cm from a healthy 21 year old volunteer. No exogenous contrast agent was used. The volumetric segmentation[17-19] of grey and white tissue and cerebrospinal fluid (CSF) was performed with the Freesurfer image analysis suite[20].

We used separate spoiled gradient echo pulse sequence scans from the same subject, one with TE=2.5ms-TR=24.3ms to distinguish the arteries and another with TE 19.3ms-TR 24.2ms to distinguish the veins. The Utrecht vesselness filter and vessel enhancing diffusion[21] were used to create binary maps of the vessels within the skull (see Fig. 1D). After combining the vessel segmentations with the brain tissue segmentation (see Fig. 1A), slice thickness was increased to 5 mm by averaging of 1 mm slices to include partial volume effects. The volume was manually registered to fit

inside noise-free CT-images of the skull phantom, resulting in a 3D, noise-free, non-contrast-enhanced head CT volume.

TIME-ATTENUATION CURVES

As outlined in[14,22-24] and according to the indicator dilution theory, the measurement of blood flow and volume can be described by considering a bolus of non-diffusible tracer given at time t = 0 in the feeding vessel(s) to a volume of interest (VOI) of tissue. The individual particles of the tracer follow different paths through the VOI and their transit times have a distribution characteristic of the passage of blood through the tissue. The probability density function of these transit times is denoted h(t), the transport function. The fraction of injected tracer still present in the VOI at time t is described by the tissue residue function R(t):

$$R(t) = \left[1 - \int_0^t h(\tau) d\tau \right] \qquad (1)$$

Where τ is a bound variable for integration purposes. The concentration $C_{VOI}(t)$ of tracer within a given VOI of tissue is given by:

$$C_{VOI}(t) = F_{tis} \int_0^t C_a(\tau) R(t-\tau) d\tau = F_{tis} R(t) \otimes C_a(t)$$

Where F_{tis} is the local blood flow in the tissue, $C_a(t)$ is the AIF, a time-attenuation curve (TAC) measured at the feeding artery. When scaled by F_t in equation (2), the tissue residue function will describe the main perfusion parameters used in CTP analysis: the CBF by the maximum value of the function, the MTT by the first moment, and the CBV by the area under the function. The residue functions used in this study are constant until MTT seconds after which a mono-exponentially decay follows (See also Fig. 2). This model assumes the tracer remains intravascular i.e. the blood brain

barrier is intact. The perfusion values CBF, MTT and CBV used for the various tissue types were acquired from literature[25] and are detailed in the table 1. The values used to define the tissue residue functions we consider to be the input values of CBF, MTT and CBV for the hybrid phantom. Accuracy of the result of an analysis method (i.e. the output of the brain perfusion software package) is defined by comparison with these input values.

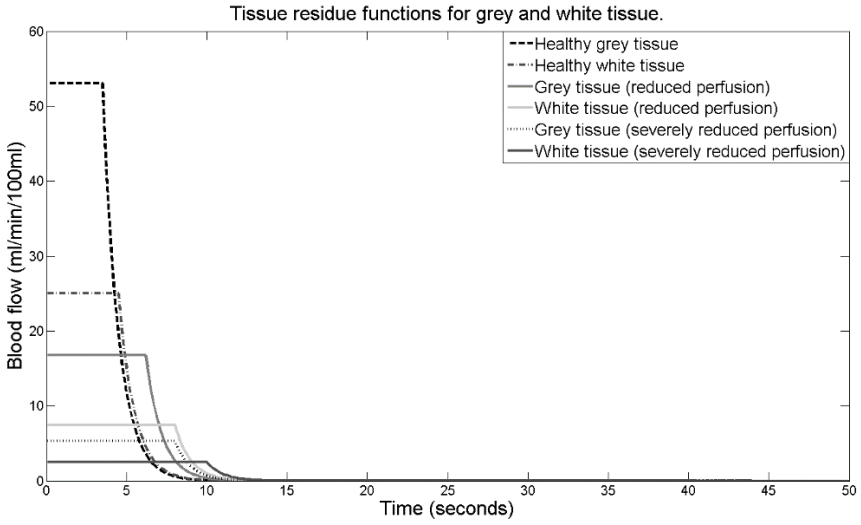

Figure 2: Tissue residue functions are scaled by the respective CBF values, the level of the plateau represents the CBF. Shown here are tissue residue functions modeled to represent grey tissue, white tissue, diseased grey tissue and diseased white tissue. The longer MTT of the diseased tissue is evident by the broader functions. The relationship between CBF, MTT and CBV (the area under the curve) is defined by the CVP. (Note: Blood flow is defined as ml of blood per 100ml of tissue per minute)

The TAC of the AIF ($C_a(t)$) and VOF (Venous Output Function) used in the hybrid head phantom were based on an average of several AIF/VOF extracted from main arteries from a single healthy (originally admitted with stroke symptoms) clinical CTP scan (See Fig 3). The (retrospective) clinical CTP data used for AIF and VOF TAC definition followed standard CTP protocol: forty millilitres of nonionic contrast agent (Iopromide, Ultravist, 300 mg iodine/ml; Schering, Berlin, Germany) was injected into the cubital

vein (18-gauge needle) at a rate of 5 ml/s followed by a 40-mL saline flush at a rate of 5 ml/s by using a dual power injector (Stellant Dual CT injector; Medrad Europe, Beek, the Netherlands), the standard CTP scanner protocol and tube settings described above were used. The properties of this standard protocol are thus inherited by the vessel TAC used in the hybrid head phantom. To correct for partial volume effects in the AIF measurements, the averaged AIF was rescaled (multiplied) to have the same area under the curve (AUC) of a VOF measured from the same patient.[26]

Equation 2 shows that convolving the AIF with a residue function scaled by F_{tis} defines $C_{VOI}(t)$, the tissue TAC. Also accounted for is the fact that CT contrast material remains in the extracellular fraction of the blood. Before convolution with R(t), $C_a(t)$ is multiplied by $1/Hct_L$, where Hct_L is the hematocrit factor of large vessels. The result of the convolution, $C_{VOI}(t)$ (the tissue TAC) is then multiplied by Hct_S, the hematocrit factor of small vessels. The values for Hct_L and Hct_S used in this work are 0.45 and 0.25 respectively[27,28].

Table I: Values used to define tissue residue function parameters for the various tissue types. These values were chosen from the mean values defined in [25]

	Grey matter	White matter	Grey matter (Reduced perfusion)	Grey matter (Severely reduced perfusion)	White matter (Reduced perfusion)	White matter (Severely reduced perfusion)
CBV(ml/100ml)	3.3	1.9	1.73	0.71	1	0.42
MTT(sec)	3.5	4.9	6.5	8	8	10
CBF(ml/100ml/min)	53	25	16.0	5.3	7.5	2.5

Six types of tissue TAC were generated using different (scaled) R(t). Healthy tissue (grey and white, normal CBF defined by table 1), tissue with reduced perfusion (grey and white, CBF reduced to 30%, table 1), and tissue with severely reduced perfusion (grey and white, CBF reduced to 10%, table 1). The tissues with reduced perfusion also have corresponding higher MTT, delayed arrival of contrast, and a reduced CBV[29], for each of the tissues, the relationship between CBF, MTT, and CBV is

defined by the Central Volume Principle (CVP). This provided TACs for every type of tissue found in the phantom, (Fig. 3).

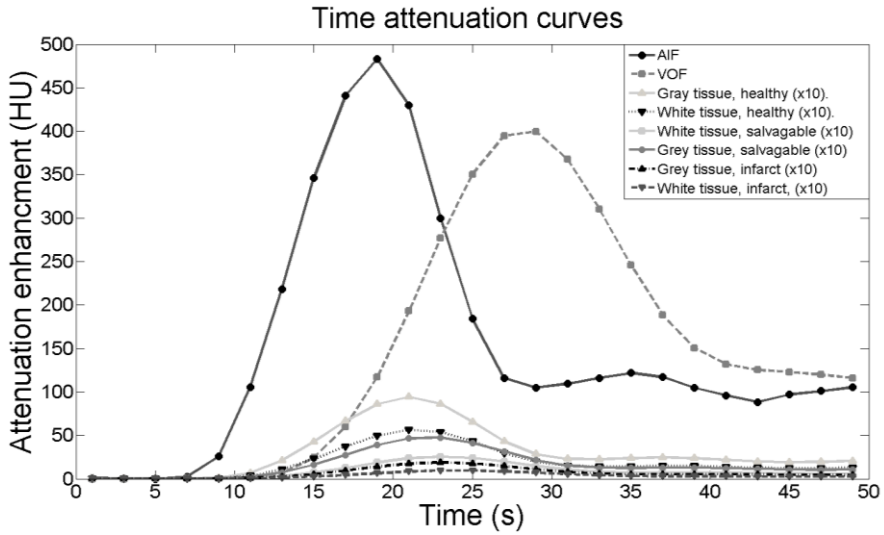

Figure 3: TAC of the clinically acquired AIF (rescaled using the AUC of the VOF) and VOF. The gray and white matter TAC's are generated using equation 2. These curves represent the attenuation enhancement before the effects of partial volume and noise. Tissue time attenuation curves have been multiplied by 10 for clarity.

All the tissue, vessel and cerebrospinal fluid segmentations were assigned a base value corresponding to the CT number or HU generally observed[30] for that particular tissue or vessel (Grey tissue 35HU, white tissue 29HU, vessels 40HU and CSF 12HU). Each voxel in the 3D hybrid head phantom then is assigned a TAC dependent on the type of tissue/vessel represented by that voxel, resulting in a 4D phantom. Regions of reduced perfusion were designated to simulate an occlusion of the middle cerebral artery and assigned a corresponding TAC generated using reduced input CBF values. Also tested was an algorithm's sensitivity to the case where the damaged tissue is perfused by an artery which has a delayed arrival of the contrast bolus, because of a partially occluded artery or tissue being fed by circumventing collateral vessels. To mimic this, we convolved the tissue residue function with an AIF that is delayed 3 seconds relative to the normal AIF used elsewhere in the brain.

EMULATION OF CT LIMITATIONS

To realistically include CT image limitations, besides the previously introduced thick slices and subsequent partial volume effects, two more CT effects were applied to the final hybrid head phantom. First, resolution limitations were simulated using a 3D Gaussian blurring function with a FWHM = 1.4 mm. With an original pixel size of 0.39 mm and given the discrete nature of the features, this will result in a final image resolution of 1.45 mm. The desired image resolution was defined by scanning an image quality phantom using the CTP protocol. Second, to add CT noise to the images, the noise images described above (also averaged to 5 mm slices) were added to each frame to generate clinical (150 mAs) and high (305 mAs) dose phantoms. A unique noise image could be generated for each frame using the large number of acquisitions from the skull phantom. For an example of a frame of a single 5mm slice from the head phantom with a dose of 150 mAs see Fig. 1C.

EVALUATION AND APPLICATION OF THE DIGITAL HEAD PHANTOM

ASSESSMENT OF THE LINEARITY OF THE BRAIN PERFUSION SOFTWARE

Three hybrid head phantom data sets, at 305 mAs, at 150 mAs and noise-free (no noise overlay added), were processed using the PMA software (both bcSVD and sSVD) and the Philips brain perfusion package. Since CBF is a primary parameter for stroke diagnosis[29,31], is the most challenging parameter to calculate and analysis of one parameter suffices for demonstration of the hybrid head phantom, this study focuses on the CBF maps with reference to CVB and MTT maps. In practice, MTT and CBV maps are also critical for diagnosis, since normal CBF in diseased tissue may be restored by auto-regulation and may only be observed by decreased CBV or increased MTT values. Knowing which CBF map voxels represent which types of tissue, we are able to group voxels of equal tissue types for analysis and define the average of the calculated CBF for each tissue type and compare it to the input CBF. To quantify the accuracy of the CTP software, we assess a linear relationship between calculated and input CTP values. This was done by examining slope and y-axis intercept of a linear fit to input vs. calculated CBF values. To examine the time sensitivity[12,15] of the algorithms, the same analysis was carried out on a hybrid head

phantom generated without simulation of delayed arrival of blood to the diseased tissue.

COMPARISON OF THE HYBRID HEAD PHANTOM TO CLINICAL CTP SCANS

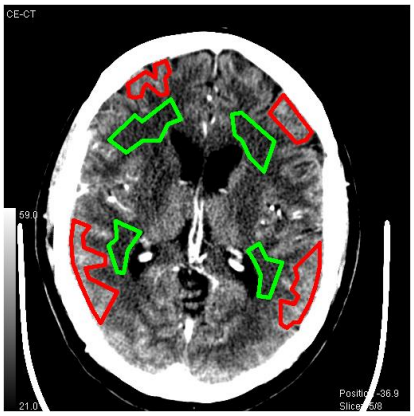

Figure 4: An example of the ROI's drawn on white tissue (green) and grey tissue (red) on a time-maximum-intensity image of clinical CTP data. These ROI's were saved and transferred to the CTP parameter maps where the ROI statistics were used to compare typical clinical results with the hybrid head phantom.

To confirm that the dynamic behaviour of the hybrid head phantom accurately represents the perfusion observed in clinical CT perfusion scans, we performed a direct comparison. In four patient scans and in the phantom at clinical dose, several regions of interest (ROI) (figure 4) were drawn by a radiologist containing healthy white or grey matter on CBF maps calculated with the software, using a time-maximum intensity projection of the CTP data as a reference to distinguish grey and white tissue. For each patient the same ROI set was used for each calculation. From the ROI values an average CBF for both tissue types was determined for each patient and from this value we derived the CBF found by each of the software packages. The same process was used for selecting ROIs on the hybrid head phantom results. As CBF in diseased tissue is extremely variable and dependant on the extent of ischemia only healthy tissue was included in this comparison. The average white and grey matter CBF values in patients were compared to the phantom results. The purpose of this comparison is to examine how typical perfusion values observed in clinically acquired data compare with results observed in the hybrid head phantom. Furthermore the dependency of the CBF values on CTP calculation method was compared between clinical and phantom data. This indicates realistic behaviour of the phantom.

As a second investigation of the agreement between clinical data and the head phantom, we used the head phantom at clinical dose to find altered bcSVD algorithm settings that lead to better CBF linearity and better separation between the CBF values of the various tissue types. We changed i) the Gaussian filter applied to the data by the bcSVD software, and ii) a noise suppression method used in bcSVD, the oscillation index[14]. Subsequently, the standard PMA settings and the altered settings were also applied to the clinical data and their effects on CBF values were compared to the CBF measured in the head phantom.

RESULTS

ASSESSMENT OF THE LINEARITY OF THE BRAIN PERFUSION SOFTWARE

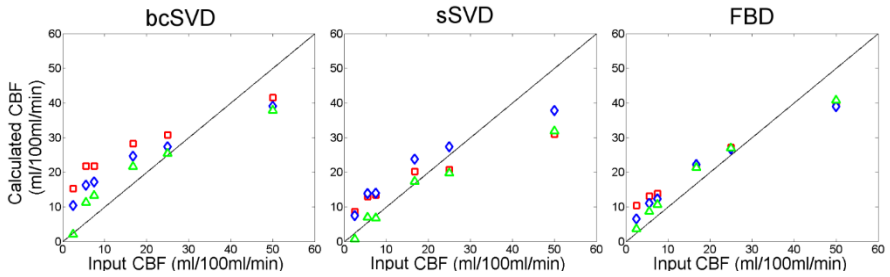

Figure 5: Scatter plot showing correlation between input CBF (defined by generated TAC) and calculated CBF (output from perfusion software) when using bcSVD, sSVD and FBD. Noise-free head phantom: ∆, with clinical dose (150 mAs): □, and with high dose (305 mAs): ◊. The solid line represents an ideal correlation, data points above this line are overestimated, and data points under the line are underestimated.

Fig. 5 shows the relationship of input vs. calculated (output) CBF values for the different software/deconvolution methods and noise levels. This relationship is assessed by a linear fit to the data. Although a good linear fit ($R^2 > 0.92$) is found in all cases, a bias is observed for all CT dose levels in the head phantom and for all software examined (Table 2), i.e. y-axis intercept > 0 and a slope < 1, indicating an

overestimation of low CBF values and an underestimation of CBF in high flow regions. In all cases, the bias was lowest in the high dose phantom. In table 3, the sensitivity of CBF measured for delayed arrival time is summarized by comparing values from the original head phantom with delayed arrival in the diseased regions to a second head phantom without arrival time delay. To best highlight the sensitivity of the algorithms, the values shown are measured using the noise-free phantom. The bcSVD method proved insensitive to the delayed arrival of blood, with no substantial change in calculated CBF. However with sSVD and FBD a substantial dependency is observed.

	bcSVD		sSVD		FBD	
Dose	Slope	Y intercept	Slope	Y intercept	Slope	Y intercept
Infinite	0.67	6.62	0.62	2.88	0.76	5.06
305 mAs	0.56	12.47	0.60	9.93	0.66	7.72
150 mAs	0.50	17.59	0.44	10.04	0.62	9.86

Table 2: Results of linear fit to mean measured CBF vs. real CBF for the three software packages using the hybrid head phantom at different dose levels. The ideal result is a slope of 1 and a y-intercept of 0. All linear fits showed a good R^2 correlation (>0.92), indicating that the results are linear, but with a bias dependant on the dose.

Table 3: Sensitivity of perfusion algorithms to delayed arrival time of blood in diseased tissue. All values are CBF in ml/100ml/min. (Noise-free phantom only.)

	Grey matter (Reduced perfusion)	White matter (Reduced perfusion)	Grey matter (Severely reduced perfusion)	White matter (Severely reduced perfusion)
True CBF value	16.00	7.50	5.3	2.50
bcSVD				
Delayed arrival	21.74	13.31	11.37	2.16
No delay	22.68	12.90	11.88	2.16
sSVD				
Delayed arrival	17.42	6.80	7.07	0.76
No delay	21.30	9.19	8.20	1.00
FBD				
Delayed arrival	21.34	10.69	8.72	3.66
No delay	26.12	13.06	10.84	4.50

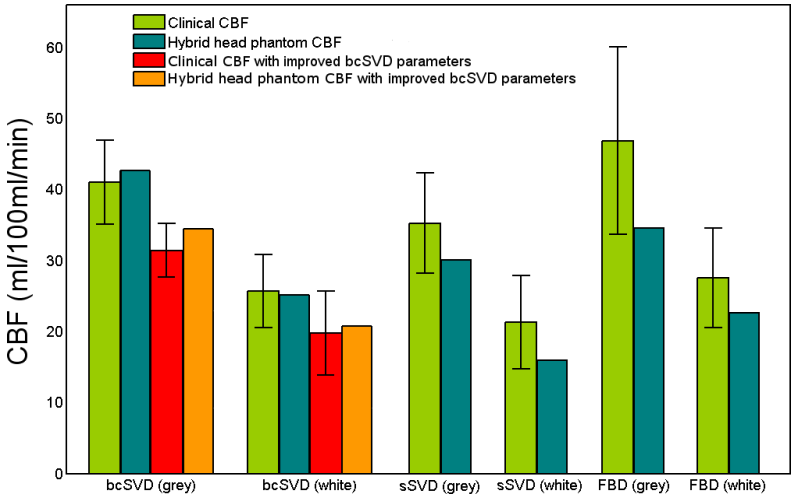

Figure 6: Correlation between CBF (in healthy tissue defined by a radiologist) calculated from clinical data (Green bars) and the result calculated from the head phantom (Blue bars), error bars represent variability of the mean CBF in clinical results (1 standard deviation). The red (clinical) and orange (head phantom) bars show how the mean CBF values are changed by altered bcSVD calculation parameters.

Fig. 6 shows the results of a comparison of the CBF maps from the head phantom and clinical data using the different CTP software packages. A linear regression of the mean CBF values for each of the software packages and settings from the clinical data (green colored bars) versus the mean CBF values measured using the head phantom (blue colored bars) and the same software gives a slope of 0.92 (ideal case being 1) and an R^2 correlation of 0.84. Fig. 7 shows CBF variance in tissue in both the clinical data CBF maps (blue colored bars) and the hybrid head phantom CBF maps (purple colored bars).

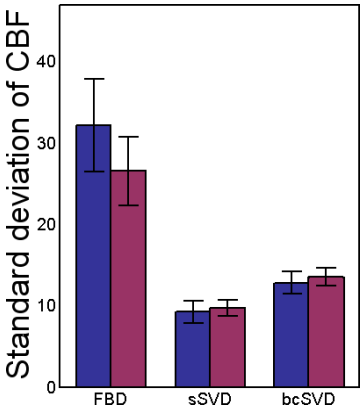

Figure 7: Comparison of variance (standard deviation) in clinical CBF maps (Blue) and head phantom CBF maps (Purple).

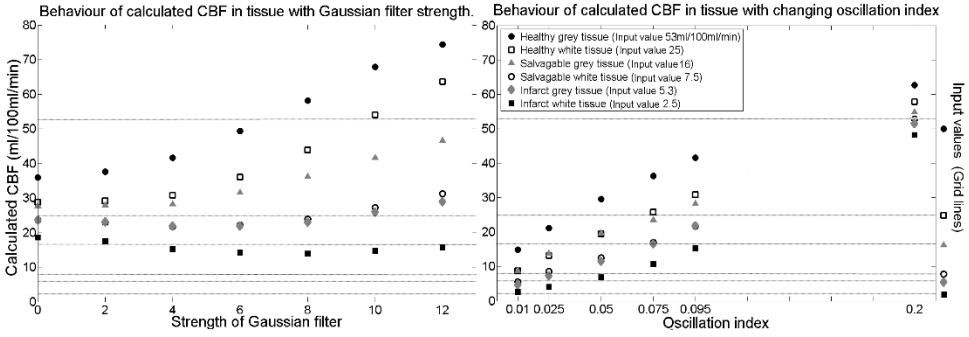

Figure 8: Effects of varying the strength of the Gaussian filter (left) and the oscillation index (right) in the bcSVD based calculations on the head phantom. Dotted lines define real CBF values for comparison and are labelled on the far right.

The effects of changing bcSVD settings in PMA are shown in Fig. 8. Increasing the strength of the blurring filter results in better separation (increased vertical divergence of data points) of CBF values of different tissue/perfusion-states, but at the cost of increased overestimation. Decreasing the oscillation index (Fig. 8) from the default value of 0.095 reduced overestimation (see Table 2). Based on these results, a Gaussian filter strength of 6 and oscillation index of 0.075 were defined as the

improved settings. In clinical data these settings visually improved image noise level and contrast between the tissue types/states on CBF maps (Fig. 9).

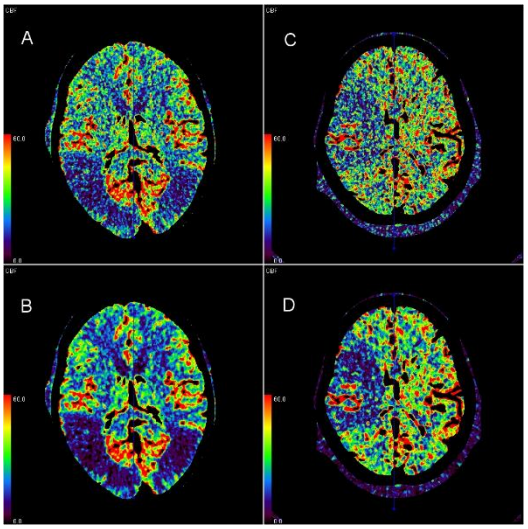

Figure 9: CBF diagnostic image quality improvement using the head phantom to alter bcSVD. A: Clinical data CBF map with default PMA parameters. B: Clinical data CBF map after optimization. C: head phantom CBF map with default PMA parameters. D: head phantom CBF map after optimization

Although the different flow regions may be clearly observed in the results from the noise free head phantom, they cannot be clearly spatially delineated in the noisy parameter maps. Furthermore, the effects of the improved settings on CBF values are similar for the head phantom and in clinical data, a common reduction in the CBF values by about 20% (See Fig. 6; red and orange bars). The improved setting also improved the bias in the CBF values measured in the head phantom, using the ground truth of the phantom we able to measure a bias with a slope of 0.67 and a y-axis intercept of 12.20, a considerable improvement in linearity for the clinical dose of 150 mAs (see table 2 for measurement at default settings.). Fig. 10 displays MTT and CBV maps from the bcSVD algorithm, a good visual agreement between the maps derived from clinical data and the head phantom is observed

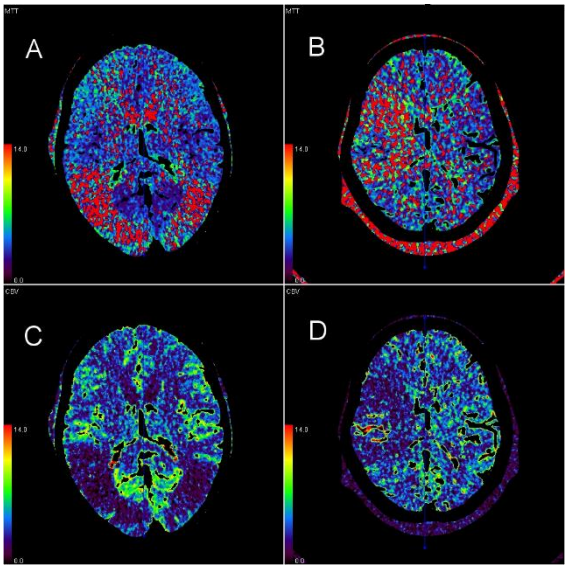

Figure 10: MTT and CBV maps showing good agreement between the results from the clinically acquired data and the head phantom. (Vessels have been excluded). A: Clinical MTT map, B: Phantom MTT map, C: Clinical CBV map, D: Phantom CBV map.

DISCUSSION AND CONCLUSIONS

A hybrid head phantom is developed to realistically mimic dynamic CT brain scans including image noise as observed in clinical scans and is used to evaluate and optimize brain CTP methods. Dependence of CBF values on dose level, algorithm parameters, and pre-processing settings correlates convincingly between clinically acquired data and phantom data (Fig. 6, Fig. 7). These results suggest that the methods and models used to generate vessel and tissue TACs, anatomical features, noise and partial volume effects are realistic and that analysis carried out using the hybrid head phantom will be representative of what is found using real clinical CTP data, with the advantage of a ground truth.

We acknowledge several limitations of the phantom. Although realistic, clinically observed CTP parameters were used for the construction, the shape of underlying residue function used to generate TAC is theoretical since it cannot be measured

directly. However, detailed and computation extensive finite element simulations of blood flow dynamics, have indicated that the used residue functions can be regarded as very accurate approximations[24]. Deconvolution methods outlined in [15,24] are applied to clinical data to construct a shape which approximates the tissue residue function. When validating perfusion analysis methods with data generated using convolution with such a shape an unwanted bias may be introduced, however we found no evidence of such a bias. A second limitation is that the arterial and venous TACs have identical timing throughout the 3D volume (with the exception of delayed arrival time in the diseased tissue).

In reality the contrast agent will perfuse upwards through the brain, meaning that the vessel and tissue lower in the head will be perfused slightly before the upper sections. Also slightly different path lengths for each vessel will result in a small variance in contrast arrival time. However both these effects are on a time scale less than the time resolution of this particular CTP protocol (2 seconds), and will not have a significant effect on the results. Furthermore, the flexibility of the hybrid phantom allows inclusion of extensive location dependent timing of all TAC when more information about the nature and level of phenomenon has been gathered. Beam hardening in the head phantom is incorporated by using CT images acquired from the physical head phantom. At this point it is unclear if beam hardening due to contrast agent plays a significant role in brain CTP results and may be a limitation of the head phantom. We intend on investigating the magnitude and ways to include this effect in the head phantom.

This study found that decreasing CT dose leads to increased CBF bias for all software packages considered. This bias is observed as a slope of less than one and an axis interception of greater than zero in a linear fit to the data, and results in an overestimation of low CBF values and an underestimation of high CBF values. This is similar to the bias observed by Wintermark et al[32]. (in terms of the nature and magnitude of the bias of the linear fit) when comparing CBF results from CT perfusion measured with SVD to stable Xenon CT (considered to be a quantitative measurement of CBF).

The results also confirm the previously published observations[33] : Firstly, that the bcSVD method is insensitive to delayed arrival of contrast in the tissue relative to the AIF. Secondly, that for a positive delay as simulated here, the CBF values calculated by sSVD will be lower than in the case on no delay, see table 3. The FBD method also exhibits delay sensitivity very similar to that of sSVD, this is expected as the FBD does not account for delayed arrival of contrast bolus. This lowering of CBF values as a result of time sensitivity paradoxically reduces the difference between the input and measured values for some CBF values.

Also, the dependence on pre-processing and type of perfusion algorithms concurs with an earlier clinical study[7]. In this study Kudo compared the ratio of measured CBF in healthy tissue to that of diseased tissue for the same three software packages examined in this study. Comparing these clinical ratios to the ratios found with the head phantom CTP results yields a correlation (linear regression) of 0.97 when using the noise-free phantom, 0.95 (clinical dose phantom) and 0.99 (high dose phantom). This excellent correspondence with clinical data is further evidence of the viability of the head phantom for emulating clinical scans.

Altogether, this makes the hybrid head phantom a useful tool for assessing and optimizing CT brain perfusion acquisition, reconstruction and analysis protocols.

References

1. Klotz E, Konig M. Perfusion measurements of the brain: using dynamic CT for the quantitative assessment of cerebral ischemia in acute stroke. *European journal of radiology.* Jun 1999;30(3):170-184.

2. Mayer TE, Hamann GF, Baranczyk J, et al. Dynamic CT perfusion imaging of acute stroke. *AJNR. American journal of neuroradiology.* Sep 2000;21(8):1441-1449.

3. Lev MH, Segal AZ, Farkas J, et al. Utility of perfusion-weighted CT imaging in acute middle cerebral artery stroke treated with intra-arterial thrombolysis: prediction of final infarct volume and clinical outcome. *Stroke; a journal of cerebral circulation.* Sep 2001;32(9):2021-2028.

4. Murphy BD, Fox AJ, Lee DH, et al. White matter thresholds for ischemic penumbra and infarct core in patients with acute stroke: CT perfusion study. *Radiology.* Jun 2008;247(3):818-825.

5. Nambu K, Takehara R, Terada T. A method of regional cerebral blood perfusion measurement using dynamic CT with an iodinated contrast medium. *Acta neurologica Scandinavica. Supplementum.* 1996;166:28-31.

6. Wintermark M, Smith WS, Ko NU, Quist M, Schnyder P, Dillon WP. Dynamic perfusion CT: optimizing the temporal resolution and contrast volume for calculation of perfusion CT parameters in stroke patients. *AJNR. American journal of neuroradiology.* May 2004;25(5):720-729.

7. Kudo K, Sasaki M, Yamada K, et al. Differences in CT perfusion maps generated by different commercial software: quantitative analysis by using identical source data of acute stroke patients. *Radiology.* Jan 2010;254(1):200-209.

8. Teslow TN, Robb RA. X-ray computed tomographic (CT) phantom designed for the development of techniques for measurement of myocardial perfusion. *Physics in medicine and biology.* Oct 1991;36(10):1407-1413.

9. Ebrahimi B, Swanson SD, Chupp TE. A microfabricated phantom for quantitative MR perfusion measurements: validation of singular value decomposition deconvolution method. *IEEE transactions on bio-medical engineering.* Nov 2010;57(11).

10. Maciak A, Kronfeld A, Muller-Forell W, Wille C, Kempski O, Stoeter P. [A capillary-based perfusion phantom for the simulation of brain perfusion for MRI]. *RoFo : Fortschritte auf dem Gebiete der Rontgenstrahlen und der Nuklearmedizin.* Oct 2010;182(10):883-890.

11. Haberland U, Cordes J, Lell M, Abolmaali N, Klotz E. A biological phantom for contrast-media-based perfusion studies with CT. *Investigative radiology.* Oct 2009;44(10):676-682.

12. Sasaki M, Kudo K, Ogasawara K, Fujiwara S. Tracer delay-insensitive algorithm can improve reliability of CT perfusion imaging for cerebrovascular steno-occlusive disease: comparison with quantitative single-photon emission CT. *AJNR. American journal of neuroradiology.* Jan 2009;30(1):188-193.

13. Axel L. A method of calculating brain blood flow with a CT dynamic scanner. *Advances in neurology.* 1981;30:67-71.

14. Ostergaard L, Weisskoff RM, Chesler DA, Gyldensted C, Rosen BR. High resolution measurement of cerebral blood flow using intravascular tracer bolus passages. Part I: Mathematical approach and statistical analysis. *Magnetic resonance in medicine : official journal of the Society of Magnetic Resonance in Medicine / Society of Magnetic Resonance in Medicine.* Nov 1996;36(5):715-725.

15. Wu O, Ostergaard L, Weisskoff RM, Benner T, Rosen BR, Sorensen AG. Tracer arrival timing-insensitive technique for estimating flow in MR

perfusion-weighted imaging using singular value decomposition with a block-circulant deconvolution matrix. *Magnetic resonance in medicine : official journal of the Society of Magnetic Resonance in Medicine / Society of Magnetic Resonance in Medicine.* Jul 2003;50(1):164-174.

16. *Perfusion mismatch analyser* [computer program]. Version 3.0.0.02006.

17. Dale AM, Fischl B, Sereno MI. Cortical surface-based analysis. I. Segmentation and surface reconstruction. *NeuroImage.* Feb 1999;9(2):179-194.

18. Fischl B, Dale AM. Measuring the thickness of the human cerebral cortex from magnetic resonance images. *Proceedings of the National Academy of Sciences of the United States of America.* Sep 26 2000;97(20):11050-11055.

19. Fischl B, Liu A, Dale AM. Automated manifold surgery: constructing geometrically accurate and topologically correct models of the human cerebral cortex. *IEEE transactions on medical imaging.* Jan 2001;20(1):70-80.

20. *Freesurfer analysis suite* [computer program]. Boston, USA.

21. Koopmans PJ, Manniesing R, Niessen WJ, Viergever MA, Barth M. MR venography of the human brain using susceptibility weighted imaging at very high field strength. *Magma.* Mar 2008;21(1-2):149-158.

22. Meier P, Zierler KL. On the theory of the indicator-dilution method for measurement of blood flow and volume. *Journal of applied physiology.* Jun 1954;6(12):731-744.

23. Zierler KL. Equations for Measuring Blood Flow by External Monitoring of Radioisotopes. *Circulation research.* Apr 1965;16:309-321.

24. Bredno J, Olszewski ME, Wintermark M. Simulation model for contrast agent dynamics in brain perfusion scans. *Magnetic resonance in medicine : official journal of the Society of Magnetic Resonance in Medicine / Society of Magnetic Resonance in Medicine.* Jul 2010;64(1):280-290.

25. Parkes LM, Rashid W, Chard DT, Tofts PS. Normal cerebral perfusion measurements using arterial spin labeling: reproducibility, stability, and age and gender effects. *Magnetic resonance in medicine : official journal of the Society of Magnetic Resonance in Medicine / Society of Magnetic Resonance in Medicine.* Apr 2004;51(4):736-743.

26. van der Schaaf I, Vonken EJ, Waaijer A, Velthuis B, Quist M, van Osch T. Influence of partial volume on venous output and arterial input function. *AJNR. American journal of neuroradiology.* Jan 2006;27(1):46-50.

27. Larsen OA, Lassen NA. Cerebral Hematocrit in Normal Man. *Journal of applied physiology.* Jul 1964;19:571-574.

28. Sakai F, Nakazawa K, Tazaki Y, et al. Regional cerebral blood volume and hematocrit measured in normal human volunteers by single-photon emission computed tomography. *Journal of cerebral blood flow and metabolism : official journal of the International Society of Cerebral Blood Flow and Metabolism.* Jun 1985;5(2):207-213.

29. Reivich M. Blood flow metabolism couple in brain. *Research publications - Association for Research in Nervous and Mental Disease.* 1974;53:125-140.

30. Weinstein MA, Duchesneau PM, MacIntyre WJ. White and gray matter of the brain differentiated by computed tomography. *Radiology.* Mar 1977;122(3):699-702.

31. Hossmann KA. Viability thresholds and the penumbra of focal ischemia. *Annals of neurology.* Oct 1994;36(4):557-565.

32. Wintermark M, Thiran JP, Maeder P, Schnyder P, Meuli R. Simultaneous measurement of regional cerebral blood flow by perfusion CT and stable xenon CT: a validation study. *AJNR. American journal of neuroradiology.* May 2001;22(5):905-914.

33. Kudo K, Sasaki M, Ogasawara K, Terae S, Ehara S, Shirato H. Difference in tracer delay-induced effect among deconvolution algorithms in CT perfusion analysis: quantitative evaluation with digital phantoms. *Radiology.* Apr 2009;251(1):241-249.

CHAPTER 3: IMPROVEMENTS IN ACCURACY AND DOSE EFFICIENCY OF CTP BY APPLICATION OF A REALISTIC DIGITAL PHANTOM

Alan J. Riordan, Edwin Bennink, Max A. Viergever, Hugo W. A. M. de Jong

Submitted for publication

ABSTRACT

Purpose: Digital phantoms may prove to be a valuable tool for optimizing CTP protocols. The purpose of this study is to investigate the impact of algorithm settings, dose, temporal resolution, and filtering on the accuracy and dose efficiency of CT cerebral blood flow measurements. This was done by the application of a realistic digital head phantom.

Materials and methods: A realistic anthropomorphic head phantom was used to simulate CTP scans with 50, 100, 150 and 250mAs/rot and at 1, 2, 3, and 4 second intervals giving a range of total 16 CT doses from 25 to 500 mGy (CTDI-vol). These CTP scans were filtered using either a Gaussian filter ('clinical standard') or an advanced 4D filter and then analysed using the widely used block-circulant singular value decomposition (bSVD) algorithm with different settings. Accuracy was assessed by calculating the Pearson correlation coefficient and linear regression between resultant CBF maps and the ground truth.

Results: Accuracy of CTP (Pearson correlation with ground truth) improved an average of 38% with application of advanced filtering and optimized algorithm settings/parameters tailored to suit protocol temporal resolution. With these improvements it was found there was no substantial gain in accuracy (<5%) for protocols with CT dose over 100mGy.

Conclusion: Temporal resolution, CT dose, algorithm settings/parameters, and filtering method have significant impact on accuracy of CTP. A digital head phantom is used to quantify and optimize performance, allowing for substantial reduction of CT dose relative to current clinical protocols

INTRODUCTION:

Computed tomography perfusion (CTP) is used for assisting in diagnosis of acute ischemic stroke, hemodynamic ischemia and subarachnoid hemorrhage[1-7]. In CTP, a time series of CT images is acquired to monitor the in-flow and wash-out of contrast agent. The resulting functional perfusion maps produced by analysis software show several parameters such as cerebral blood flow (CBF), cerebral blood volume (CBV), and mean transit time (MTT). These parameters may be calculated from the time series of CT images using a variety of methods including the maximum slope algorithm[6], deconvolution methods based on singular value decomposition (SVD)[8-11], box modulation transfer function[12], and analytical fit-based de-convolutions[13]. The parameter maps can be used to estimate the location and intensity of perfusion defects with respect to normal parenchyma. The quantitative accuracy of CTP maps is important to allow for establishment of general empirical thresholds of CBF, CBV and MTT values to distinguish diseased areas from healthy, and to allow for patient prognoses by comparing these maps to follow up scans that have determined patient out-come.

The quantitative accuracy may depend on the choice of calculation method[14,15]. Several studies have demonstrated the superior performance of SVD, mainly because the algorithm can cope with locally delayed arterial contrast bolus arrival in diseased areas that are fed by collaterals[8,14]. Due to this, the extensive documentation on the methods used[8,9], and the consensus among CTP researchers[16], this study will focus on using this software. The algorithm's large computational load explains the fact that these are only recently introduced clinically. A second limitation is the sensitivity of the SVD method to noise in the source CT images. To reduce the noise, filtering is done by excluding the least significant high frequency components during de-convolution[9,11] which may compromise the accuracy of the perfusion parameters if used incorrectly.

Noise is generally also reduced before application of the CTP algorithm. In addition to the common spatial image filters, a number of advanced noise reduction methods have been introduced, including iterative reconstruction of the CT source images[17]. Recently there have been advanced filters introduced that exploit the specific dynamic

or 4D nature of the CTP data such as the HYPR[18-20] and TIPS filters[21,22]. Together with the acquisition parameters such as temporal resolution[23,24] and mAs or radiation dose[24,25], specific choices in algorithm and image processing settings can have profound impact on quantitative accuracy and dose efficiency.

It is difficult to find the optimal analysis method/settings with a specific protocol as this requires a ground truth with which to compare the calculated parameters. Earlier studies have shown how to evaluate CTP by comparison to Xenon CT[26] or PET[27], however such studies are impractical to carry out on a significant scale and comparison between modalities will always run the risk of inheriting a bias. Likewise, choosing the most optimal acquisition protocol is difficult for the same reasons, and would also require multiple CT scans to evaluate different protocols, which of course is not possible due to dose limitations. We propose to use a realistic digital phantom which has the advantage of being able to simulate multiple CTP protocols/scans on a single subject while also providing a ground truth with which to evaluate the performance of these protocols.

The objective of this study is to use the digital head phantom to improve accuracy of CBF measurements calculated using bSVD analysis, and evaluate various clinically viable acquisition protocols with a view to increasing dose efficiency. This will be achieved by optimization of the analysis software and application of TIPS advanced 4D filtering.

MATERIALS AND METHODS:

THE DIGITAL HEAD PHANTOM.

A previously published digital head phantom was used to simulate multiple CTP protocols. This phantom was validated by direct comparison to clinical CTP data[28].

While a detailed explanation of the construction can be found in the original publication, a brief description will be given here. CT acquisitions of a physical head phantom providing the skull and CT images characteristics such as noise and beam

hardening effects were combined with clinically acquired (non-dynamic) MRI data. The CT data was acquired at 80 kVp and various mAs/rot, from a Philips iCT 256 scanner with 13 slices, each 5mm thick. Noise masks were generated by subtracting noise-free average images. The MRI data provided the structure of soft tissue of the brain via volumetric tissue segmentation of different tissue types[29-32] and the vessels by applying a vesselness filter[33]. The tissue and vessel volumes were elastically registered[34] to fit inside the imaged skull of the physical CT phantom. Dynamic contrast bolus passage through vessels and tissue was simulated by using tracer-kinetic theory[35,36]. Contralateral flow, often observed in stroke patients, is simulated in the digital phantom by temporal offset of TAC's in specific regions. The simulation uses arterial contrast enhancement measurements from the ICA of clinical CTP data. These patients were injected with forty milliliters of nonionic contrast agent (Iopromide, Ultravist, 300 mg iodine/ml; Schering, Berlin, Germany) into the cubital vein (18-gauge needle) at a rate of 6 ml/s followed by a 40-mL saline flush at a rate of 6 ml/s by using a dual power injector (Stellant Dual CT injector; Medrad Europe, Beek, the Netherlands).

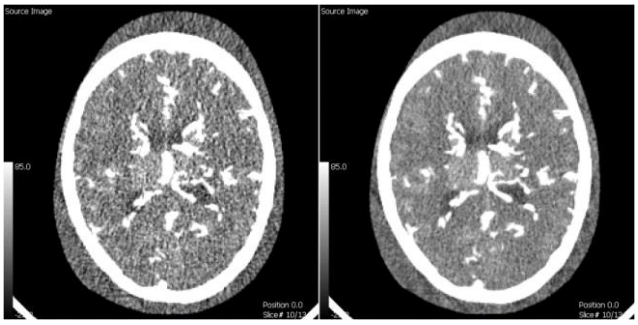

Figure 1: A slice of the digital head phantom with a CT dose of 50mAs/rot (left) and 150mAs/rot (right) before filtering and analysis showing contrast enhancement in the vessels and different levels of image noise. The scale on the left is HU value.

SIMULATION OF CTP PROTOCOLS.

The head phantom was used to simulate CTP source images using scan protocols with varying temporal resolution and CT dose. The same bolus shape and resultant time-attenuation curves (TAC) were used for all temporal resolutions. Temporal resolution was varied by sampling the time-attenuation curves produced by the perfusion model at different points on the time-axis. The temporal resolutions used were 1s, 2s, 3s and 4s. These temporal resolutions were typical of current CTP protocols[37]. The scan time for each protocol was 50 seconds which is sufficient to image wash in and egress of the contrast in the tissue and is considered clinically acceptable for a stroke patient. The resulting head phantoms, with 13 slices of 5mm slice thickness (total coverage of 65 mm as generated by Philips Brilliance iCT 256), had 50, 25, 17 and 13 frames per scan, respectively. Spatial resolution was simulated by 3D blurring of the image data before noise was added to the images as described in[28]. For all temporal resolutions, the CT doses used were varied between 50, 100, 150 and 250mAs/rot by adding the varying noise masks to the phantom data. The CT dose index volumes (CTDI-vol) for the entire CTP scans were estimated by comparing the mAs/rot and number of time frames the clinical CTP protocol used in our institute (150mAs/rot with 25 frames results in 150 CTDI-vol, Philips iCT 256), assuming CT dose varied linearly with mAs and number of frames. A set of head phantoms at each of the different temporal resolutions, but without any added noise, were also generated.

NOISE FILTERS.

The most commonly used image filters are so called spatially-invariant, such as a Gaussian filter which strength is set by its width and which can be considered as clinical standard. These filters smooth the frames spatially (2D or 3D) but can also include the temporal dimension. The 4D nature of CTP data is exploited to filter noise in specialized processing algorithms such as clustering[38], HYPR[18-20] and the Time–Intensity Profile Similarity (TIPS) bilateral filter[21] that all make use of the temporal information to average specific TACs. To illustrate the impact of these advanced filters, in addition to processing the digital head phantom using Gaussian filtering, the

phantoms were also processed after application of TIPS. This filter was previously developed by Mendrik et. al. and averages TACs based on both their proximity and similarity in shape. The filter was utilized as follows: Firstly a 4 second temporal Gaussian filtering (SD) was applied to the TAC's, followed by the application of TIPS with 3x3x3 mm spatial kernel size (SD) and 50 HU^2 profile similarity kernel size (SD).

THE CTP SOFTWARE.

The bSVD de-convolution algorithm implemented in Perfusion mismatch analyzer[39] was used to generate parameter maps from the head phantom CTP data. The bSVD method determines a so-called tissue residue function for each tissue pixel in the CTP data by de-convolving the TAC with the arterial input function. From these functions it is possible to imply the CBF, CBV and MTT of the local tissue[8,27]. This software and method has been extensively documented and forms the basis for many other commercial software packages used in CTP and MRI perfusion analysis[14]. Software using bSVD is also delay-insensitive, meaning it will not be affected by the arrival time of the bolus in the tissue or artery, a situation this is particularly of importance in diseased regions fed by collaterals The deconvolution of the tissue residue function is sensitive to noise and discrete sampling frequency of the tissue time-attenuation curve and the arterial input function (AIF). The resulting higher frequency oscillations can be filtered to leave only the physiologically realistic low frequency signal. This is typically done by applying an automated, adaptive, filtering process such as described by Gobbel and Fike[11] which effectively removes higher frequency components in the solution of the tissue residue function until the solution has an "oscillation index" below a predefined threshold. In clinical software this OI is commonly set to predefined default value and not adjusted for different scan protocols.

The head phantoms used in this experiment have varying temporal resolutions and image noise, data of differing temporal resolutions can only be expected to contain frequencies allowed by the sampling rate. This means that to effectively filter the noise, different values for the OI must be set for each of the temporal resolutions. The head phantoms, both the Gaussian and TIPS filtered, were processed with a range of OI, 0.005 to 0.17 in steps of 0.015.

ANALYSIS OF THE CBF MAPS.

The resulting CBF maps were compared on a pixel by pixel basis to the “ground truth” CBF maps used to generate the phantoms. A Pearson correlation co-efficient and a linear regression of the all the pixel values was calculated to assess correlation, of the CBF estimates to the true values, a similar analysis method was previously used by Kudo et al[40]. A higher Pearson correlation indicates that a given combination of protocol/filter returns CBF estimates that have a higher correlation with the ground true CBF, while the slope and intercept of the linear regression indicate scaling and offset errors with the ideal values for each being one and zero respectively. Both the Pearson correlation and the linear regression must be considered together as the Pearson correlation is also an indicator of the image noise; it is possible for a very noisy poor quality CBF map to have an ideal slope and intercept, yet still be too noisy to be clinically useful. For this reason we considered the OI that returned the best Pearson correlation to be the optimal OI for a given protocol.

RESULTS.

The relationship between Pearson correlation score and Oscillation index on TIPS filtered data a 150mAs for is demonstrated in figure 1. The optimal OI was found to be dependent on the temporal resolution (0.02, 0.05, 0.065 and 0.11 for 1, 2, 3 and 4 second temporal resolution respectively).

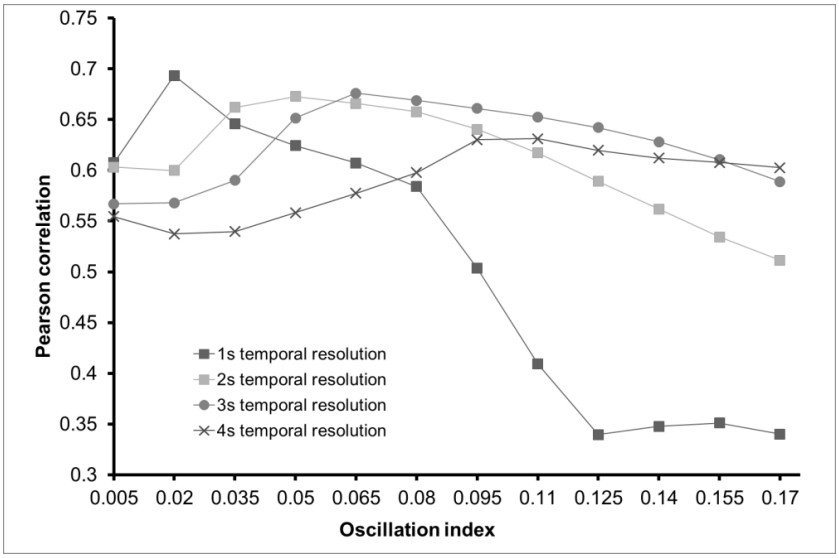

Figure 2. Demonstration of how Pearson correlation score is affected by Oscillation Index. Protocols shown are TIPS filtered with 150 mAs/rot at 1,2,3 and 4s temporal resolution. Similar behaviour is observed for other protocols with and without the TIPS filter. The default, clinically used value for OI is 0.095.

				Pearson correlation scores				Linear regression (With optimised OI)			
				Gaussian filtering		TIPS filtering		Gaussian filtering		TIPS filtering	
#	mAs/rot	Temporal resolution (s)	Est. CTDI-vol (mGy)	Optimized OI	ρ (Default OI)	ρ (Optimised OI)	ρ (Default OI)	ρ (Optimised OI)	Slope	Intercept	Slope	Intercept
1	50	1	100	0.020	0.32	0.49	0.47	0.67	0.64	24.81	1.59	6.31
2	50	2	50	0.050	0.46	0.53	0.56	0.58	0.70	21.80	1.11	16.17
3	50	3	33	0.080	0.46	0.46	0.48	0.48	0.54	26.29	0.33	24.54
4	50	4	25	0.110	0.44	0.44	0.45	0.45	0.56	28.52	0.55	29.95
5	100	1	200	0.020	0.38	0.58	0.52	0.69	1.03	19.33	1.64	4.53
6	100	2	100	0.050	0.53	0.58	0.63	0.66	0.84	17.29	1.31	7.23
7	100	3	67	0.080	0.54	0.54	0.63	0.64	0.76	20.76	0.91	10.54
8	100	4	50	0.110	0.49	0.50	0.58	0.58	0.52	24.25	0.28	16.32
9	150	1	300	0.020	0.39	0.61	0.50	0.69	1.09	16.66	1.59	3.66
10	150	2	150	0.050	0.55	0.59	0.64	0.67	0.78	16.54	1.40	6.32
11	150	3	100	0.080	0.56	0.56	0.66	0.67	0.70	18.88	0.48	7.21
12	150	4	75	0.110	0.53	0.54	0.63	0.63	0.68	21.58	0.29	12.05
13	250	1	500	0.020	0.41	0.65	0.53	0.69	1.21	14.35	1.59	3.74
14	250	2	250	0.050	0.58	0.62	0.66	0.68	0.94	13.49	1.42	5.40
15	250	3	167	0.080	0.58	0.60	0.67	0.68	0.75	15.19	1.52	5.41
16	250	4	125	0.110	0.54	0.55	0.66	0.66	0.78	19.69	0.72	8.36

Table 1: Pearson correlation and linear regression (slope and axis intercept) of CBF results from selected head phantoms with the true CBF values. Optimized OI are those found to produce the best Pearson correlation for individual protocols. Linear regression results are shown for the optimal OI only.

Table 1 shows the Pearson correlation scores from the CBF parameter maps obtained by processing the CTP head phantoms using the default and optimized oscillation index (defined as the OI with the best Pearson correlation for a given protocol). With the default OI a higher CT-dose does not always imply a higher correlation with the ground truth. For example; the protocol with 150 mAs / 2 s. (#10) has a slightly lower correlation than the protocol with 150 mAs / 3s (#11), despite the latter utilizing less frames at the same CT dose corresponding to 33% less CT dose. This is addressed by optimizing the OI. Table 1 also shows the Pearson correlations obtained with the optimal OI, i.e. the OI that returned the best Pearson score, compared to the clinical OI used by bSVD (0.095). Linear regression is only shown where the OI is at its optimal. Without optimization the linear regression for some of the head phantoms (particularly those with high temporal resolution and low CT dose) was higher than many of the other protocols simply because they were extremely noise images (with poor Pearson correlation). This further illustrates why the Pearson correlation and linear regression should be taken as complimentary with the Pearson correlation being the primary metric of quality.

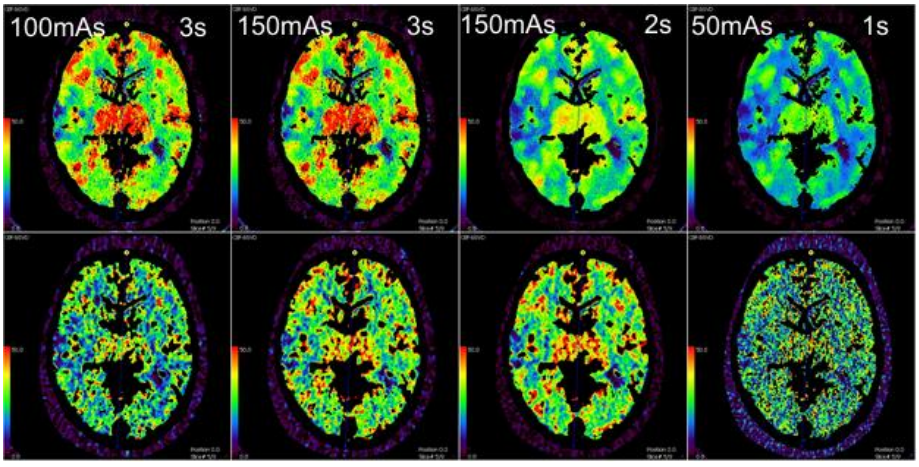

Figure 2: Demonstration of the effect of the TIPS filter on CTP data, the top row shows CBF maps calculated from TIPS filtered data while the bottom shows the same phantoms analysed using standard Gaussian filters. Left to right the protocols are: 100mAs/rot, 3s temporal resolution.150mAs/rot, 3s temporal resolution, 150mAs, 2s

temporal resolution and 50mAs/rot, 1s temporal resolution All colour maps are between 0 (Dark purple) and 50 ml/100ml/min (Red), the optimal OI was used in all cases.

It is clear from table 1 that the TIPS filtered data gives significantly better correlation than data where noise reduction is done by simple spatial and temporal smoothing. This is also clear in the image quality, figure 2 shows a sample comparison of both cases. The combination of the TIPS filter and optimized OI significantly improves the Pearson correlation score of all the protocols (average 35% higher), especially the protocols using higher temporal resolution of 1 frame per second, for example protocol number 1, 50mAs/rot with a frame every second, improves by a factor of two, again this improvement is reflected in the image quality (Figure 2.). In nearly all cases the standard filter gives more desirable slope and intercept, this will be discussed in the discussion section.

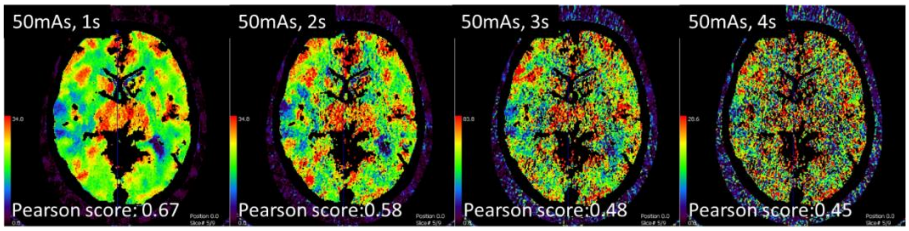

Figure 3: Lower Pearson correlation scores corresponds with poorer image quality.

Figure 3 demonstrates the relationship between Pearson correlation score and diagnostic image quality. The images shown are the CBF maps calculated from data with a CT dose of 50mAs at all four temporal resolutions. For these images the PMA program automatically set the colour scale to suit the range of CBF values and the optimal OI is used. It is clear that as the Pearson correlation decreases, so does the image quality. Similar results are found with the other protocols.

Temporal Resolution (s)	OI (Optimal)	Pearson Correlation	Slope	Intercept
1	0.020	0.7639	1.34	2.71
2	0.065	0.7613	1.14	5.13
3	0.080	0.7608	1.40	5.41
4	0.110	0.7241	1.34	6.77

Table 2 Pearson correlation, slope and intercept measured with head phantoms at the 4 different temporal resolutions without added noise.

Table 2 shows the result obtained from the noise-free head phantoms, showing that even without noise there is a fundamental limitation to the accuracy of the bSVD method. Again the OI was optimized to maximize the Pearson correlation score and there is little difference between the temporal resolutions.

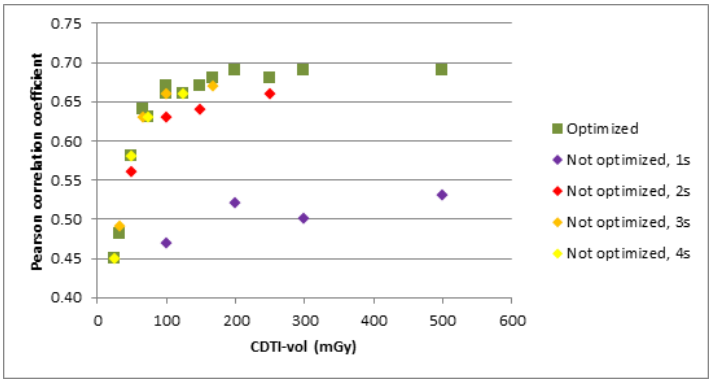

Figure 4. The relationship between the estimated CT dose and Pearson correlation for all of the protocols. These results are with optimized OI and TIPS filtering.

Figure 4 demonstrates that above 100mGy there is little difference between protocols (<5% difference), while below 100mGy the score is strongly correlated with the CT dose.

DISCUSSION

In this study we demonstrated how CTP acquisition and processing protocol can be optimized by using a digital phantom with the goal of improving the accuracy and dose efficiency of bSVD based CTP analysis.

All of the head phantoms originate from the same ground truth, a clinical analogy would be if the same patient was scanned repeatedly with the different CTP protocols and the results of the perfusion measurements compared. The demonstrated [28] realism of the head phantom, with anatomical accuracy, real CT noise, and realistic perfusion model make it suitable for this task. The head phantom allows us to examine protocols that may be unethical to apply to clinical studies, such as unreasonably high or low CT dose, but which also give information on the limitations of the methods used. For example, the results of the “noise-free” phantoms shown in figure 3 are effectively simulating an extremely high CT dose, and show that there is a limitation to how high the Pearson correlation can be even in the absence of noise, this limitation is partially due to the realistic features of the head phantom such as partial volume effects, resolution limitations, but also due to mathematical limitations of the bSVD algorithm itself, a perfect de-convolution cannot be achieved with discrete sampling points.

The Pearson correlation and linear regression results must be taken as complimentary. A very noisy CBF parameter map, although clinically usable may potentially still return ideal slope and intercept from the linear regression. The Pearson correlation tests for linearity, which means that such noisy data could be disregarded due to its low score. A good linear regression combined with high correlation implies that the radiologist, or computer aided diagnosis software would better be able to

differentiate between different tissue states (such as infarct core, penumbra and healthy tissue) and tissue types.

The scores found in this work are lower than that those found in a study by Kudo et al[40]. The reasons for this may be twofold; firstly, Kudo calculates the correlation based on average values of uniform tissue ROIs with a size of 28x28 pixels which lowers in the impact of image noise, whereas this study examines the correlation on a pixel by pixel basis. Secondly, the digital head phantom includes partial volume effects on tissue and vessels, with realistic anatomical structures; this was not a factor in Kudo's study.

Each CTP data set was filtered using both a standard Gaussian filter and the TIPS filter. The results show that without optimization of the OI, certain CTP protocols underperformed, scoring lower than other protocols with lower dose. Optimizing the OI caused the protocols to correspond to the order expected based on the CT dose. The protocols perform much better after optimization (figure 4), particularly those with 1 second temporal resolution. The implication of this is that to maximize the performance of the software it must be adjusted for the temporal resolution of the protocol using a method such as the digital head phantom.

When the scoring of the protocols is examined after the OI has been optimized several interesting conclusions can be drawn. The TIPS filter is highly effective at improving Pearson correlation (table 1) and image quality (figure 2). The best performing protocols using the Gaussian filtering are outperformed by nearly all the protocols when the TIPS filter is used. If the two protocols with excessively low CT dose are excluded (50mAs/rot with frames every 3 or 4 seconds showed only marginal improvement) then every protocol sees at least a 16% improvement in performance, with an average of 38% improvement. One protocol in particular, 50mAs/rot with a frame every second, with a score of 0.32, was unusable clinically, but after application of the TIPS filter and optimized OI has a score of 0.67 and vastly improved image quality (Figure 2, column 4) making it one of the best performing protocols (figure 2). In table 1 we can see that the Gaussian filter performs better in terms of slope and

intercept in many cases, however since in every case the Pearson correlation is lower than with the TIPS filter this is not an indicator of better quantitative accuracy.

We also observe that after application of the TIPS filter that many protocols that have a large difference in total CT dose have little or no difference in Pearson correlation score. Most interestingly there is little difference (<5%) in performance between protocols above 100mGy even including protocols with excessively high CT dose up to 500mGy (Table 1). This is primarily due to the effectiveness of the TIPS filter in reducing noise and limitations of the bSVD method.

Combining the application of the TIPS filter and optimization of the bSVD algorithm gives a significant reduction in CT dose compared to most currently clinically used protocols[37] while significantly improving correlation and accuracy, at least 17% improvement (table 1), and image quality (figure 2).

There are several limitations to this study that must be considered. Although the theoretical model used to generate the TAC's in the head phantom returns curves that correspond very well to those seen in clinical data, the curves are generated using a matrix based de-convolution (although with extremely high (0.1s) temporal resolution). This may have unintended bias when then de-convolving the curves with the same matrix based methodology. As with any simulation, there may of course be sources of error in clinical data not included in the phantom, or visa-versa. The results here should be taken as a reliable indicator of what would be observed in clinical data and not as an absolute definition.

This work only evaluated the bSVD method and the optimization of the OI is specific to this method, although it is likely that other filters that reduce noise in the temporal dimension should be tuned in a similar manner. The optimization of the OI index, although very specific is also intended as a demonstration of the utility of the digital phantoms to maximize the accuracy of CTP algorithms. Furthermore, this study only evaluates the performance of the software in measuring the CBF parameter since this is the most difficult parameter to measure, however it is possible that these

optimizations have detrimental effects on the bSVD calculation of the CBV and MTT. There are however simpler and more reliable ways to measure these parameters[13].

The TIPS filter applied in this study was not optimized for specific temporal resolutions or CT dose. There are several parameters such as the temporal Gaussian filtering, spatial kernel size, profile similarity kernel size that would most likely give further improvements and these optimizations will constitute a future body of work.

Ideally the findings of this work would be independently confirmed by clinical application of the better performing protocols, application of the TIPS filter, and appropriate optimization of the perfusion software all in conjunction with validation by follow up scans that assess patient outcome. However this is another body of work. For now these findings can be taken as a reliable indicator of what would happen clinically.

This study demonstrates that temporal resolution, CT dose, algorithm settings/parameters, and filtering method have significant impact on accuracy of bSVD based CTP. Application of digital head phantoms facilitate optimization of the CTP software, and demonstrate effectiveness of advanced filtering such as TIPS. The results show that it is possible to significantly improve accuracy and image quality while simultaneously allowing for substantial reduction of CT dose relative to current clinical protocols by application of phantom.

References

1. Wintermark M. Brain perfusion-CT in acute stroke patients. *European radiology.* Nov 2005;15 Suppl 4:D28-31.

2. Konstas AA, Wintermark M, Lev MH. CT perfusion imaging in acute stroke. *Neuroimaging clinics of North America.* May 2011;21(2):215-238, ix.

3. Mayer TE, Hamann GF, Baranczyk J, et al. Dynamic CT perfusion imaging of acute stroke. *AJNR. American journal of neuroradiology.* Sep 2000;21(8):1441-1449.

4. Wintermark M, Bogousslavsky J. Imaging of acute ischemic brain injury: the return of computed tomography. *Current opinion in neurology.* Feb 2003;16(1):59-63.

5. Koenig M, Klotz E, Luka B, Venderink DJ, Spittler JF, Heuser L. Perfusion CT of the brain: diagnostic approach for early detection of ischemic stroke. *Radiology.* Oct 1998;209(1):85-93.

6. Klotz E, Konig M. Perfusion measurements of the brain: using dynamic CT for the quantitative assessment of cerebral ischemia in acute stroke. *European journal of radiology.* Jun 1999;30(3):170-184.

7. Michel P, Reichhart M, Wintermark M, Meuli R, Bogousslavsky J. Perfusion-CT guided acute stroke management. *Rinsho shinkeigaku = Clinical neurology.* Nov 2003;43(11):728-731.

8. Wu O, Ostergaard L, Weisskoff RM, Benner T, Rosen BR, Sorensen AG. Tracer arrival timing-insensitive technique for estimating flow in MR perfusion-weighted imaging using singular value decomposition with a block-circulant deconvolution matrix. *Magnetic resonance in medicine : official journal of the Society of Magnetic Resonance in Medicine / Society of Magnetic Resonance in Medicine.* Jul 2003;50(1):164-174.

9. Ostergaard L, Weisskoff RM, Chesler DA, Gyldensted C, Rosen BR. High resolution measurement of cerebral blood flow using intravascular tracer bolus passages. Part I: Mathematical approach and statistical analysis. *Magnetic resonance in medicine : official journal of the Society of Magnetic Resonance in Medicine / Society of Magnetic Resonance in Medicine.* Nov 1996;36(5):715-725.

10. Kudo K, Sasaki M, Ostergaard L, et al. Susceptibility of Tmax to tracer delay on perfusion analysis: quantitative evaluation of various deconvolution algorithms using digital phantoms. *Journal of cerebral blood flow and metabolism : official journal of the International Society of Cerebral Blood Flow and Metabolism.* Mar 2011;31(3):908-912.

11. Gobbel GT, Fike JR. A deconvolution method for evaluating indicator-dilution curves. *Physics in medicine and biology.* Nov 1994;39(11):1833-1854.

12. Nambu K, Takehara R, Terada T. A method of regional cerebral blood perfusion measurement using dynamic CT with an iodinated contrast medium. *Acta neurologica Scandinavica. Supplementum.* 1996;166:28-31.

13. Axel L. A method of calculating brain blood flow with a CT dynamic scanner. *Advances in neurology.* 1981;30:67-71.

14. Kudo K, Sasaki M, Ogasawara K, Terae S, Ehara S, Shirato H. Difference in tracer delay-induced effect among deconvolution algorithms in CT perfusion analysis: quantitative evaluation with digital phantoms. *Radiology.* Apr 2009;251(1):241-249.

15. Kudo K, Sasaki M, Yamada K, et al. Differences in CT perfusion maps generated by different commercial software: quantitative analysis by using identical source data of acute stroke patients. *Radiology.* Jan 2010;254(1):200-209.

16. Wintermark M, Albers GW, Broderick JP, et al. Acute Stroke Imaging Research Roadmap II. *Stroke; a journal of cerebral circulation.* Sep 2013;44(9):2628-2639.

17. Willemink MJ, de Jong PA, Leiner T, et al. Iterative reconstruction techniques for computed tomography Part 1: technical principles. *European radiology.* Jun 2013;23(6):1623-1631.

18. Speidel MA, Bateman CL, Tao Y, et al. Reduction of image noise in low tube current dynamic CT myocardial perfusion imaging using HYPR processing: a time-attenuation curve analysis. *Medical physics.* Jan 2013;40(1):011904.

19. Wu Y, Wieben O, Mistretta CA, Korosec FR. Evaluation of temporal and spatial characteristics of 2D HYPR processing using simulations. *Magnetic resonance in medicine : official journal of the Society of Magnetic Resonance in Medicine / Society of Magnetic Resonance in Medicine.* May 2008;59(5):1090-1098.

20. O'Halloran RL, Wen Z, Holmes JH, Fain SB. Iterative projection reconstruction of time-resolved images using highly-constrained back-projection (HYPR). *Magnetic resonance in medicine : official journal of the Society of Magnetic Resonance in Medicine / Society of Magnetic Resonance in Medicine.* Jan 2008;59(1):132-139.

21. Mendrik AM, Vonken EJ, van Ginneken B, et al. TIPS bilateral noise reduction in 4D CT perfusion scans produces high-quality cerebral blood flow maps. *Physics in medicine and biology.* Jul 7 2011;56(13):3857-3872.

22. Bennink E, Riordan AJ, Horsch AD, Dankbaar JW, Velthuis BK, de Jong HW. A fast nonlinear regression method for estimating permeability in CT perfusion imaging. *Journal of cerebral blood flow and metabolism : official journal of the International Society of Cerebral Blood Flow and Metabolism.* Nov 2013;33(11):1743-1751.

23. Wintermark M, Smith WS, Ko NU, Quist M, Schnyder P, Dillon WP. Dynamic perfusion CT: optimizing the temporal resolution and contrast

volume for calculation of perfusion CT parameters in stroke patients. *AJNR. American journal of neuroradiology.* May 2004;25(5):720-729.

24. Wiesmann M, Berg S, Bohner G, et al. Dose reduction in dynamic perfusion CT of the brain: effects of the scan frequency on measurements of cerebral blood flow, cerebral blood volume, and mean transit time. *European radiology.* Dec 2008;18(12):2967-2974.

25. Li ZL, Li H, Zhang K, et al. Improvement of image quality and radiation dose of CT perfusion of the brain by means of low-tube voltage (70 KV). *European radiology.* Jun 4 2014.

26. Wintermark M, Thiran JP, Maeder P, Schnyder P, Meuli R. Simultaneous measurement of regional cerebral blood flow by perfusion CT and stable xenon CT: a validation study. *AJNR. American journal of neuroradiology.* May 2001;22(5):905-914.

27. Sasaki M, Kudo K, Ogasawara K, Fujiwara S. Tracer delay-insensitive algorithm can improve reliability of CT perfusion imaging for cerebrovascular steno-occlusive disease: comparison with quantitative single-photon emission CT. *AJNR. American journal of neuroradiology.* Jan 2009;30(1):188-193.

28. Riordan AJ, Prokop M, Viergever MA, Dankbaar JW, Smit EJ, de Jong HW. Validation of CT brain perfusion methods using a realistic dynamic head phantom. *Medical physics.* Jun 2011;38(6):3212-3221.

29. Fischl B, Liu A, Dale AM. Automated manifold surgery: constructing geometrically accurate and topologically correct models of the human cerebral cortex. *IEEE transactions on medical imaging.* Jan 2001;20(1):70-80.

30. Dale AM, Fischl B, Sereno MI. Cortical surface-based analysis. I. Segmentation and surface reconstruction. *NeuroImage.* Feb 1999;9(2):179-194.

31. *Freesurfer analysis suite* [computer program]. Boston, USA.

32. Fischl B, Dale AM. Measuring the thickness of the human cerebral cortex from magnetic resonance images. *Proceedings of the National Academy of Sciences of the United States of America.* Sep 26 2000;97(20):11050-11055.

33. Koopmans PJ, Manniesing R, Niessen WJ, Viergever MA, Barth M. MR venography of the human brain using susceptibility weighted imaging at very high field strength. *Magma.* Mar 2008;21(1-2):149-158.

34. Klein S, Staring M, Murphy K, Viergever MA, Pluim JP. elastix: a toolbox for intensity-based medical image registration. *IEEE transactions on medical imaging.* Jan 2009;29(1):196-205.

35. Bredno J, Olszewski ME, Wintermark M. Simulation model for contrast agent dynamics in brain perfusion scans. *Magnetic resonance in medicine : official journal of the Society of Magnetic Resonance in Medicine / Society of Magnetic Resonance in Medicine.* Jul 2010;64(1):280-290.

36. Ostergaard L, Chesler DA, Weisskoff RM, Sorensen AG, Rosen BR. Modeling cerebral blood flow and flow heterogeneity from magnetic resonance residue data. *Journal of cerebral blood flow and metabolism : official journal of the International Society of Cerebral Blood Flow and Metabolism.* Jun 1999;19(6):690-699.

37. Medicine AAoPi. *Adult Brain Perfusion CT Protoc.* 2012.

38. Baumgartner C, Gautsch K, Bohm C, Felber S. Functional cluster analysis of CT perfusion maps: a new tool for diagnosis of acute stroke? *Journal of digital imaging.* Sep 2005;18(3):219-226.

39. *Perfusion mismatch analyser* [computer program]. Version 3.0.0.02006.

40. Kudo K, Christensen S, Sasaki M, et al. Accuracy and reliability assessment of CT and MR perfusion analysis software using a digital phantom. *Radiology.* Apr 2013;267(1):201-211.

CHAPTER 4: THE EFFECT OF HEAD MOVEMENT ON CT PERFUSION SUMMARY MAPS: SIMULATIONS WITH CT HYBRID PHANTOM DATA

F. Fahmi, A. Riordan, L.F.M. Beenen, G. J. Streekstra, N.Y. Janssen, H. de Jong, C.B.L. Majoie, E. van Bavel, H.A. Marquering

Published in Medcial and biological engineering and computing, Feburary 2014

ABSTRACT

Head movement is common during CT Brain Perfusion (CTP) acquisition of patients with acute ischemic stroke. The effects of this movement on the accuracy of CTP analysis has not been studied previously. The purpose of this study was to quantify the effects of head movement on CTP analysis summary maps using simulated phantom data. A dynamic digital CTP phantom dataset of 25 time-frames with a simulated infarct volume was generated. Head movement was simulated by specific translations and rotations of the phantom data. Summary maps from this transformed phantom data were compared to the original data using the volumetric Dice Similarity Coefficient (DSC). DSC for both penumbra and core strongly decreased for rotation angles larger than approximately 1^0, 2^0, and 7^0 for respectively pitch, roll and yaw. The accuracy is also sensitive for small translations in the z-direction only. Sudden movements introduced larger errors than gradual movement. These results indicate that CTP summary maps are sensitive to head movement, even for small rotations and translations. CTP scans with head movement larger than the presented values should be interpreted with extra care.

INTRODUCTION

CT Brain Perfusion imaging (CTP) is emerging as a promising diagnostic tool for initial evaluation of acute ischemic stroke patients [1-3]. In CTP images, areas of the brain with perfusion defects can be detected after the onset of clinical symptoms and it facilitates the distinction between the irreversibly damaged infarct core and the salvageable damaged infarct penumbra, which is important in choosing the most suitable therapy [3-5].

Perfusion images are obtained by monitoring the dynamic passage of an iodinated contrast agent bolus through the cerebral vasculature and tissue. The perfusion analysis is based on local time-attenuation curves during contrast in- and outflow. The analysis provides estimation for local perfusion parameters such as Cerebral Blood Volume (CBV), Cerebral Blood Flow (CBF), and Mean Transit Time (MTT). Using pre-

defined thresholds and contra-lateral comparison, these maps are combined in a summary map estimating the volume of infarct core and penumbra [6,7].

CTP analysis assumes that a specific location in the images is associated with a single anatomical position, ignoring the possibility of head movement. However, previous study revealed that 24% of acute ischemic stroke patients had considerable or severe head movement during CTP acquisition. As a result, almost 16% of CTP source data sets were judged unsuitable for accurate CTP analysis by experienced radiologists [8]. It is currently not clear to what extent the patients' head movement actually affects the CTP analysis. The aim of this study was to quantify the relationship between the extent of rotation and translation to alternations in CTP summary maps using a digital dynamic head phantom.

METHODS

DIGITAL PHANTOM DATA

All simulated CTP datasets were generated from a digital hybrid phantom, which was based on a combination of CT images of an anthropomorphic head phantom with clinically acquired MRI brain images to quantify the different tissues. These data were combined with processed high resolution 7T clinical MRI images to include healthy and diseased brain parenchyma, as well as the cerebral vascular system. Time attenuation curves emulating contrast bolus passage based on perfusion as observed in clinical studies were added. This resulted in a dynamic 3D, noise-free, non-contrast-enhanced CT volume of 104 thin slices (0.8mm), 25 time-frames with a 2 seconds interval [9]. Noise was not added to the images in order to study the effects of the movement solely.

Infarct and penumbra volume was designated according to clinical experiences. The infarct volume used in this study was positioned at the right part of the brain. The volume of infarct core and penumbra were created proportionally by applying mask to the digital hybrid phantom data. The imposed size and location of infarct volume will be used as ground truth for further analysis.

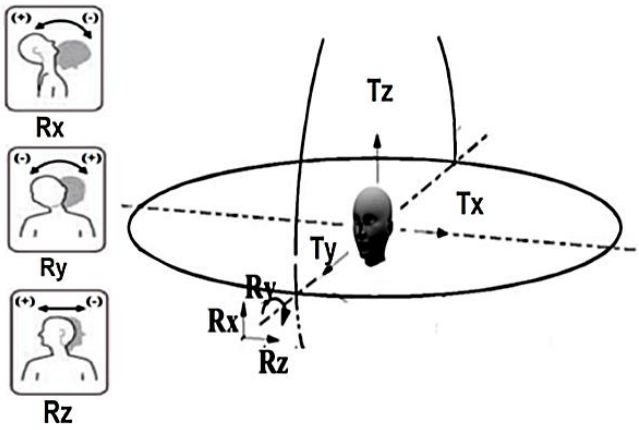

Fig. 1 Types of head rotation and translation.

To simulate head movement, the CTP phantom data were rotated and translated using Transformix an accompanying toolbox in Elastix[10]. Translations and rotations were performed along and around each coordinate axis (Fig. 1). The ranges of the motion parameters applied in the simulations were based on a previous study that quantified the patients' head movement during clinical CTP acquisition [8]. Based on these observations, the simulated rotation angles were set from -10 to +10 degrees around the z-axis (yaw), and -5 to +5 degree for the x-axis (pitch) and y- axis (roll), with steps of one degree. The translations were set from -10 to +10 mm for all three axes. The head movement was simulated in the time frames 8 to 20.

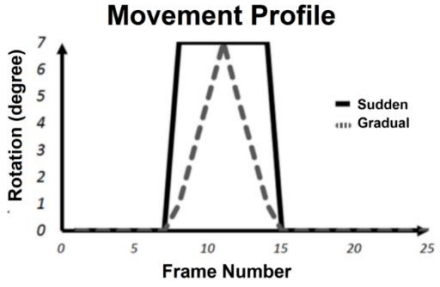

Fig. 2 Sudden vs Gradual Movement, for 7 degree yaw rotation.

We simulated both sudden and gradual movement by applying different speeds of movement: gradual movements with rotation angle of 0.5^0/s (pitch and roll) and 1^0/s (yaw) and sudden movement with rotation angle up to 2^0/s (pitch and roll) and 3.5^0/s (yaw). These movement profiles are illustrated in Fig. 2.

CTP PERFUSION ANALYSIS

The thin slice CTP phantom data volume was averaged along the z-direction to generate 6 slices of 4.8 mm thickness, representing the slice thickness that is used in most clinical practices. The original and transformed CTP datasets were processed by a trained operator using Philips Extended Brilliance Workspace version 3.5 Brain CT Perfusion Package (Philips Healthcare, Cleveland, OH).

The standard clinical procedure was used to produce the CTP summary maps. The arterial input function (AIF) and venous output function (VOF) regions were confirmed by an experienced radiologist. The classification of infarct core and penumbra was performed using default software settings: the infarct core was defined as pixels with a relative MTT > 1.5 and CBV<2.0 ml/100gr, and the area of penumbra defined based on a relative MTT > 1.5 and CBV>2.0 ml/100gr [11]. The image registration of the software package was applied if it produced a better match between successive frames, and skipped otherwise.

VOLUME SIMILARITY MEASUREMENT

The effects of head movement in CTP analysis was determined by comparing volumes of core, penumbra and total infarct presented in summary maps generated from both original and transformed CTP phantom data. We calculated the volume similarity and the spatial agreement using the Dice Similarity Coefficient (DSC). DSC is a measurement of spatial overlap of volumes, widely used for comparing segmentation results [12]. The DSC, ranging from 0 to 1, is defined as two times the volume of the intersection divided by the union of the two volumes.

The summary map of the original CTP phantom data is shown in Fig. 3. The regions of artificial infarct core (red) and penumbra (green) are shown in the left part of the image.

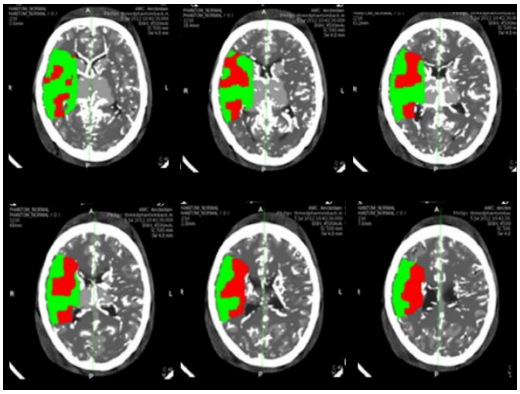

Fig. 3 Summary map of the original CTP hybrid phantom data. Perfusion abnormalities (infarct core–red and penumbra-green) can be seen in the right side of the brain.

The size of core, penumbra and total infarct, is plotted in Fig. 4. For pitch and roll rotations (Fig. 4 a-b), errors in volume estimations fluctuated strongly. For positive pitch rotations, an increase in infarct volume is accompanied with a decrease in penumbra. In roll rotation the size of penumbra decreased compared to the penumbra of data while the size of core increased.

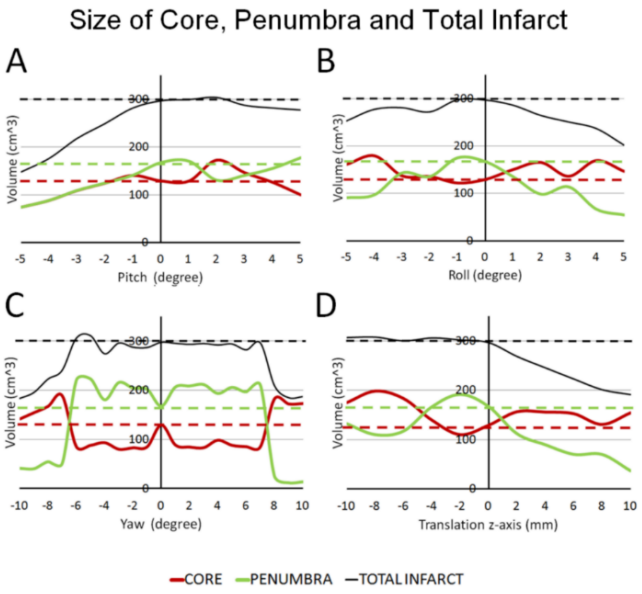

Fig. 4 Size of infarct core, penumbra, and total infarct volume; plotted for every simulated rotation angle (a-c), and translation in the z-direction (d). The dashed lines represent the value of original phantom.

For yaw rotation (Fig. 4 c), the estimated total infarct volume was nearly constant between +/- 7^0. In this range, the size of penumbra was overestimated by 20-25%, while the core volume was underestimated by 30-35%. For rotation angles beyond this range, the total infarct volume decreased rapidly.

Translation in the x- and y- direction for a range of 0 to 10 mm did not have a noticeable effect on the calculated volumes and are therefore not plotted in this figure. Positive translations in the z-direction had large effects on the infarct size estimates (Fig. 4 d).

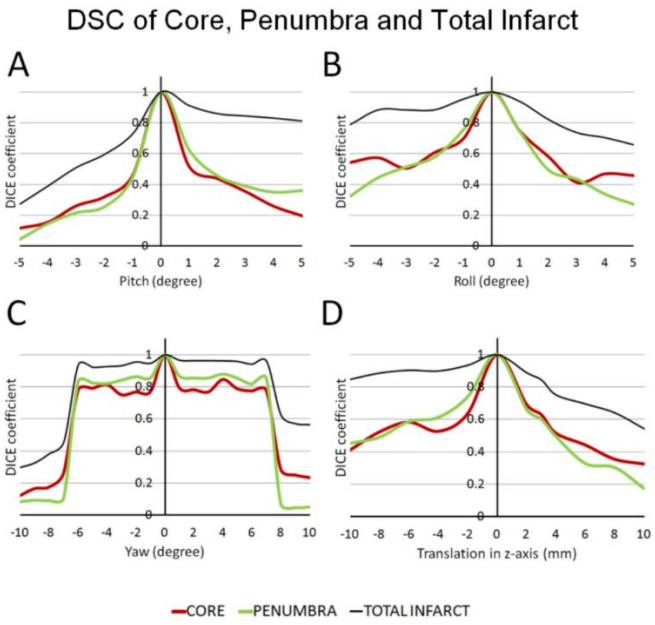

Fig. 5 DSC value of the infarct core, penumbra and total infarct volume; plotted for every simulated rotation angle (a-c), and translation in the z-direction (d).

The DSC values are shown in Fig. 5. This figure shows that the DSC were nearly constant within narrow ranges of rotation (-7^0 to 7^0 for yaw, -1^0 to 1^0 for pitch, and -2^0 to 2^0 for roll). The DSCs for positive translations in the x- and y-direction were all close to 1. For translation in z- direction, DSC values dropped even for small translations of 2 mm.

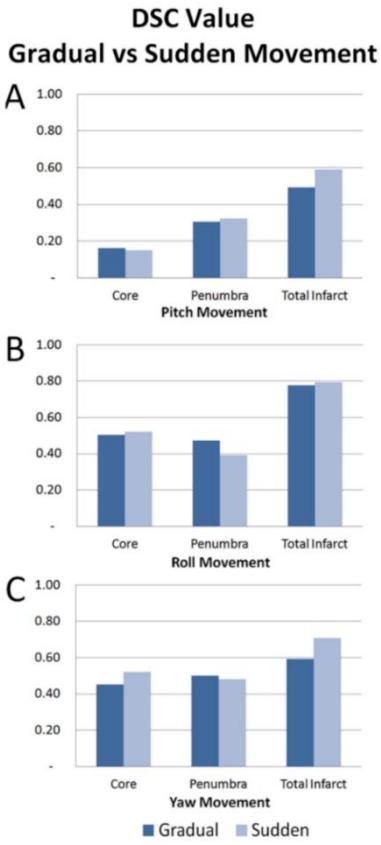

Fig. 6 Comparison of DSC for gradual and sudden head movement for + and - 4 degrees pitch (a), + and - 4 degrees roll (b), and + and – 7 degrees yaw (c).

The comparison of the DSC for gradual and sudden movements is shown in Fig. 6. This figure shows that there is no large difference between the DSC values for gradual and sudden movement.

DISCUSSION

This study showed that simulated head movement has strong effects on the summary map of brain perfusion CT with inaccurate classifications of size and location of core and penumbra, even for small rotation and or translation.

Restricting head movement during CTP acquisition would be part of the solution. Several methods to minimize head movement include foam headrest, molded plastic masks, tapes, orthopaedic collars-straps, and vacuum-lock bags [13,14]. However, restrictions that limit the rotation and translation are not trivial to implement and would have a risk of inducing further movement problems [15,16].

Our previous study revealed that head movement in patients with acute ischemic stroke is quite common (about a quarter of all clinical patients during CTP acquisitions), with a range of rotations between 2.0^0-3.5^0 for moderate and 5.6^0-14^0 for severe movement [8]. This study emphasizes the importance of the severe effects that this range of movement can have on CTP analysis.

Out of plane movement such as pitch, roll, and translation in z direction, deteriorated the summary maps more than in plane movement (yaw and translation in x and y direction). The image registration function available in the software package is only able to correct the in plane motion, but not the out of plane movement. As a result, the out of plane movement causes large error in estimating infarct volume and its spatial location.

Nevertheless, it is somewhat surprising that in plane movement also contributes to inaccuracies in infarct volume and location in CTP analysis. Our results suggest a limitation of the available registration of yaw rotation more than 7^0 for example. This finding suggests that even for in plane head movement, the CTP analysis should be carried out with care.

Previous studies on general axial CT scanning showed that the speed of movement instead of the range of the movement was also crucial [17]. The effects of rotation might also depend on the dynamics of such movement, sudden or immediate movements tend to cause larger mismatches on the summary map. In this study we showed that for the total infarct area there was a larger mismatch for sudden movement than for gradual movement, for all rotations. However, both the accuracy of the core and penumbra estimation was less sensitive to the speed of the movement.

Core and penumbra classification is performed using estimations of relative MTT, CBV, and CBF values in combination with estimations of the arterial input function and venous output function. Head movement was expected to alter AIF, VOF and local attenuation curves and therefore produced error in estimations of core and penumbra. Fig. 7 shows examples of how different movement patterns can alter the AIF and VOF

curves. However, it was beyond the scope of this study to evaluate the effects of different movement patterns on local attenuation curves.

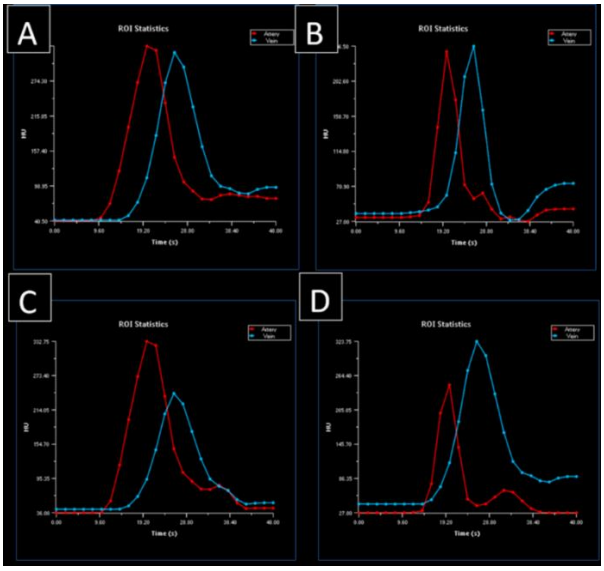

Fig. 7 AIF -VOF of original phantom data (a), and transformed phantom data: with 4 degrees pitch (b), 5 degrees roll (c), and 7 degrees yaw (d). AIF was selected at Anterior Communicating Artery (ACA) and VOF at Superior Sagital Sinus (SSS).

The current study has not addressed movement in a real patient population. However, the limits of movement were derived from a previous study in a population of 103 patients with ischemic stroke. The current study estimates the effects of movement on the summary maps and may be used in clinical practice to select image datasets that potentially deteriorate CTP analysis results. However, this would require a quantification of the movement, which is something that is not commonly available in clinical practice. Currently, the evaluation of suspicious movement is performed by visual inspection. This study shows the added value of a quantitative assessment of head movement to help radiologists identifying unsuitable CTP image data for the CTP analysis.

The effects of head motions are expected to be dependent on the scanner type, scanning protocol, and dedicated analysis software. To the best of our knowledge,

similar studies have not been performed for other settings. However, the extent and poor predictability of these artefacts suggest that also in many other cases, head movement severely affects proper estimation of core and penumbra size and location.

This study has some limitations. The simulation was done separately for individual rotations and translations. Moreover, motion was simulated as a single gradual or sudden event only, with return to baseline. Actual movement in stroke patients is far more complicated, with coupled rotation and translation in multiple directions at various times during the procedure [8]. Such complex movement could even result in less accurate infarct volume estimations. We chose to perform the analysis for various movement parameters separately to quantify the effect of each transform parameter. We generated 6 slices of 4.8 mm thickness for this study. The use of thinner slices could make the CTP analysis more robust against small head movement, but this issue was not addressed in this study. In the simulation, we only use one model of CTP phantom data with specified size and location of infarct. The DSC value of core and penumbra with smaller volume can be worse due to lack of overlap. This study utilized 2D registration function available in the software package that is only able to handle in plane movement. This way, we can never be really sure what precisely the effect of out of plane head movement to the summary map. However this was the best approach we can do, as in our knowledge 3D registration is not yet available for CTP application.

Based on the presented simulations, this study suggests that head movement can be dealt with for only a small range of movement. The head movement, even for small rotation angles and z-axis displacements, strongly alters size and position of infarct core and penumbra in the CTP analysis. The range of movement parameters for which an accurate CTP analysis result can be expected differ for the different parameters: (-1^0, 1^0) for pitch, (-2^0, 2^0) for roll and (-7^0, 7^0) for yaw and a translation in z-axis less than 2mm. This study suggests that CTP scans with a rotation angle larger than the limits should be interpreted with extra care.

References

1. Allmendinger AM, Tang ER, Lui YW, Spektor V. Imaging of stroke: Part 1, Perfusion CT--overview of imaging technique, interpretation pearls, and common pitfalls. *AJR Am J Roentgenol.* Jan 2012;198(1):52-62.

2. Konstas AA, Wintermark M, Lev MH. CT perfusion imaging in acute stroke. *Neuroimaging clinics of North America.* May 2011;21(2):215-238, ix.

3. Sandhu GS, Sunshine JL. Advanced neuroimaging to guide acute stroke therapy. *Curr Cardiol Rep.* Dec 2012;14(6):741-753.

4. Shang T, Yavagal DR. Application of acute stroke imaging: selecting patients for revascularization therapy. *Neurology.* Sep 25 2012;79(13 Suppl 1):S86-94.

5. Janjua N. Use of neuroimaging to guide the treatment of patients beyond the 8-hour time window. *Neurology.* Sep 25 2012;79(13 Suppl 1):S95-99.

6. Schaefer PW, Barak ER, Kamalian S, et al. Quantitative assessment of core/penumbra mismatch in acute stroke: CT and MR perfusion imaging are strongly correlated when sufficient brain volume is imaged. *Stroke; a journal of cerebral circulation.* Nov 2008;39(11):2986-2992.

7. Murphy BD, Fox AJ, Lee DH, et al. Identification of penumbra and infarct in acute ischemic stroke using computed tomography perfusion-derived blood flow and blood volume measurements. *Stroke; a journal of cerebral circulation.* Jul 2006;37(7):1771-1777.

8. Fahmi F, Beenen LF, Streekstra GJ, et al. Head Movement during CT Brain Perfusion Acquisition of Patients with Acute Ischemic Stroke. *Submitted For Publication.* 2012.

9. Riordan AJ, Prokop M, Viergever MA, Dankbaar JW, Smit EJ, de Jong HW. Validation of CT brain perfusion methods using a realistic dynamic head phantom. *Medical physics.* Jun 2011;38(6):3212-3221.

10. Klein S, Staring M, Murphy K, Viergever MA, Pluim JP. elastix: a toolbox for intensity-based medical image registration. *IEEE transactions on medical imaging.* Jan 2009;29(1):196-205.

11. Wintermark M, Flanders AE, Velthuis B, et al. Perfusion-CT assessment of infarct core and penumbra: receiver operating characteristic curve analysis in 130 patients suspected of acute hemispheric stroke. *Stroke; a journal of cerebral circulation.* Apr 2006;37(4):979-985.

12. Zou KH, Warfield SK, Bharatha A, et al. Statistical validation of image segmentation quality based on a spatial overlap index1: scientific reports. *Academic radiology.* 2004;11(2):178-189.

13. Beyer T, Tellmann L, Nickel I, Pietrzyk U. On the use of positioning aids to reduce misregistration in the head and neck in whole-body PET/CT studies. *J Nucl Med.* Apr 2005;46(4):596-602.

14. Green MV, Seidel J, Stein SD, et al. Head movement in normal subjects during simulated PET brain imaging with and without head restraint. *J Nucl Med.* Sep 1994;35(9):1538-1546.

15. Montgomery AJ, Thielemans K, Mehta MA, Turkheimer F, Mustafovic S, Grasby PM. Correction of head movement on PET studies: comparison of methods. *J Nucl Med.* Dec 2006;47(12):1936-1944.

16. Bloomfield PM, Spinks TJ, Reed J, et al. The design and implementation of a motion correction scheme for neurological PET. *Physics in medicine and biology.* Apr 21 2003;48(8):959-978.

17. Wagner A, Schicho K, Kainberger F, Birkfellner W, Grampp S, Ewers R. Quantification and clinical relevance of head motion during computed tomography. *Investigative radiology.* Nov 2003;38(11):733-741.

CHAPTER 5: A CT BRAIN PERFUSION PROTOCOL TO ELIMINATE THE NEED FOR SELECTING A VENOUS OUTPUT FUNCTION

Alan J. Riordan, Edwin Benink, Jan Willem Dankbaar, Max A. Viergever, Birgitta K Velthuis, Ewoud J Smit, Hugo W. A. M. de Jong

Published in American Journal of Neuro-Radiology, July 2013

ABSTRACT

Background and purpose: In CT perfusion (CTP) an arterial input function (AIF) is used for cerebral blood volume measurement. AIF's are often influenced by partial volume effects resulting in overestimated CBV. To correct for partial volume a venous output function (VOF) is manually selected. This can introduce variability. Our goal is to develop a CTP protocol that enables AIF selection unaffected by partial volume.

Methods: First, the effects of partial volume on artery sizes/types including MCA were estimated using a CTP phantom with 9 protocols (slice thickness 1, 1.8 and 5 mm and image resolution 0.5, 1 and 1.5 mm). Next, these protocols were applied to clinical CTP studies from 6 patients. The influence of the partial volume effect was measured by comparison of the time-attenuation curves from different artery locations to reference veins.

Results: AIFs from middle cerebral arteries (MCA) were unaffected by partial volume effects when using high image resolution (1mm) and medium slice thickness (1.8mm). For the clinical data a total of 104 arteries and 60 veins were selected. The data confirmed that high image resolution and thin slice thickness enables selection of MCA for AIFs free of partial volume influences. In addition, large veins were not insusceptible to partial volume effects relative to large arteries, questioning their use for partial volume correction.

Conclusions: A CTP protocol with 1.8mm slice thickness and 1mm image resolution allows AIF selection unaffected by partial volume effects in MCA arteries.

CTP is used in the diagnosis of acute ischemic stroke to non-invasively measure cerebral perfusion parameters[1-5]. Relative perfusion parameters can be obtained by normalization to the uninvolved hemisphere and are successfully applied in stroke imaging to differentiate penumbra from benign oligemia [6-8]. Accurate absolute CTP values would be desirable to improve the comparability of results. As an example, absolute CBV has been found to be an accurate method of delineating the infarct core[9] and this method is widely used in clinical practice, providing motivation to assess and improve the accuracy of CBV measurements.

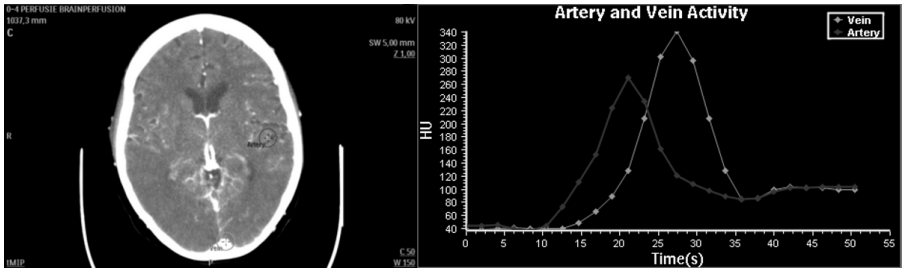

Figure 1. Semi-automatic blood vessel designation requires user definition of ROIs (circles) on the MCA and a large vein. The software then determines the voxel within the ROI representing the TAC with maximum AUC.

Calculation of CTP maps requires selection of an arterial input function (AIF) (figure 1). The AUC (the integral of contrast agent concentration over time) of the AIF is used to calculate the CBV. However, this AUC is commonly underestimated due to the partial volume effect, especially when smaller arteries like the ACA or MCA are selected. The PVE is a result of limited spatial resolution as defined by the in-plane axial image resolution and slice thickness[10-13] Since underestimation of the AUC of the AIF results in overestimation of the CBV, correction for PVE is necessary and typically performed using the VOF[14-20]. This correction assumes that without PVE, all AIFs and VOF should have equal AUCs, and that a VOF selected in a large vein like the superior sagittal sinus or the straight sinus is unaffected by PVE.

Correction of the PVE by using the VOF has limitations. It requires the user to select a second vessel besides the AIF, introducing additional user-variability. Also, the AUC of the VOF has been reported to depend on slice thickness[17] and cannot always be considered uninfluenced by PVE. Finally, although the assumption of equal AUC's in AIF and VOF is plausible, it has not been investigated so far.

The goal of this study is to develop a CTP-protocol that will enable PVE free AIF selection in the MCA by increasing image resolution and decreasing slice thickness, eliminating a step that every clinician must currently make in perfusion analysis.

MATERIALS AND METHODS

The required slice thickness and image resolution were established using phantom and patient studies.

ANTHROPOMORPHIC HEAD PHANTOM

A realistic anthropomorphic CTP head phantom, previously used to compare CTP software and protocols[21], was applied to gain insight in the PVE for a range of CTP reconstruction protocols. The phantom also allows measurement of PVE with knowledge of underlying truth. The CTP phantom is a combination of CT images (using Philips iCT 256 slice, protocol detailed in clinical data section) of a physical skull phantom together with MRI brain images. Spatially variant CT noise, effects of tube settings, and reconstruction parameters are included by scanning the skull phantom using the CTP protocol. Cerebral vessels and tissue, automatically segmented from the MRI data [22,23], were manually registered to fit inside CT-images of the skull phantom. Time-attenuation curves in the arteries and veins (AIF and VOF) were taken from clinical scans. Arterial and venous time-attenuation curves from clinical data were added and perfusion values observed in clinical studies were used to generate tissue time-attenuation curves. Pixel size and slice thickness can be set

by averaging the original image voxels, and resolution by changing the scale of a blurring kernel.

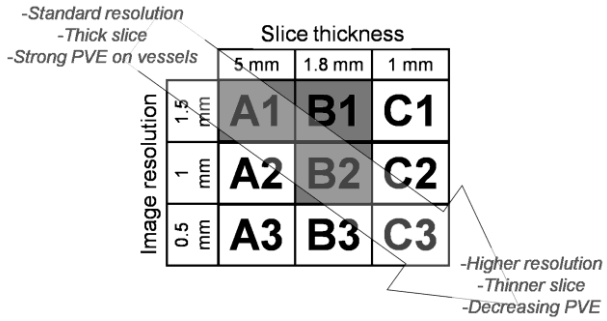

Figure 2. CTP protocols investigated using the head phantom. Protocols A1, B1, and B2 have also been used acquiring the clinical data.

Phantom data were constructed using 9 different protocols (figure 2) varying in slice thickness and in slice image resolution. These parameters mainly define the 3D spatial resolution of the CTP images and hence the strength of the PVE for a vessel[24]. The slice thicknesses used were: 1 mm; achievable with most modern scanners, 1.8mm, and 5 mm; often used in CTP protocols to reduce noise in the tissue time-attenuation curves.

The in-plane image resolution depends on several parameters including focal spot size, image reconstruction filter and pixel size, which can be set by the operator. The image resolution was expressed in the FWHM [mm] of the point spread function, and measured using an image quality phantom. For the head phantom, we choose image resolutions of 0.5 mm; a typical technical limit for most scanners, 1mm and 1.5 mm; typical of current CTP protocols. In all cases the pixel size was set to 0.2x0.2 mm. To ensure variance in the measured PVE could not be attributed to noise, the phantoms were constructed using unrealistically high mAs, approximately 100 times higher than used in a clinical setting.

CLINICAL DATA

An initial group of 30 patients was selected from participants in a national multicentre acute stroke trial, a prospective study on the prognostic value of CTP and CTA in patients with acute stroke symptoms. This study is approved by the institutional review committee and subjects gave informed consent. Inclusion criteria were as follows: (1) patients who displayed no hemorrhage or infarcted tissue on both admission and 3 day follow-up non-contrast CT, to ensure that all of the contrast agent entering via the arteries would exit via the vein and that all time-attenuation curves were fully sampled; (2) admission scan on a 256-slice scanner, to ensure a uniform quality of data; (3), CTP acquisition in thin slice mode to allow reconstruction of different slice thicknesses. Next the patients were visually assessed by an expert reader to ensure absence of any motion and that the ICA and MCA was present, resulting in 24 of these patients being discarded leaving 6 patients to be used in this study.

All data were acquired and constructed using the standard clinical protocol: 150 mAs/rot, 80 kVp, 512 x 512 matrix, 200 mm field of view, 0.39 mm^2 pixels, slice thickness/spacing of 1/0.8 mm and an acquisition series of 25 time-frames at 2 second intervals with a rotation time of 0.33 seconds. These data were subsequently reconstructed to a slice thickness of 5 mm (clinical standard) or 1.8 mm (thin slice) and an in-plane image resolution (point spread function) of 1.5 mm (clinical standard) or 1mm (high resolution) in the combinations given in figure 2.

IMAGE ANALYSIS

Both the phantom data and the clinical data were analysed in a similar fashion. Circular ROI's with a diameter 20mm to ensure complete encircling of the vessel cross section, were manually drawn over artery locations in the Maximum Intensity Projections (figure 1). These arteries were approximately perpendicular to the slice plane[17]. The contents of each ROI in the raw data were examined to determine the artery diameter and centre. The diameter and centre were estimated using a threshold technique[25], allowing grouping in artery types; ICA (diameter 4mm or higher), MCA (2-3mm) and smaller arteries (1-2mm), such as small MCA and ACA vessels. This technique proved

accurate as long as the vessel diameter was not smaller than the FWHM of the CT images[25]. Selection of the VOF was similar to the selection of the AIF, although now the ROIs were placed over large veins (sagittal sinus) that were approximately perpendicular to the imaging plane.

As the vessel centre can be considered as being least affected by partial volume, the AUC was estimated by fitting a Gaussian curve to the time-attenuation curve of the pixel determined to be at the centre. Only the centre pixel was measured to conform to methods used in clinical perfusion software and to ensure that PVE is not overestimated in smaller vessels by averaging with pixels nearer to the vessel wall. The Gaussian curve fit enabled us to distinguish the first pass bolus from the recirculation as is done in commercial software such as Philips Brain perfusion 4.0 (figure 3A). Prior to curve fitting, time-attenuation curves were corrected for background, defined as the local time-averaged HU value before bolus arrival.

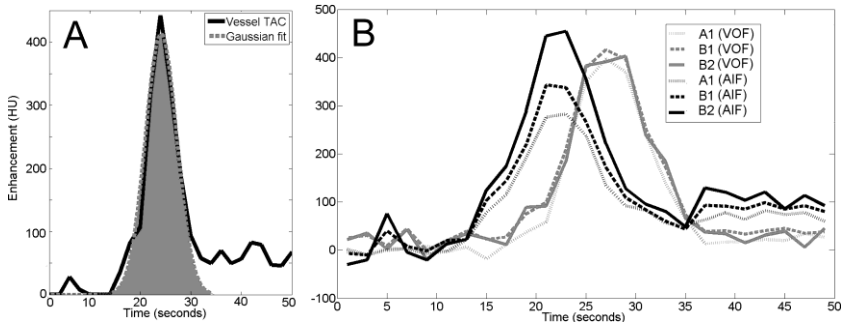

Figure 3. (A) Gaussian fit to the AUC (shaded area) of a vessel to estimate AUC of first pass of the bolus. (B) Time attenuation curves, background corrected, demonstrate the changes in enhancement for the different protocols A1, B1, B2. Black lines represent an MCA artery, and grey lines a vein from the same patient. The MCA has a higher AUC than the vein when using protocol B2.

A measure for the PVE in the vessels was calculated by dividing the AUC of the AIF by the AUC of a reference time-attenuation curve yielding a relative AUCrel. For the phantom data, the known input arterial time-attenuation curve prior to PVE influences

served as the reference time-attenuation curve. For the clinical data, the VOF measured with protocol B1 (figure 2) was used as the reference. AUC_{rel} values are expected to be equal to or smaller than 1, where 1 can be interpreted as being unaffected by PVE. Values lower than 1 can be considered as a PVE induced reduction of AUC. The relative value of 1 is a reference point so that patients with differing enhancement may be compared. Ideally we wish to find the vessel with the highest enhancement, and AUC_{rel} values greater than one are allowed for in the clinical data. The results from the clinical data were grouped according to vessel type (small arteries, MCA, ICA and large veins), and protocol used.

STATISTICAL ANALYSIS

Statistical analyses using SPSS software determined the significance and implication of the clinical measurements. Depending on the relative group size, relationship and the number of groups being compared, either a Mann-Whitney two-tailed, Friedman with post-hoc, or Wilcoxon signed-rank test was used to test the difference in PVE results between vessel groups and between CTP protocols. In all cases probability values are reported and a p-value of 0.05 was considered significant in all test types.

RESULTS

ANTHROPOMORPHIC HEAD PHANTOM

Figure 4 shows that the protocol with a slice thickness of 1.8 mm or less and an image resolution of at most 1 mm (protocol B2) shows the least PVE for the MCA vessel group. In the box plot, AUCrel values are compared between the 9 CTP protocols. The impact of PVE reduces with higher (improved) image resolution, and thinner slices (protocol B and C).

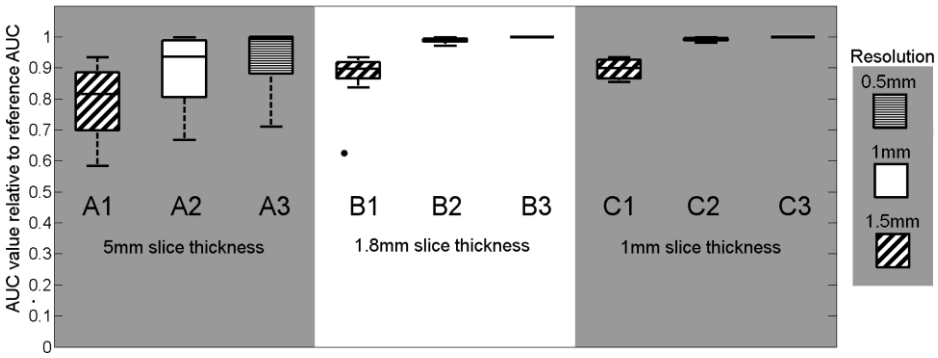

Figure 4: Results of PVE measurements applying nine different CTP protocols to the digital head phantom. The vertical axis gives a measure of the partial volume effect expressed as AUC_{rel}.

CLINICAL DATA

From the 6 patient studies a total of 104 AIF and 60 VOF locations were selected. At every AIF and VOF location the time-attenuation curve was measured using the three protocols A1, B1, B2. Examples of MCA and venous time-attenuation curves are shown in figure 3B. It can be seen that the time-attenuation curve of the AIF gets higher with smaller slice thickness and higher (improved) resolution. This effect is much less pronounced or even absent for the venous time-attenuation curves.

Figure 5, a boxplot, shows the median and range of AUC_{rel} for the three artery groups and the large veins. In all vessel groups, the protocols with smaller slice thickness and higher resolution, in the order of A1, B1 and B2, show decreasing PVE effects. This boxplot merely illustrates the distribution of the samples, table 1 contains statistical analysis which investigates the trends observable in this figure.

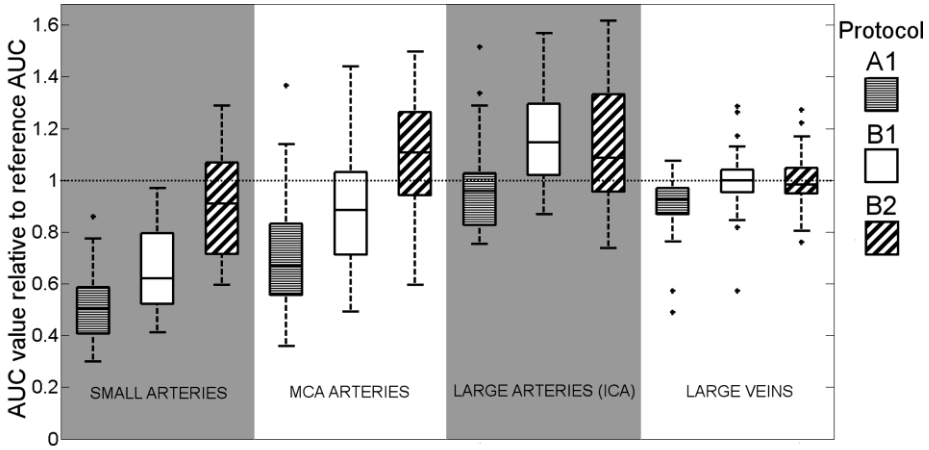

Figure 5: Box plot describing how PVE depends on CTP protocol. Vessel type/group is defined on the horizontal axis, AUC of the vessel TAC relative to AUC of the average VOF from protocol B1 (AUCrel) ,as a measure for partial volume effect is displayed on the vertical axis. Each of the groupings represent a range of vessel diameters, (Small arteries: <2mm, MCA: 2-3mm, Large (ICA): >4mm, Vein >5mm.

For the smaller arteries AUC_{rel} stays well below 1 for all evaluated protocols. For the veins the average AUC_{rel} is one, by definition, for protocol B1, and also approximately one if B2 is used. When applying protocol A1 (often used clinically) with 5 mm slice thickness the veins are still slightly affected by PVE. This is an important finding, given that in the clinical practice PVE correction is commonly based on the VOF.

For the larger arteries, the MCA group showed less PVE for protocol B2 over B1. For the ICA protocols B1 and B2 show similar results, which indicates that for large arteries protocol B1 suffices to allow AIF selection unaffected by PVE in the MCA. Interestingly, the larger arteries (MCA and ICA) groups show an AUC_{rel} larger than one. This is unexpected since current CTP methodology assumes the AUC of the arteries to be ideally equal to the veins.

Table 1 shows a summary of the statistical comparisons which confirm the significance of the results. Specific tests, Wilcoxon SRT, Friedman, and Mann-Whitney, were

carried out in consultation with a trained statistician taking into consideration the asymmetry of the distributions, number of samples per group, and number of groups being compared. The implications will be discussed further in the discussion.

Table 1: Summary of the statistical results, and implications, obtained by comparison of the vessel AUC measured in the clinical data. A p-value of 0.05 was considered significant for all tests.

Comparison	Test applied	P-value	Implication
Vein B1 - Vein B2	Wilcoxon SRT	.941	No difference in VOF's between protocols B1 and B2
Vein A1 - Vein B2	Wilcoxon SRT	<.001	VOF's significantly different (stronger PVE) with clinical standard protocol A1 as compared to protocol B2
ICA B1 – ICA B2	Wilcoxon SRT	.211	No significant difference in ICA AIF between protocols B1 and B2
ICA A1 - ICA B1	Wilcoxon SRT	<.001	ICA AIF's significantly different (stronger PVE) with clinical standard A1 as compared to protocol B1
MCA A1 - MCA B1,B2	Friedman	<.001	AIF's in MCA significantly different in all protocols
Small A1 – Small B1,B2	Friedman	<.001	AIF's in small vessels significantly different in all protocols
MCA B2 - ICA B2	Mann-Whitney	.519	No significant difference in MCA and ICA when protocol B2 is applied
ICA A1,A2,B2 - VOF A1,A2,B2	Mann-Whitney	<.001	VOF significantly lower than ICA for all protocols
Clinical results – Phantom results	Mann-Whitney	.49	PVE results from clinical data correlate with head phantom

Although previous studies [17,26] have investigated PVE under different CT protocol and conditions, there is no published data on what protocol would eliminate the need for correction of AIF measurements. Also there are no studies that have validated correction of PVE using the measurements of the VOF. The results of our phantom experiments indicated that an image resolution of 1 mm and a slice thickness of 1.8 mm enable AIF definition in MCA vessels unaffected by PVE. The application of this protocol to clinical data resulted in good agreement with the findings from the phantom study, and the area under the curve of the MCA was found to be larger or equal to the VOF.

The spread in the measured values from the protocols A1-A3 (figure 4) is mainly attributed to variance in the vessel orientation between approximately 0 and 30 degrees which has a substantial influence when using thick slices. While it is possible to reconstruct CTP volumes with a slice thickness limited only by the hardware (0.625 mm in the case of the scanner used here), the time taken to process over 100 slices for a 7-8 cm long CTP image volume can be prohibitive for a time-critical procedure where a quick diagnosis is crucial. Re-constructing to 1.8 mm thick slices is more practical (protocols B1-B3), and the phantom results indicate that thinner slices (protocol C1-C3) offer no additional benefit. For the smaller arteries AUC_{rel} stays well below 1 for all evaluated protocols, indicating that these vessels are not useable for AIF selection if PVE is to be prevented.

The measurements carried out on the clinical data (figure 5) have a noticeable variance. This can largely be attributed to uncertainty in vessel diameter measurements and vessel orientation. This is illustrated by the fact that the large veins, where vessel diameter and orientation is less of an issue, have the least variance.

The unexpected finding that for the high resolution protocols, the AUC of arteries was significantly larger than that of the veins (Table 1), is contrary to the common assumption that both AUCs are equal in the absence of PVE and hence can be used

for PVE correction. In this study every care was taken so that this difference could not be attributed to biases induced by curve fitting, background correction, delay of venous peak (the Gaussian fit is insensitive to delay), noise or other image related sources. This suggests that the PVE correction using the VOF will not be sufficient, but will still result in over-estimation of the CBV.

It has previously been observed that the hematocrit in arteries and veins can differ[27,28]. It is also well documented that the high osmolarity of CT contrast agents, which acutely increases the blood volume, causes red blood cell crenation[29]. It has been theorized that this could further change the hematocrit value in such a way that it is dependent on the size of the red blood cells and the pressure in the vessel, both of which differ between the arteries and veins[27]. This implies it might be incorrect to assume that the hematocrit factor is the same in the veins and arteries, and that the relative hematocrit is dynamic due to the changing concentration of contrast in the blood.

Several limitations to this study must be acknowledged. First, 6 patients is a small patient cohort, the inclusion criteria were stringent to minimize the influence of confounding factors. In this study we focused on the PVE, keeping all other aspects of CTP studies as constant as possible. The total number of included vessels enabled us to draw statistically significant conclusions. Second, when working with the suggested thin slice data CT noise may affect CTP map quality, since tissue time attenuation curves have lower contrast as vessel attenuation curves. To reduce noise in the tissue time-attenuation curves it may be necessary to average to thicker slices after acquisition of the AIF. An alternative method to prevent loss of valuable time may be to reconstruct a limited number of thin slices purely for the acquisition of the AIF, and to reconstruct the rest of the volume in thicker slices. In this study care was taken to minimize the effect of noise. The vessel center was chosen as the measurement location. One alternative was to measure the pixel with the maximum enhancement; however this measurement may have noise induced bias towards higher AUC values and influence the calculation of the PVE. In addition, the contrast enhancement in the vessels was high in comparison to the background noise in all protocols, allowing for constantly good fitting of the gaussian shape to the first pass of the bolus. Since the method used to measure the AUC in this work is very similar, if

not identical, to commercial CTP software the measurements will reflect any bias observed in clinical practice.

In conclusion, partial volume effects depend strongly on scan parameters and vessel diameter and can adversely affect CTP results. CTP data reconstructed with 1.8 mm slice thickness and an image resolution of 1 mm can eliminate PVE in MCA size arteries which are found in all CTP scans. This makes CTP scans less user-variant, since no VOF selection is required. Such a reconstruction protocol may increase accuracy of CTP maps and its subsequent diagnostic value.

References

1. Klotz E, Konig M. Perfusion measurements of the brain: using dynamic CT for the quantitative assessment of cerebral ischemia in acute stroke. *European journal of radiology.* Jun 1999;30(3):170-184.

2. Mayer TE, Hamann GF, Baranczyk J, et al. Dynamic CT perfusion imaging of acute stroke. *AJNR. American journal of neuroradiology.* Sep 2000;21(8):1441-1449.

3. Wintermark M, Smith WS, Ko NU, Quist M, Schnyder P, Dillon WP. Dynamic perfusion CT: optimizing the temporal resolution and contrast volume for calculation of perfusion CT parameters in stroke patients. *AJNR. American journal of neuroradiology.* May 2004;25(5):720-729.

4. Axel L. Cerebral blood flow determination by rapid-sequence computed tomography: theoretical analysis. *Radiology.* Dec 1980;137(3):679-686.

5. Axel L. A method of calculating brain blood flow with a CT dynamic scanner. *Advances in neurology.* 1981;30:67-71.

6. Lev MH, Segal AZ, Farkas J, et al. Utility of perfusion-weighted CT imaging in acute middle cerebral artery stroke treated with intra-arterial thrombolysis: prediction of final infarct volume and clinical outcome. *Stroke; a journal of cerebral circulation.* Sep 2001;32(9):2021-2028.

7. Schaefer PW, Barak ER, Kamalian S, et al. Quantitative assessment of core/penumbra mismatch in acute stroke: CT and MR perfusion imaging are strongly correlated when sufficient brain volume is imaged. *Stroke; a journal of cerebral circulation.* Nov 2008;39(11):2986-2992.

8. Kamalian S, Kamalian S, Konstas AA, et al. CT perfusion mean transit time maps optimally distinguish benign oligemia from true "at-risk" ischemic

penumbra, but thresholds vary by postprocessing technique. *AJNR. American journal of neuroradiology.* Mar 2012;33(3):545-549.

9. Wintermark M, Flanders AE, Velthuis B, et al. Perfusion-CT assessment of infarct core and penumbra: receiver operating characteristic curve analysis in 130 patients suspected of acute hemispheric stroke. *Stroke; a journal of cerebral circulation.* Apr 2006;37(4):979-985.

10. Kalender WA. *Computed Tomography. Fundamentals, System Technology, Image Quality, Applications.* New York: Wiley; 2000.

11. Barrett JF, Keat N. Artifacts in CT: recognition and avoidance. *Radiographics : a review publication of the Radiological Society of North America, Inc.* Nov-Dec 2004;24(6):1679-1691.

12. Prokop M. *Spiral and multislice computed tomography of the body.* New York: Thieme; 2003.

13. Cianfoni A, Colosimo C, Basile M, Wintermark M, Bonomo L. Brain perfusion CT: principles, technique and clinical applications. *La Radiologia medica.* Dec 2007;112(8):1225-1243.

14. Wintermark M, Reichhart M, Thiran JP, et al. Prognostic accuracy of cerebral blood flow measurement by perfusion computed tomography, at the time of emergency room admission, in acute stroke patients. *Annals of neurology.* Apr 2002;51(4):417-432.

15. Kudo K, Sasaki M, Ogasawara K, Terae S, Ehara S, Shirato H. Difference in tracer delay-induced effect among deconvolution algorithms in CT perfusion analysis: quantitative evaluation with digital phantoms. *Radiology.* Apr 2009;251(1):241-249.

16. Wintermark M, Albers GW, Broderick JP, et al. Acute Stroke Imaging Research Roadmap II. *Stroke; a journal of cerebral circulation.* Sep 2013;44(9):2628-2639.

17. van der Schaaf I, Vonken EJ, Waaijer A, Velthuis B, Quist M, van Osch T. Influence of partial volume on venous output and arterial input function. *AJNR. American journal of neuroradiology.* Jan 2006;27(1):46-50.

18. Miles K. *Multidetector Computed Tomography in Oncology CT Perfusion Imaging.* Informa; 2007.

19. Aviv RI, d'Esterre CD, Murphy BD, et al. Hemorrhagic transformation of ischemic stroke: prediction with CT perfusion. *Radiology.* Mar 2009;250(3):867-877.

20. Konstas AA, Goldmakher GV, Lee TY, Lev MH. Theoretic basis and technical implementations of CT perfusion in acute ischemic stroke, part 2: technical implementations. *AJNR. American journal of neuroradiology.* May 2009;30(5):885-892.

21. Riordan AJ, Prokop M, Viergever MA, Dankbaar JW, Smit EJ, de Jong HW. Validation of CT brain perfusion methods using a realistic dynamic head phantom. *Medical physics.* Jun 2011;38(6):3212-3221.

22. Dale AM, Fischl B, Sereno MI. Cortical surface-based analysis. I. Segmentation and surface reconstruction. *NeuroImage.* Feb 1999;9(2):179-194.

23. Koopmans PJ, Manniesing R, Niessen WJ, Viergever MA, Barth M. MR venography of the human brain using susceptibility weighted imaging at very high field strength. *Magma.* Mar 2008;21(1-2):149-158.

24. Bushberg JT. *The essential physics of medical imaging.* 3rd ed. Philadelphia: Wolters Kluwer Health/Lippincott Williams & Wilkins; 2012.

25. Hoffmann KR, Nazareth DP, Miskolczi L, et al. Vessel size measurements in angiograms: a comparison of techniques. *Medical physics.* Jul 2002;29(7):1622-1633.

26. Tang C, Blatter DD, Parker DL. Accuracy of phase-contrast flow measurements in the presence of partial-volume effects. *Journal of magnetic resonance imaging : JMRI.* Mar-Apr 1993;3(2):377-385.

27. Lapin GD, Allen CV, Groothuis DR. Noninvasive measurement of arterial blood plasma concentration of iodinated contrast agents from CT scans of human brain. *Journal of computer assisted tomography.* May-Jun 1994;18(3):363-369.

28. McHedlishvili G, Varazashvili M, Kumsishvili T, Lobjanidze I. Regional hematocrit changes related to blood flow conditions in the arterial bed. *Clinical hemorheology and microcirculation.* 2003;29(2):71-79.

29. Aspelin P. Effect of ionic and non-ionic contrast media on whole blood viscosity, plasma viscosity and hematocrit in vitro. *Acta radiologica: diagnosis.* 1978;19(6):977-989.

CHAPTER 6: COMPARISON OF PARTIAL VOLUME EFFECTS IN ARTERIAL AND VENOUS CONTRAST CURVES IN CT BRAIN PERFUSION IMAGING

Alan J. Riordan, Edwin Benink, Jan Willem Dankbaar, Max A. Viergever, Birgitta K Velthuis, Ewoud J Smit, Hugo W. A. M. de Jong

Published in PloS one, May 2014

ABSTRACT

Purpose: In brain CT perfusion (CTP), the arterial contrast bolus is scaled to have the same area under the curve (AUC) as the venous outflow to correct for partial volume effects (PVE). This scaling is based on the assumption that large veins are unaffected by PVE. Measurement of the internal carotid artery (ICA), usually unaffected by PVE due to its large diameter, may avoid the need for partial volume correction. The aims of this work are to examine i) the assumptions behind PVE correction and ii) the potential of selecting the ICA obviating correction for PVE.

Methods: The AUC of the ICA and sagittal sinus were measured in CTP datasets from 52 patients. The AUCs were determined by i) using commercial CTP software based on a Gaussian curve-fitting to the time attenuation curve, and ii) by simple integration of the time attenuation curve over a time interval. In addition, frames acquired up to 3 minutes after first bolus passage were used to examine the ratio of arterial and venous enhancement. The impact of selecting the ICA without PVE correction was illustrated by reporting cerebral blood volume (CBV) measurements.

Results: In 49 of 52 patients, the AUC of the ICA was significantly larger than that of the sagittal sinus ($p=0.017$). Measured after the first pass bolus, contrast enhancement remained 50% higher in the ICA just after the first pass bolus, and 30% higher 3 minutes later. CBV measurements were significantly lowered when the ICA was used without PVE correction.

Conclusions: Contradicting the assumptions underlying PVE correction, contrast in the ICA was significantly higher than in the sagittal sinus, even 3 minutes after the first pass of the contrast bolus. PVE correction might lead to overestimation of CBV if the CBV is calculated using the AUC of the time attenuation curves.

CT perfusion (CTP) is used in the diagnosis of acute ischemic stroke to non-invasively measure tissue perfusion parameters[1-5]. Although relative perfusion parameters such as relative cerebral blood volume (rCBV), obtained by normalization to the contra-lateral hemisphere, are successfully applied in stroke imaging[6-8], the absolute CBV is a more accurate measure for delineating the infarct core[9]. Accurate absolute perfusion values would also be desirable to improve the comparability between different CTP modalities and allow for better comparison within large patient groups or databases. The latter allows for establishment of accurate correlations between CTP parameter values and clinical prognostic information.

Calculation of CTP maps requires selection of an arterial input function (AIF) which is typically measured in the middle cerebral artery (MCA) or anterior cerebral artery (ACA). While several methods exist to calculate CBV, including the impulse residue function approach [10], the determination of CBV by comparing the area under the curve (AUC) of the tissue time–attenuation curves to the AUC of a reference curve is the most widely used method and the focus of this study. The AUC of the first pass bolus of the AIF is used to calculate the CBV by taking the ratio of the tissue and AIF AUC's (Eq 1.) after correction for difference in hematocrit[11].

$$CBV = AUC_{\text{tissue curve}} / AUC_{\text{reference curve}}. \quad \text{(Eq 1)}$$

Hence, the AIF should ideally be taken as the reference curve in Eq 1. However, the amplitude of the AIF is commonly underestimated as a result of small-diameter (MCA and ACA) vessels and limited spatial resolution (defined by the in-plane axial image resolution and slice thickness[12-15]). Since underestimation of the AUC of the AIF results in overestimation of the CBV (see equation 1), correction for this partial volume effect (PVE) is necessary and typically performed using the venous output function (VOF)[16-22]. This correction is based on two assumptions: first, that the centre pixels of a large vein like the superior sagittal sinus (SSS) or the straight sinus, is unaffected by PVE: and second, that without PVE (i.e. an ideal imaging situation), all AIFs and VOF should have equal AUCs. Thus, to perform a correction for the PVE, the VOF is

taken as the reference curve in Eq.1. This current clinical method to correct for PVE in the arteries has been necessary for lack of an alternative, and although it is commonly used clinical validations have not been published.

Recent development of CT scanners with larger scan coverage allows selection of the internal carotid artery (ICA) as the AIF reference artery. The large diameter of the ICA, 4.8 mm on average in adult humans[23] and orientation (perpendicular to the slices) potentially allows for direct measurement of the inflow without the need to apply a PVE correction derived from the venous outflow. This is desirable as it reduces potential for user variability, anatomical variations, and measurement errors.

The purpose of this study is to investigate the suitability of selecting the ICA to measure the reference curve for calculation of CBV, and to examine the assumptions behind the clinically used method of PVE correction using the venous time-attenuation curve.

MATERIALS AND METHODS

PATIENT DATA SELECTION

An initial group of 80 patients were retrospectively selected from participants in a multicentre stroke trial (the DUtch acute Stroke Trial; (DUST) ClinicalTrials.gov Identifier: NCT00880113). DUST is a prospective study on the prognostic value of CTP and CTA in patients with acute stroke symptoms. The DUST study has been approved by the Medical Ethics Review Committee of the University Medical Centre Utrecht, and all subjects gave written informed consent. Inclusion criteria for this sub-study were as follows: (1) admission scan on a 256-slice scanner (Brilliance iCT, Philips Healthcare, Best, the Netherlands), to ensure a uniform quality of data; (2), CTP with an extended acquisition protocol (detailed below), in thin-slice mode. This initial group of patients was visually assessed by an expert reader to ensure no movement was observable after motion correction, and the ICA was included in the

scan coverage. This resulted in 28 patients being discarded and a final patient cohort of 52 patients.

CTP PROTOCOL

All data were acquired and reconstructed using an extended clinical protocol: 150 mAs/rot, 80 kVp, 512 x 512 matrix, 200 mm field of view, 0.39x0.39mm pixels, 81 reconstructed slices with thickness/spacing of 1.0/0.8 mm and a rotation time of 0.33 seconds. The in plane image resolution, measured with an image quality phantom with a 10 µm tungsten wire, was 1.46mm (FWHM). The geometry of the cone beam with a large field of view meant that the data sets were restricted to 6.5cm axial coverage. The thin 1mm slice thickness is required to ensure the absence of PVE in the AIF taken from the ICA should it cross the slice plane at an oblique angle [19,24]. Forty millilitres of nonionic contrast agent (Iopromide, Ultravist, 300 mg iodine/ml; Schering, Berlin, Germany) was injected into the cubital vein (18-gauge needle) at a rate of 6 ml/s followed by a forty millilitres saline flush at a rate of 6 ml/s by using a dual power injector (Stellant Dual CT injector; Medrad Europe, Beek, the Netherlands). An initial acquisition series of 25 time-frames at 2-second intervals was immediately followed by a second series of acquisitions with six time-frames at 30 second intervals. The initial acquisition constitutes the standard stroke CTP protocol used in our institute, the total CT dose (CTDI-vol) including the extended acquisition was 185 mGy.

MEASUREMENT OF ARTERIAL AND VENOUS AUC'S

The AUC of the arterial and venous contrast bolus first-pass was measured at the ICA and SSS. These AUCs were measured using both commercial software employing a Gaussian fit and an alternative method using Trapezoidal Integration (Table 1).

Table 1. Outline of AUC measurement methods and analysis.

First pass of contrast bolus		
AUC method	ROI definition	Pixel choice
Gaussian fit (Philips EBW 4.0)	Manual (circle)	Maximum enhancement within ROI
Trapezoidal Integration	Manual (circle)	Centre of vessel
After first pass of contrast bolus		
Method	ROI definition	Pixel choice
Temporal ratio of ICA and SSS	Manual (circle)	Centre of vessel

MEASUREMENT OF AUC USING COMMERCIAL SOFTWARE

Direct measurement of the AUC of the ICA and SSS was performed using clinical software (EBW 4.0, Brain Perfusion Package, Philips Healthcare, Best, the Netherlands). The ICA and SSS were selected to be approximately perpendicular to the slice plane[19,24]. Circular ROIs were manually drawn on the blood vessel locations on the maximum intensity projection of the patient data. The software selects the pixel within the circular ROI's with the time-attenuation curve (TAC) that has the maximum enhancement over time. Subsequently, the software estimated the AUCs by fitting a Gaussian curve to the TAC[5]. A Gaussian curve fit distinguishes the first pass bolus from the recirculation (Figure 1).

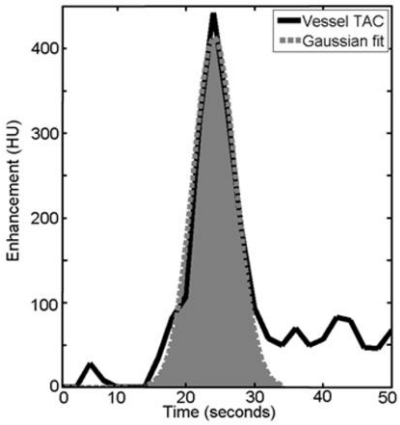

Figure 1: Gaussian fitting of the first pass of the bolus in the ICA time-attenuation curve.

The AUC of the bolus is therefore defined as the area under the Gaussian shape. This measurement included correction for background, defined as the average HU value before bolus arrival. All post-reconstruction image filtering/smoothing was disabled to minimize any additional averaging of the vessels with the surrounding structures that could influence the partial volume effect. Image registration was performed by the software. For each patient, 4 (+/-1) vessel locations were selected on the ICA in the lower slices at the cavernous sinus portion and ten or more vessel locations were selected in SSS.

MEASUREMENT OF AUC USING TRAPEZOIDAL INTEGRATION.

Measuring the TAC at the pixel with maximum enhancement, although common in clinical software, may theoretically introduce a bias towards artificially higher TACs owing to noise. Furthermore, fitting a Gaussian curve to the TACs may introduce an under- or over-estimation to the AUC. To avoid potential bias due to these two factors, an independent set of measurements was carried out on the same vessels without using the commercial software.

Since the vessel centre is the least affected by partial volume from surrounding tissue, the TACs of the vessels were measured at the pixel determined to be at the vessel centre (VC) using a threshold technique applied to the average of all frames of the CTP[25]. Trapezoidal integration of these vessel TACs over the time interval between the bolus arrival and 6 seconds after the peak value was recorded. The bolus arrival time and peak value were determined independently for the arteries and veins, to avoid influence of delayed bolus arrival in the veins on AUC measurement. Prior to this analysis motion correction was applied by a 3D rigid image registration

technique[26]. Background correction was also applied by subtracting the average HU value of the frames before arrival of the contrast bolus in the same way as the commercial software.

ANALYSIS OF AUC DURING FIRST PASSAGE OF THE CONTRAST BOLUS.

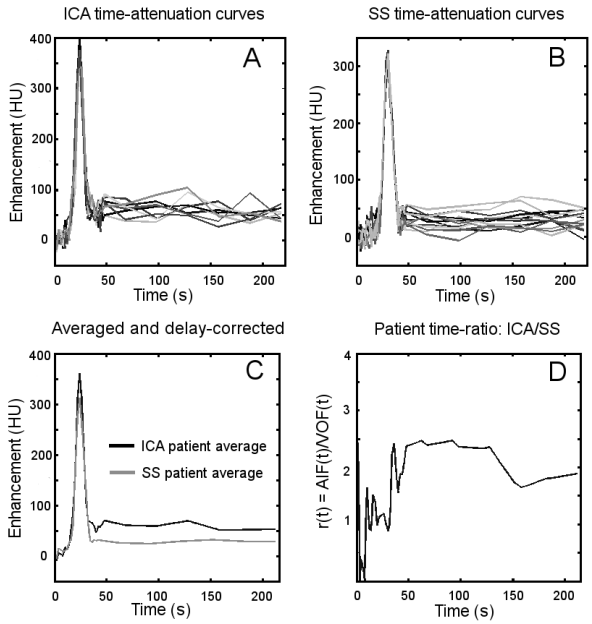

Figure 2: Examples of acquired time-attenuation curves from one patient.

The time-attenuation curves were separated into ICA (panel A) and SSS (panel B) measurements. Averaging of these groups gives a typical time-attenuation curve for each vessel, the SSS is then shifted in time to correct for the delay of bolus arrival time in the veins (panel C). The curves are then interpolated to allow a ratio to be calculated in the frames of the extended protocol (panel D).

In order to compare the results between patients, the average AUC measured in the ICA measurements of each patient was divided by the average AUC of the SSS measurements in that patient (Figure 2): $r_{AUC} = AUC_{ICA}/AUC_{SSS}$. This can be considered to be an inter-patient normalization. The ratio r_{AUC} was independently calculated for the AUCs found with the clinical software and with trapezoidal integration described above.

CONTRAST ENHANCEMENT AFTER FIRST PASSAGE OF THE BOLUS.

The frames from the extended acquisition were used to examine the change in contrast enhancement after the first pass of the bolus (Table 1). The ratio of r(t) = AIF(t)/VOF(t) produces a curve that represents how the enhancement in the average of all the ICA (AIF) compares to the average of all the SSS (VOF) throughout the extended acquisition on a single patient. This ratio does not describe the total amount of contrast in the system, merely the relative enhancement over a time period of 3 minutes. This ratio was calculated independently and based on at least 3 arterial TACs and venous TACs for each patient.

For the calculation of r(t), the first the peak enhancement of the TACs were aligned with respect to their timing to correct for the delay of the venous signal relative to the arterial signal. This was done as it was thought that it may be inaccurate to compare a contrast enhancement at a particular time in the vein to that of the artery when the same concentration of contrast had passed though the artery a few seconds earlier. This temporal alignment was accomplished with linear interpolation of the tails so that the 30 second temporal resolution of the extended protocol would not be an issue when comparing time points on the AIF and the time-shifted VOF. A Wilcoxon signed-rank test was used to determine whether there was a statistically significant difference in r(t) at the beginning of the extended scan (t=60s) and near the end of the scan (t=180s). This difference could indicate a trend or convergence towards equilibrium.

CBV ANALYSIS

To illustrate the impact of AUC variations on CBV calculations, on all 52 patients white matter ROI's (6-8cm^2) in the frontal lobe were manually drawn and three average tissue CBV's for each patient were calculated according to equation 1, where the AUC(reference curve) was taken from i) the MCA (AIF is MCA with no PVE correction), ii) SSS (AIF is MCA with VOF based PVE correction) and iii) ICA (AIF is ICA with no PVE correction) respectively. All CBV measurements were performed using the Philips EBW 4.0, Brain Perfusion Package Software.

RESULTS

From the data 52 patients a total of 202 ICA and 674 SSS locations were selected and measured. Examples of ICA and SSS TACs are shown in Figure 2 A/B. In Figure 2C, the SSS curve has been shifted on the time axis to align the peak of the ICA and SSS curves.

ANALYSIS OF AUC DURING FIRST PASSAGE OF THE CONTRAST BOLUS.

Figure 3: Standard boxplots (with outliers) showing the average ratio rAUC = AUC_{ICA}/AUC_{SSS} of all 52 patients. The measurements shown are the AUC determined by the clinical Gaussian fitting at the pixel at the vessel centre (VC) and by integration of the curve at the pixel with maximum enhancement (ME).

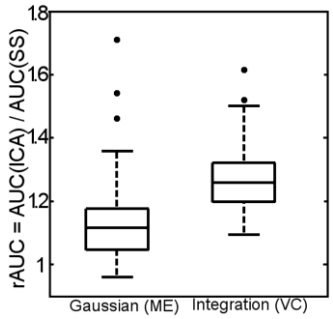

Figure 3 shows a standard-type boxplot, with excluded outliers, of r_{AUC} for all 52 patients. In 49 of the patients the AUC of the ICA was larger than that of the SSS for

both measurement methods. The average r_{AUC} was 1.12 when measured with the clinical software and 1.26 when measured by the simple integration method.

CONTRAST ENHANCEMENT AFTER FIRST PASSAGE OF THE BOLUS.

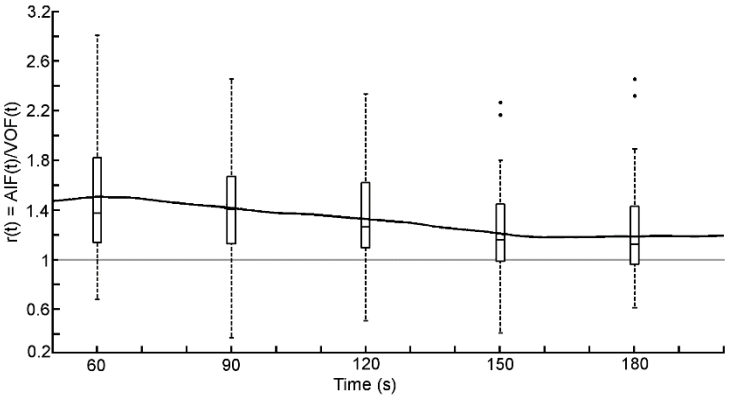

Figure 4: The ratio of the ICA to the SSS over the duration of the extended scan.

Each point on the black line is an average of 52 time-ratios. At 30 second intervals a box plot (Solid line is the median value at that time point) representing all 52 patients illustrates the spread of the data across all patients at that point in time

Figure 4 shows $r_{average}(t)$ over the duration of the extended scan. This plot is the result of averaging the r(t) curves from each of the 52 patients. At 30-second intervals a box plot representing all 52 patients illustrates the spread of the data across all patients at that point in time. The Wilcoxon signed-rank test comparing the distribution of the 52 measurements at 60s to those at 180s showed a drop in the mean value of the ratio over 3 minutes to be significant, with a p-value of 0.0014 indicating a significantly decreasing trend.

CBV ANALYSIS

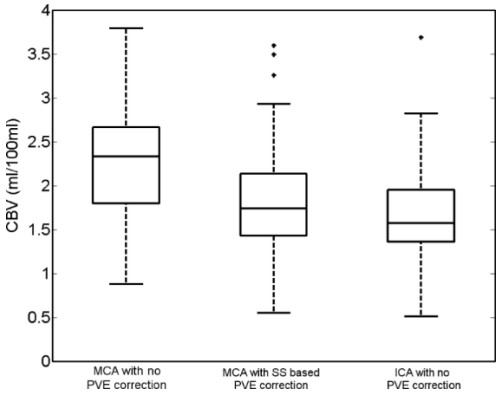

Figure 5. Standard boxplots (with outliers) showing the CBV measurements of ROI drawn on white matter in the 52 patients. Each box represents 52 CBV values calculated from identical ROI but with different vessels selected as the reference vessel. Differences in the CBV between the vessels are therefore directly related to the AUC of the vessel used, and reflect the result found in the direct measurements of the AUC of the vessel time-attenuation curves.

The CBV measurements from each patient, using the MCA, SSS and ICA in turn as the reference vessel are shown in a standard-type boxplot in Figure 5. On average the CBV in white tissue was 2.33ml(blood)/100ml(tissue) when calculated using only the MCA, 1.81 ml/100ml when calculated using the SSS to correct for PVE, and 1.62 ml/100ml when only the ICA was used without partial volume correction. The differences between the CBV measured in the ICA and VOF corrected measurements were shown to be statistically significant with a Wilcoxon signed-rank test p-value of 0.017.

Modern scanners with large-volume coverage allow for inclusion of the ICA in the CTP scan volume. The large size of the ICA gives the potential for AIF selection without the necessity to correct for partial volume, i.e. without selecting a VOF. This study demonstrates that the ICA is large enough to be unaffected by partial volume on thin slices, implied by the ICA having consistently higher AUC than the VOF in the SSS. This makes PVE correction redundant when calculating CBV from the AUC of the TAC.

Our finding is also contrary to assumptions underlying the clinically applied VOF correction and implies that the ICA is the only viable location to measure the inflow unaffected by PVE when using this clinical protocol and CT scanner. Other scanners may have additional options for AIF selection unaffected by PVE, particularly if they have better image resolution. It is important to recognize from this study that if the VOF is used to correct for PVE it is likely that the CBV will be overestimated.

The CBV measurements illustrate the direct relationship between the AUC measured and the CBV calculated using those AUC. The CBV results using the ICA and SSS reflect the difference found in the more extensive measurement of the AUC of the vessels. The CBV values reported in this study do not represent typical CBV values for healthy brain tissue, the patient group includes patients who have suffered acute stroke of varying severity. No attempt was made to avoid diseased tissue when drawing ROI's to measure the CBV since the only relevant point is how a given ROI returns different values of CBV when the ICA and sagittal sinus are used.

In this study care was taken to avoid biases induced by curve fitting and noise. This was done by measuring the vessels in several independent ways: first, using a curve fit at the pixel with maximum enhancement; second, by simple integration of the curve at the pixel at the centre of the vessel. Additional indications that measurement errors do not underlie our findings can be taken from Figures 2 and 4. These figures present the relative values of the arterial TAC to the venous TAC and show that the venous

TAC is lower than the arterial TAC in the frames from the extended protocol. These measurements do not incorporate any curve fitting or integration.

It was observed that at the end of the extended protocol, three minutes after start of contrast administration, the ratio $r_{average}(t)$ had dropped steadily to a value of 1.3, as compared with a value of 1.5 after one minute. This decline was found to be statistically significant. A similar effect, measuring similar ratios at one and three minutes, was also observed by Lapin et al[27]. With an even longer scan duration Lapin found that it took nearly ten minutes before the enhancement in the arteries and veins was equal, however our clinical protocol does not allow for such a long acquisition period so we are not able to confirm this last finding.

Since a different ratio r_{AUC} is found with the commercial software and integration method, it is reasonable to assume that one or both of these methods may have a bias due to the measurement method. Methods measuring the AUC of the first pass of the contrast bolus may have bias due to potential sources of error, such as differentiating the first pass from the recirculated contrast or imperfect curve-fitting.

As mentioned in the methods section, trapezoidal integration over a set time period may induce a bias considering the dispersion in the TAC of the vein. However, given that this bias would derive from missing about one second of enhancement on the edge of the shape of the bolus (measured with a temporal resolution of 2 seconds) it is unlikely that it accounts for the large difference (~25%) between the AUC of the ICA and SSS measured with this method. However we do acknowledge that some of this difference may be due to dispersion.

The third measurement, examining the enhancement after the first pass of the bolus, is an uncomplicated measurement where no assumptions are made in terms of integration or curve fitting. However, all three measurements agree that the average enhancement in the ICA is higher than the SSS, at least 12% higher using the commercial software, and possibly 50% higher when observing the contrast enhancement after the first pass of the bolus.

This last result is the most surprising as it is expected that the contrast, and hence the enhancement, in the entire vascular system should quickly approach an equilibrium after the first passage of the bolus. However, what is observed is that the enhancement in the vessels does not go to an equilibrium for the entire 3 minute duration of the extended scan. The enduring difference in enhancement between artery and vein, observed in all three of the measurements, cannot be explained by calcification in the ICA wall as this is filtered out by the background correction applied by subtracting the average HU value of the first 6 frames before contrast arrival. The difference may be a result of a difference in the hematocrit values between arteries and veins [27,28,]. This hematocrit difference could explain the difference in enhancement observed in the ICA and SSS in the extended frames, while also allowing for the amount of contrast in the entire vascular system to be in equilibrium.

However the possible difference in hematocrit is not sufficient to explain the declining ratio observed in the extended protocol. It has been documented that the high osmolarity of CT contrast agents can acutely increase the blood volume, causing red blood cell crenation[29]. This process may further change the hematocrit value in a way that it is dependent on the size of the red blood cells and the pressure in the vessel, both of which are different in arteries and veins[27]. The hematocrit may thus be dynamic due to the changing concentration of contrast in the blood, thereby explaining our results. However, this explanation is merely a theory, and further study is required to explain why the contrast enhancement remains higher in the ICA long after the system has reached equilibrium.

At present, most commercial CTP software uses thicker slices (3-5 mm) to enhance speed and simplicity of the CTP analysis. These thicker slices may also introduce more partial volume effects[24]. In particular measurements from vessels not perpendicular to the slice plane may suffer from partial volume effects, which will affect the ICA more than the larger venous sinus. This may affect the applicability of our findings to thick-slice CTP data.

One must also realize that the currently used CTP thresholds for defining infarct and penumbra are based on limited-coverage, 5mm CTP data using the small ACA or

MCA as arterial input and venous sinus as compensation for the partial volume effects of these small arteries[9]. Our results show that the AUC of the ICA is higher than the VOF in 94% of the cases on thin-slice data and therefore using the VOF will likely underestimate the arterial inflow and subsequently overestimate the CBV. More accurate CBV results using thin slice ICA as input may therefore require reassessment of thresholds defining the infarct core.

One technical limitation to this study must be acknowledged. Subtle movement of the subject between time frames that cannot be detected visually could affect consistent measurement of TAC, although this can to some extent be corrected for by image registration. This would lower values in the arterial inflow (due to the smaller vessel diameter of the ICA relative to the SSS) more than in the venous outflow, hence finding the AUC of the ICA to be larger than the VOF is in spite of this limitation and not as a result of it.

In conclusion, increased spatial coverage and thin-slice CTP data allows for measurement of the ICA inflow unaffected by partial volume effects. Our results cast doubt on the reliability of the widely used method of partial volume correction that uses the AUC of the venous outflow, since the AUC the large ICA was larger than that of the veins, contrary to the common assumption that both AUCs are equal in the absence of PVE. Selecting a smaller artery, requiring correction for partial volume effect using the VOF, will probably underestimate the AUC of the arterial inflow and therefore overestimate the CBV if calculated using the AUC of the time attenuation curves.

References

1. Klotz E, Konig M. Perfusion measurements of the brain: using dynamic CT for the quantitative assessment of cerebral ischemia in acute stroke. *European journal of radiology.* Jun 1999;30(3):170-184.

2. Mayer TE, Hamann GF, Baranczyk J, et al. Dynamic CT perfusion imaging of acute stroke. *AJNR. American journal of neuroradiology.* Sep 2000;21(8):1441-1449.

3. Wintermark M, Smith WS, Ko NU, Quist M, Schnyder P, Dillon WP. Dynamic perfusion CT: optimizing the temporal resolution and contrast volume for calculation of perfusion CT parameters in stroke patients. *AJNR. American journal of neuroradiology.* May 2004;25(5):720-729.

4. Axel L. Cerebral blood flow determination by rapid-sequence computed tomography: theoretical analysis. *Radiology.* Dec 1980;137(3):679-686.

5. Axel L. A method of calculating brain blood flow with a CT dynamic scanner. *Advances in neurology.* 1981;30:67-71.

6. Lev MH, Segal AZ, Farkas J, et al. Utility of perfusion-weighted CT imaging in acute middle cerebral artery stroke treated with intra-arterial thrombolysis: prediction of final infarct volume and clinical outcome. *Stroke; a journal of cerebral circulation.* Sep 2001;32(9):2021-2028.

7. Schaefer PW, Barak ER, Kamalian S, et al. Quantitative assessment of core/penumbra mismatch in acute stroke: CT and MR perfusion imaging are strongly correlated when sufficient brain volume is imaged. *Stroke; a journal of cerebral circulation.* Nov 2008;39(11):2986-2992.

8. Kamalian S, Kamalian S, Konstas AA, et al. CT perfusion mean transit time maps optimally distinguish benign oligemia from true "at-risk" ischemic penumbra, but thresholds vary by postprocessing technique. *AJNR. American journal of neuroradiology.* Mar 2012;33(3):545-549.

9. Wintermark M, Flanders AE, Velthuis B, et al. Perfusion-CT assessment of infarct core and penumbra: receiver operating characteristic curve analysis in 130 patients suspected of acute hemispheric stroke. *Stroke; a journal of cerebral circulation.* Apr 2006;37(4):979-985.

10. Wu O, Ostergaard L, Weisskoff RM, Benner T, Rosen BR, Sorensen AG. Tracer arrival timing-insensitive technique for estimating flow in MR perfusion-weighted imaging using singular value decomposition with a block-circulant deconvolution matrix. *Magnetic resonance in medicine : official journal of the Society of Magnetic Resonance in Medicine / Society of Magnetic Resonance in Medicine.* Jul 2003;50(1):164-174.

11. Rempp KA, Brix G, Wenz F, Becker CR, Guckel F, Lorenz WJ. Quantification of regional cerebral blood flow and volume with dynamic susceptibility contrast-enhanced MR imaging. *Radiology.* Dec 1994;193(3):637-641.

12. Kalender WA. *Computed Tomography. Fundamentals, System Technology, Image Quality, Applications.* New York: Wiley; 2000.

13. Barrett JF, Keat N. Artifacts in CT: recognition and avoidance. *Radiographics : a review publication of the Radiological Society of North America, Inc.* Nov-Dec 2004;24(6):1679-1691.

14. Prokop M. *Spiral and multislice computed tomography of the body.* New York: Thieme; 2003.

15. Cianfoni A, Colosimo C, Basile M, Wintermark M, Bonomo L. Brain perfusion CT: principles, technique and clinical applications. *La Radiologia medica.* Dec 2007;112(8):1225-1243.

16. Wintermark M, Reichhart M, Thiran JP, et al. Prognostic accuracy of cerebral blood flow measurement by perfusion computed tomography, at the time of emergency room admission, in acute stroke patients. *Annals of neurology.* Apr 2002;51(4):417-432.

17. Kudo K, Sasaki M, Ogasawara K, Terae S, Ehara S, Shirato H. Difference in tracer delay-induced effect among deconvolution algorithms in CT perfusion analysis: quantitative evaluation with digital phantoms. *Radiology.* Apr 2009;251(1):241-249.

18. Wintermark M, Albers GW, Alexandrov AV, et al. Acute stroke imaging research roadmap. *AJNR. American journal of neuroradiology.* May 2008;29(5):e23-30.

19. van der Schaaf I, Vonken EJ, Waaijer A, Velthuis B, Quist M, van Osch T. Influence of partial volume on venous output and arterial input function. *AJNR. American journal of neuroradiology.* Jan 2006;27(1):46-50.

20. Miles K. *Multidetector Computed Tomography in Oncology CT Perfusion Imaging.* Informa; 2007.

21. Aviv RI, d'Esterre CD, Murphy BD, et al. Hemorrhagic transformation of ischemic stroke: prediction with CT perfusion. *Radiology.* Mar 2009;250(3):867-877.

22. Konstas AA, Goldmakher GV, Lee TY, Lev MH. Theoretic basis and technical implementations of CT perfusion in acute ischemic stroke, part 2: technical implementations. *AJNR. American journal of neuroradiology.* May 2009;30(5):885-892.

23. Krejza J, Arkuszewski M, Kasner SE, et al. Carotid artery diameter in men and women and the relation to body and neck size. *Stroke; a journal of cerebral circulation.* Apr 2006;37(4):1103-1105.

24. Riordan AJ, Bennink E, Viergever MA, Velthuis BK, Dankbaar JW, de Jong HW. CT brain perfusion protocol to eliminate the need for selecting a venous output function. *AJNR. American journal of neuroradiology.* Jul 2013;34(7):1353-1358.

25. Hoffmann KR, Nazareth DP, Miskolczi L, et al. Vessel size measurements in angiograms: a comparison of techniques. *Medical physics.* Jul 2002;29(7):1622-1633.

26. Thevenaz P, Ruttimann UE, Unser M. A pyramid approach to subpixel registration based on intensity. *IEEE transactions on image processing : a publication of the IEEE Signal Processing Society.* 1998;7(1):27-41.

27. Lapin GD, Allen CV, Groothuis DR. Noninvasive measurement of arterial blood plasma concentration of iodinated contrast agents from CT scans of human brain. *Journal of computer assisted tomography.* May-Jun 1994;18(3):363-369.

28. McHedlishvili G, Varazashvili M, Kumsishvili T, Lobjanidze I. Regional hematocrit changes related to blood flow conditions in the arterial bed. *Clinical hemorheology and microcirculation.* 2003;29(2):71-79.

29. Aspelin P. Effect of ionic and non-ionic contrast media on whole blood viscosity, plasma viscosity and hematocrit in vitro. *Acta radiologica: diagnosis.* 1978;19(6):977-989.

CHAPTER 7: SUMMARY AND GENERAL DISCUSSION

The focus of this thesis is to examine the technical CTP process as performed in an acute stroke setting and identify elements of patient motion, scanner acquisition protocol, pre-processing, and analysis that affect the (quantitative) accuracy of the diagnostic perfusion imaging and define the optimal where possible. This was primarily done by application of a digital head phantom alongside measurements on clinically acquired data. The results suggest that by optimizing many facets of the CTP process it is possible to achieve significantly improved diagnostic image quality and quantitative accuracy without the need to increase CT dose. This may strengthen the clinical impact of CTP and advance its application and acceptance.

CHAPTER 2: VALIDATION OF CT BRAIN PERFUSION METHODS USING A REALISTIC DYNAMIC HEAD PHANTOM

The introduction of this thesis highlighted the need for a gold standard to investigate how specific parameters affect the accuracy of the diagnostic perfusion maps. In chapter 2 we detail the development of a digital CTP head phantom to fulfil that requirement.

The first requirement of the digital CTP phantom was that it would behave like real clinical CTP data in all relevant aspects. This was achieved by simulation of perfusion by indicator-dilution theory[1,2], by using anatomically accurate structure and by inclusion of real CT features as noise, limited resolution and artefacts[3] After a clinical validation we demonstrate how the head phantom could be used to measure the difference in behaviour and performance of different CTP analysis software, and how the software performed when the image noise on the CT data was varied. This provides us with the tool needed to investigate and evaluate changes in the CTP process which will be used extensively in the following chapters.

CHAPTER 3: IMPROVEMENTS IN ACCURACY AND DOSE EFFICIENCY OF CTP BY APPLICATION OF A REALISTIC DIGITAL PHANTOM.

In the third chapter the flexibility and specific features of the hybrid head phantom is utilized to investigate a wide array of CTP scanner protocols, many of which have never been used clinically. The purpose of this chapter was twofold; to improve the reliability of cerebral blood flow measurements using CT perfusion by optimizing CT perfusion protocols and filters and to further demonstrate the usefulness of a digital head phantom as a tool for optimization and calibration.

The data was analysed by bSVD based perfusion software and the results allow us to identify the best performing protocols. Optimization of the perfusion software for different temporal resolutions demonstrated how simple alterations can significantly improve results in specific situations. Application of the TIPS bilateral filter proved that advanced filtering methods can not only further improve the image quality by removing noise as was demonstrated earlier[4], but also significantly improve the quantitative performance of CTP. The results of this chapter identify several scanner protocols that, with application TIPS filter and optimized perfusion software, offer much improved diagnostic image quality and accuracy with significantly less CT dose when compared to current clinically used CTP scanner protocol.

CHAPTER 4: THE EFFECT OF HEAD MOVEMENT ON CT PERFUSION SUMMARY MAPS: SIMULATIONS WITH CT HYBRID PHANTOM DATA

In chapter 4 the digital head phantom is used to assess the effect of patient head movement on CTP summary maps. Investigation of the effects of patient movement has received little attention relative to other aspects of CTP considering the detrimental effect it can have on the results. A study that served as a precursor and motivation for this chapter showed that 24% of CTP patients had severe head movement, rendering 16% of CTP perfusions results unreliable[5].

Many conclusions that can be drawn from large patient databases, for example determining quantitative thresholds for use in computer aided diagnosis, require that one must either prevent patient movement, or exclude patients from the database, or

correct for patient movement. For the latter two of these three options it is important to know how much patient movement means that the data will be unreliable, and how effective correction methods are in correcting for patient movement.

Although this can be done to some extent with clinical data, to quantitatively measure the effect it is better to first perform a perfusion analysis on a ground truth, with known perfusion values and regions of tissue states, and then to measure perfusion properties a second time after patient movement is simulated. In this way one can directly measure the effect of the movement, allowing for definition of acceptable ranges and speed of movement. With these definitions clinical datasets could automatically red flagged for more careful assessment.

It is intended that this line of study using the digital head phantom will continue further to investigate more advanced methods of image registration and investigation of other aspects of CTP such thinner slices.

CHAPTER 5: CT BRAIN PERFUSION PROTOCOL TO ELIMINATE THE NEED FOR SELECTING A VENOUS OUTPUT FUNCTION

Partial volume effects are an unavoidable aspect of imaging small, high contrast objects, limited image resolution and slice thickness means that there will always be averaging of neighbouring (anatomical) structures[6]. The main problem with PVE in CTP imaging is averaging of the time-attenuation curve of the artery (high concentration of contrast and high enhancement) with surrounding tissue (low concentration, low enhancement) resulting in a AIF curve that has lower enhancement and does not accurately represent the volume of the inflow to the tissue[6-8]. This causes the blood volume and blood flow to be overestimated. This is currently corrected for by using the area under the curve measured in the sagittal sinus, based on the assumption that all of the contrast agent entering the tissue via the arteries will leave the system via the veins.

The diameters of the vessels used to define the arterial inflow e.g. the MCA and ACA, are of such a (small) scale with respect to the image resolution that they are affected by PVE. But by increasing the image resolution and decreasing slice thickness it is

possible to reduce PVE to the point where at least the pixel representing the centre of these vessels is unaffected by PVE. Finding the minimum resolution and slice thickness that allows this was the goal of this chapter.

Simulations with the head phantom indicated that such a scanner protocol would be feasible. Indeed, applying a slice thickness of 1.8mm and an image resolution of 1mm to clinical CTP data showed that the MCA and ACA vessels could be used as the AIF without need for correction for partial volume effect, implied by the measurements of these vessels having the same area under the curve as the ICA (which at 4-5mm is large enough to be unaffected by PVE) and a greater area under the curve than the sagittal sinus (diameter 5-7mm).

This image resolution and slice thickness can be achieved by most scanners. However, increasing the image resolution will increase image noise so additional/stronger filtering will be required after the measurement of the AIF for calculation of perfusion parameters. Reconstructing the CTP volume with 1.8mm thick slices increases the time needed for reconstruction, depending on the computational power available this construction time may be prohibitive.

However, since the vessels which we want to measure are found only midlevel in the brain, it should be practical to only reconstruct several thin slices in this region, with high resolution, solely for the acquisition of the AIF. This solution would require scanner manufacturers to implement a reconstruction of one small volume of several 1.8mm slices with high resolution for measurement of the AIF, and another for calculation of the perfusion parameters as normal.

Although this would require some changes on the part of the scanner manufacturers, there would be no negative impact on the CTP process aside from a few seconds of addition reconstruction time. Although this would allow arterial inflow measurements unaffected by PVE, it raises two important questions;

Firstly, why not just select the ICA as the AIF?

Selection of the ICA is only possible when using scanners with large coverage, around 8cm of coverage is required to include both the ICA and the majority of the brain. Such coverage is usually only possible with the latest generation of scanners and which are not widely available yet. However the ICA is indeed the best choice when available.

Secondly, why not just continue to correct the AIF using the area under the curve of the sagittal sinus?

Our original answer to this question, before this research was carried out, was that elimination of a user input (selection of the sagittal sinus) would save time and reduce variability. However, measurement of the sagittal sinus on the clinical CTP data revealed that the sagittal sinus had, on average, a significantly lower area under the curve than that of the ICA.

It is this last finding that is arguably the most important of this chapter, if true, such a result would invalidate the assumption upon most PVE correction methods in CTP are based. If this is the case then a scan protocol that eliminates the need for such a correction, such as outlined in this chapter becomes even more important for scanners that do not have the coverage to include the ICA in the scan volume. This result required further investigation with a separate study, with a larger patient cohort and will be discussed in chapter 6

CHAPTER 6 COMPARISON OF PARTIAL VOLUME EFFECTS IN ARTERIAL AND VENOUS CONTRAST CURVES IN CT BRAIN PERFUSION IMAGING

In chapter 5 we observed that the area under the time-attenuation curve of the sagittal sinus was significantly lower than that of the ICA. In chapter 6 we repeat this measurement on a much larger patient cohort, measuring area under the curve of the ICA and sagittal sinus time-attenuation curves in 52 patients. The results confirm the observation made in chapter 5 with several independent measurement methods, fitting of a Gaussian curve and simple trapezoidal to the first passage of the bolus, and

examination of the difference in contrast enhancement after the first passage of the bolus.

This result appears to contradict the assumption upon which CTP PVE correction is based; that the veins allow quantitative measurement of the contrast agent over time and that the total amount of contrast that enters via the arteries must leave via the veins. More specifically, that the contrast agent of the first passage of the bolus measured in the sagittal sinus, although delayed and dispersed is what must have entered through the arteries. What we measure in this chapter implies that there is more contrast going in via the ICA than leaves via the sagittal sinus. Where does the missing contrast agent go? There are two scenarios that we investigated to account for the missing contrast.

Firstly, it is possible that a portion of the contrast agent is being delayed so long by passage through the tissue that it does not arrive in the sagittal sinus until after the first passage of the bolus. To investigate this we looked at the contrast enhancement after the first passage of the bolus. Since the CTP patient data was a part of the DUST study (http://dutchstroketrial.nl/), the protocol included 6 extra frames scanned every 30 seconds for 3 additional minutes after the standard scan that image the first passage of the bolus. It was found that not only did the missing contrast agent not appear, but that the contrast enhancement remained significantly lower in the sagittal sinus for the 3 additional minutes. So long after the first passage of the bolus we would expect the amount of contrast agent in the system to be in equilibrium, with equal enhancement in the arteries and veins.

The second scenario that could account for the missing contrast agent is a difference in haematocrit in the arteries and veins. We previously assumed that there was no difference in haematocrit since the vessel sizes are similar. Previous studies[9] found small differences between the cerebral arteries and veins, but not enough difference to account for the difference we observed in this chapter.

However, these studies did not measure haematocrit in the presence of contrast agent. In the discussion of this chapter we postulate that the high osmolarity of CT

contrast agents acutely increases the blood volume, causing red blood cell crenation. It has been previously theorized that this could further change the haematocrit value in such a way that it is dependent on the size of the red blood cells and the pressure in the vessel[10,11], both of which differ between the arteries and veins. This implies that it may be incorrect to assume that the hematocrit factor is the same in the veins and arteries, and that the hematocrit is dynamic due to the changing concentration of contrast in the blood.

Although this scenario potentially explains the "missing" contrast agent, we cannot confirm this without highly invasive measurements of the haematocrit in the cerebral arteries and veins during passage of contrast bolus.

The implication of this theory is that the assumption that all the contrast being fed by the arteries leaves via the veins is correct, but that the assumption that they have the same haematocrit is incorrect. This would mean that for the PVE correction method work as intended, we would first need to account for the difference in haematocrit. This is not a simple task considering that the results also indicate that the difference in haematocrit is dependent on the concentration of contrast agent, and may be dynamic, changing as contrast agent is removed from the blood.

We recognise that we have not provided a concrete explanation of the effect observed in this chapter and the implication that that has for the scientific strength of this finding. We are however confident that the observation of the effect is not due to measurement errors, having potential implications for calculation of the CBV when the area under the curve of the VOF is used to correct for PVE in the arteries. To the best of our knowledge there was never any clinical (or otherwise) validation of this PVE correction method, which may be surprising considering the simplicity of the methodology used in this chapter, simple comparison of the vein and artery in the absence of PVE.

However, before making a drastic dismissal of a method that has been used in the field of CTP for decades, we must also acknowledge that this is a single study, carried out with CT data acquired on a single CT scanner with a specific protocol, where the patients were all suspected of one condition (acute ischemic stroke). Certainly further

studies that addresses these limitations should be carried out to confirm our findings. In the meantime the PVE correction method should at least be considered to have a shadow of doubt cast across it, raising a need for alternatives to PVE correction such as the protocol suggested in chapter 5, or the inclusion of the ICA in the scan volume. Aside from the increased quantitative error with the CBV being overestimated, the current PVE correction will mean an additional variance between patients, increased lack of reproducibility that may hamper the sensitivity and specificity of CTP.

DEFINITION OF AN OPTIMAL CTP PROCESS

The introduction of this thesis outlined the steps of the CTP process and the complexity and potential variability of CTP. In the following chapters we see how many of these parameters can have a strong influence on the diagnostic perfusion maps. Throughout this work we see large differences in results when these parameters are varied and these inconstancies are reflected in clinical practice.

The parameters that were examined were: CT dose (per frame), temporal and spatial resolution, slice thickness, noise reduction/filtering, perfusion analysis method, oscillation index of bSVD, patient head movement, and partial volume effect correction. For all of these parameters we expanded our understanding of these processes and how they affect the CTP diagnostic maps and also propose optimal values.

From these optimal values we can propose a CTP process that maximizes quantitative accuracy, reduces CT dose (relative to current clinical protocols), reduces risk of errors induced by patient movement, and eliminates the need for use of a seemingly flawed method of correction for PVE.

SCANNER PROTOCOL:

From chapter 3 we see that with use of the TIPS filter the large amount of noise due to such a low dose is suppressed giving good quantitative performance (score of 0.67) with a dose that is 33% lower than our current clinical protocol (also scoring 0.67). The

1 second temporal resolution means that the nyquist criteria will be satisfied for short tissue MTT such as grey matter (~3.5s) and offers some potential to take advantage of some more exotic contrast bolus shapes such as double bolus. Although it must be noted that in chapter 3 there was no strongly negative effect in the CBF correlation due to longer temporal resolutions that should not always satisfy the nyquist criteria such as 2 and 4 seconds.

DATA RECONSTRUCTION:

Following from the findings of chapter 5 and 6, in the absence of the ICA in the scan volume, we should reconstruct several slices from mid-level in the scan with the highest resolution possible, preferably less than 1mm, and a slice thickness of less than 1.8mm for measurement of the arterial inflow from the ACA or MCA unaffected by PVE. For scanners with larger coverage which include the ICA, the ICA should be chosen as the arterial inflow. Use of iterative reconstruction techniques such as iDose [12-14] that further reduce the noise may allow for even lower CT dose.

IMAGE REGISTRATION:

Chapter 4 showed the necessity for 3D image volume registration. For large patient data bases it would also be useful to have an image registration process that measures the degree of patient movement and marks them for closer examination or exclusion based on the results from chapter 4.

PRE-PROCESSING AND FILTERING:

Chapter 3 showed conclusively that the TIPS filter significantly improves CTP results allowing for much lower CT dose. The TIPs filter does require additional processing time (~20-40 seconds dependant on hardware, the process benefits from multi-threading), but this is not prohibitive. Alternatively the HYPR filter has also been shown to be effective[15].

PERFUSION ANALYSIS SOFTWARE:

Kudo et al. demonstrated the superior performance of the Perfusion Mismatch Analyser software, and the bSVD method has been the standard for CTP analysis for several years. The choice of oscillation index, 0.02 is defined by the temporal resolution of 1 second, derived from the results in chapter 3. Computer Aided Diagnosis with maps that clearly and accurately define regions of reduced perfusion, and differentiate between tissue that would be salvageable after reperfusion and tissue that has already died is highly desirable. Such systems already exist[16] and have been used to assist in patient selection, but many physicians remain doubtful of its accuracy based. The main role of CTP is to assist the physician in selecting candidates for rtPA[17,18], and CAD could potentially simplify this process greatly. However CAD will only ever be as accurate, consistent and reliable as the quantitative accuracy of the parameter maps upon which it is defined. In my opinion, the current state of CTP does not fulfil these requirements, this will be discussed further in the conclusion.

GENERAL DISCUSSION OF LIMITATIONS.

Each of the studies carried out in this work have specific limitations that have been outlined in their respective chapters however there are some general issues that apply to all of the work outlined in this thesis.

With regards to the clinical data used in this study, the majority of the data was acquired using scanner protocol outlined in the DUST study. Although this protocol is well designed with regards to current opinion on ideal CTP acquisition, the fact that the majority of this work uses only one protocol results in a lack of variety in our clinical data. Ideally we would have explored the effects of various CT scanner protocol on some of the findings in this thesis. That said, chapter 3 does fill this gap somewhat using the digital head phantom and that in itself demonstrates the usefulness of the phantom. Likewise, another limitation is that the majority of clinical data analysed in this thesis comes from a single CT scanner, the Philips ICT at UMC Utrecht.

Chapter 2 and 3 rely heavily on the realism of the digital head phantom, and to a lesser extent, chapters 4 and 5. We must recognise that the digital head phantom is attempting to simulate both blood perfusion through the brain, whilst also emulating the imaging of this system with CTP. No doubt there are aspects of both the perfusion of the blood flow and the acquisition that are not included in the digital head phantom. However we aimed to emulate the most important aspects that most affect the CTP acquisition. As such we feel that the digital head phantom may be taken as a reliable indication of what would happen in the scenario's it aims to emulate, we recognise that it will never be an exact simulation.

The perfusion analysis software used in this thesis is also limited to several instances. Philips healthcare Extended Brilliance Workspace brain perfusion package is the software used at our institution for CTP analysis. Although this software allowed us to avail of two different analysis algorithms (bSVD[19] and fit based deconvolution[20]), we did not have to opportunity to utilize/evaluate other commercial software packages such as those offered by Siemens, Toshiba, and General electric. Although these software also utilize similar algorithms as a consensus emerges[21,22] they have different implementations to suit the capabilities of scanners. However we attempt to remain objective and make our findings non-specific to the Philips software (unless specifically evaluating it like in chapter 2). We also used the software package Perfusion Mismatch Analyser[23] extensively, written by Kudo, utilizing the methodology outlined by Ostergaard, Wu and Gobbel[24-26]. The implementation of the bSVD method in this software is well documented and validated to perform well in relative to other software packages[27].

Many of the findings in this thesis, specifically those in chapter 3 and 4 lack assessment of clinical impact. The general assumption underlying this work was that CTP studies will clinically benefit from more quantitative, reproducible perfusion measurements with less noise using less radiation dose. In the case of chapter 3, which evaluates an array of different protocols and processing, most the scanner protocols that are simulated are not clinically validated or in even feasible some cases (with regards to dose limitations). Even if we had the opportunity to use such protocols clinically, to validate the findings of the head phantom in this chapter would require

multiple scans on patients. The clinical impact of the work presented in chapter 4 was evaluated in a separate study not included in this thesis[16].

GENERAL CONCLUSIONS

A lack of consensus and standardisation[27,28] means an inconstancy in results from different vendors or research groups. Although many groups have campaigned for standardization[21,22,29-34], the field of CTP has been developing at such a fast pace that this goal has been difficult to reach. This has a negative impact on the credibility of CTP as a quantitative measurement of perfusion, and greatly hinders the advancement of CAD diagnosis. Ideally diagnosis in stroke imaging should be based in quantitative thresholds, these thresholds may be defined by analysis of large patient databases that include patient outcome. However, definition and application of these thresholds will be unreliable if there are inconstancies in the quantitative accuracy of the results between patients, methods, and institutes.

One reason for the lack of consistency in CTP is the lack of a gold standard with which to validate, compare, and quantitatively assess new ideas and developments. Previously new developments have been tested by use of follow up scans or other less clinically orientated methods. With a tool such as the head phantom new ideas can be tested and presented in a manner which makes it clear to the field of CTP if a change is worthwhile and suitable for universal adoption. Aside from the work presented in this thesis we have recently seen other groups using head phantoms which have helped to form a consensus on certain aspects of CTP[27,35-38].

The more widespread use of digital head phantoms may lead to a standardized ‘toolbox’ for testing and developing new ideas in CTP and would pave the way for uniform CTP methodology. This may ultimately strengthen the clinical impact of CTP and advance its application and acceptance.

References

1. Bredno J, Olszewski ME, Wintermark M. Simulation model for contrast agent dynamics in brain perfusion scans. *Magnetic resonance in medicine : official journal of the Society of Magnetic Resonance in Medicine / Society of Magnetic Resonance in Medicine.* Jul 2010;64(1):280-290.

2. Meier P, Zierler KL. On the theory of the indicator-dilution method for measurement of blood flow and volume. *Journal of applied physiology.* Jun 1954;6(12):731-744.

3. Riordan AJ, Prokop M, Viergever MA, Dankbaar JW, Smit EJ, de Jong HW. Validation of CT brain perfusion methods using a realistic dynamic head phantom. *Medical physics.* Jun 2011;38(6):3212-3221.

4. Mendrik AM, Vonken EJ, van Ginneken B, et al. TIPS bilateral noise reduction in 4D CT perfusion scans produces high-quality cerebral blood flow maps. *Physics in medicine and biology.* Jul 7 2011;56(13):3857-3872.

5. Fahmi F, Beenen LF, Streekstra GJ, et al. Head Movement during CT Brain Perfusion Acquisition of Patients with Acute Ischemic Stroke. *Submitted For Publication.* 2012.

6. van der Schaaf I, Vonken EJ, Waaijer A, Velthuis B, Quist M, van Osch T. Influence of partial volume on venous output and arterial input function. *AJNR. American journal of neuroradiology.* Jan 2006;27(1):46-50.

7. Niesten JM, van der Schaaf IC, Riordan AJ, de Jong HW, Mali WP, Velthuis BK. Optimisation of vascular input and output functions in CT-perfusion imaging using 256(or more)-slice multidetector CT. *European radiology.* May 2013;23(5):1242-1249.

8. Riordan AJ, Bennink E, Viergever MA, Velthuis BK, Dankbaar JW, de Jong HW. CT brain perfusion protocol to eliminate the need for selecting a venous output function. *AJNR. American journal of neuroradiology.* Jul 2013;34(7):1353-1358.

9. McHedlishvili G, Varazashvili M, Kumsishvili T, Lobjanidze I. Regional hematocrit changes related to blood flow conditions in the arterial bed. *Clinical hemorheology and microcirculation.* 2003;29(2):71-79.

10. Aspelin P. Effect of ionic and non-ionic contrast media on whole blood viscosity, plasma viscosity and hematocrit in vitro. *Acta radiologica: diagnosis.* 1978;19(6):977-989.

11. Lapin GD, Allen CV, Groothuis DR. Noninvasive measurement of arterial blood plasma concentration of iodinated contrast agents from CT scans of

human brain. *Journal of computer assisted tomography.* May-Jun 1994;18(3):363-369.

12. O'Halloran RL, Wen Z, Holmes JH, Fain SB. Iterative projection reconstruction of time-resolved images using highly-constrained back-projection (HYPR). *Magnetic resonance in medicine : official journal of the Society of Magnetic Resonance in Medicine / Society of Magnetic Resonance in Medicine.* Jan 2008;59(1):132-139.

13. Willemink MJ, de Jong PA, Leiner T, et al. Iterative reconstruction techniques for computed tomography Part 1: technical principles. *European radiology.* Jun 2013;23(6):1623-1631.

14. Niesten JM, van der Schaaf IC, Riordan AJ, et al. Radiation dose reduction in cerebral CT perfusion imaging using iterative reconstruction. *European radiology.* Feb 2014;24(2):484-493.

15. Speidel MA, Bateman CL, Tao Y, et al. Reduction of image noise in low tube current dynamic CT myocardial perfusion imaging using HYPR processing: a time-attenuation curve analysis. *Medical physics.* Jan 2013;40(1):011904.

16. Fahmi F, Marquering HA, Streekstra GJ, et al. Automatic detection of CT perfusion datasets unsuitable for analysis due to head movement of acute ischemic stroke patients. *Journal of healthcare engineering.* 2014;5(1):67-78.

17. von Kummer R, Allen KL, Holle R, et al. Acute stroke: usefulness of early CT findings before thrombolytic therapy. *Radiology.* Nov 1997;205(2):327-333.

18. Hacke W, Kaste M, Bluhmki E, et al. Thrombolysis with alteplase 3 to 4.5 hours after acute ischemic stroke. *The New England journal of medicine.* Sep 25 2008;359(13):1317-1329.

19. Sasaki M, Kudo K, Ogasawara K, Fujiwara S. Tracer delay-insensitive algorithm can improve reliability of CT perfusion imaging for cerebrovascular steno-occlusive disease: comparison with quantitative single-photon emission CT. *AJNR. American journal of neuroradiology.* Jan 2009;30(1):188-193.

20. Axel L. A method of calculating brain blood flow with a CT dynamic scanner. *Advances in neurology.* 1981;30:67-71.

21. Wintermark M, Albers GW, Broderick JP, et al. Acute Stroke Imaging Research Roadmap II. *Stroke; a journal of cerebral circulation.* Sep 2013;44(9):2628-2639.

22. Zhu G, Michel P, Zhang W, Wintermark M. Standardization of Stroke Perfusion CT for Reperfusion Therapy. *Translational stroke research.* Jun 2012;3(2):221-227.

23. *Perfusion mismatch analyser* [computer program]. Version 3.0.0.02006.

24. Wu O, Ostergaard L, Weisskoff RM, Benner T, Rosen BR, Sorensen AG. Tracer arrival timing-insensitive technique for estimating flow in MR perfusion-weighted imaging using singular value decomposition with a block-circulant deconvolution matrix. *Magnetic resonance in medicine : official journal of the Society of Magnetic Resonance in Medicine / Society of Magnetic Resonance in Medicine.* Jul 2003;50(1):164-174.

25. Ostergaard L, Weisskoff RM, Chesler DA, Gyldensted C, Rosen BR. High resolution measurement of cerebral blood flow using intravascular tracer bolus passages. Part I: Mathematical approach and statistical analysis. *Magnetic resonance in medicine : official journal of the Society of Magnetic Resonance in Medicine / Society of Magnetic Resonance in Medicine.* Nov 1996;36(5):715-725.

26. Gobbel GT, Fike JR. A deconvolution method for evaluating indicator-dilution curves. *Physics in medicine and biology.* Nov 1994;39(11):1833-1854.

27. Kudo K, Christensen S, Sasaki M, et al. Accuracy and reliability assessment of CT and MR perfusion analysis software using a digital phantom. *Radiology.* Apr 2013;267(1):201-211.

28. Kudo K, Sasaki M, Ogasawara K, Terae S, Ehara S, Shirato H. Difference in tracer delay-induced effect among deconvolution algorithms in CT perfusion analysis: quantitative evaluation with digital phantoms. *Radiology.* Apr 2009;251(1):241-249.

29. Wintermark M, Warach SJ, Stir, Virtual International Stroke Trials Archive - Imaging I. Acute stroke imaging research roadmap II and international survey of acute stroke imaging capabilities: we need your help! *AJNR. American journal of neuroradiology.* Sep 2013;34(9):1671.

30. Leiva-Salinas C, Wintermark M. The future of stroke imaging: what we need and how to get to it. *Stroke; a journal of cerebral circulation.* Oct 2010;41(10 Suppl):S152-153.

31. Jauch EC, Saver JL, Adams HP, Jr., et al. Guidelines for the early management of patients with acute ischemic stroke: a guideline for healthcare professionals from the American Heart Association/American Stroke Association. *Stroke; a journal of cerebral circulation.* Mar 2013;44(3):870-947.

32. Wintermark M, Sanelli PC, Albers GW, et al. Imaging recommendations for acute stroke and transient ischemic attack patients: A joint statement by the American Society of Neuroradiology, the American College of Radiology, and the Society of NeuroInterventional Surgery. *AJNR. American journal of neuroradiology.* Nov-Dec 2013;34(11):E117-127.

33. Saver JL, Warach S, Janis S, et al. Standardizing the structure of stroke clinical and epidemiologic research data: the National Institute of Neurological Disorders and Stroke (NINDS) Stroke Common Data Element (CDE) project. *Stroke; a journal of cerebral circulation.* Apr 2012;43(4):967-973.

34. Leiva-Salinas C, Hom J, Warach S, Wintermark M. Stroke imaging research road map. *Neuroimaging clinics of North America.* May 2011;21(2):239-245, ix.

35. Brauweiler R, Eisa F, Hupfer M, Nowak T, Kolditz D, Kalender WA. Development and evaluation of a phantom for dynamic contrast-enhanced imaging. *Investigative radiology.* Aug 2012;47(8):462-467.

36. Lee Q. Dynamic CT head phantom for perfusion and angiography studies. Medical Imaging 2010: Biomedical Applications in Molecular, Structural, and Functional Imaging; 2010.

37. van den Boom R. Effect of dose reduction on cerebral CT perfusion maps: results from a hybrid digital perfusion phantom. European Congress of Radiology; 2013.

38. Fahmi F, Riordan A, Beenen LF, et al. The effect of head movement on CT perfusion summary maps: simulations with CT hybrid phantom data. *Medical & biological engineering & computing.* Feb 2014;52(2):141-147.

NEDERLANDSE SAMENVATTING

ACHTERGROND EN MOTIVATIE

Beroerte veroorzaakt 9% van alle sterfgevallen wereldwijd, is de meest voorkomende doodsoorzaak na ischemische hartziekten en vormt meer dan 4% van zorguitgaven in westerse landen. Verschillende behandelingen zijn in de afgelopen jaren beschikbaar gekomen, die over het algemeen gericht zijn op het verwijderen van de blokkerende bloedprop. Snelle en nauwkeurige diagnose is cruciaal voor het bepalen van de juiste behandeling waaronder het niet risicoloos toedienen van speciale bloedverdunners (rtPA). CT perfusie (CTP) van de hersenen is een veelbelovend instrument om artsen te helpen bij maken van deze keus, door verschillende perfusie parameters in het de hersenen in kaart kan brengen. De klinische bruikbaarheid van de CTP methodiek moet echter nog overtuigend bewezen worden. Tot op heden is er nog geen goede objectieve manier om de CTP techniek te valideren en is er nog geen consensus over hoe te CTP metingen moeten verlopen en de data moeten worden geanalyseerd.

CT PERFUSIE BEELDVORMING

CTP beeldvorming van de hersenen is een techniek die gebruikt kan worden om bij patiënten met een (acuut) CVA (beroerte) de cerebrale doorbloeding of perfusie te beoordelen. In gespecialiseerde ziekenhuizen worden deze CTP beelden gewoonlijk verkregen naast een gewone niet-contrast CT en een CT-angiografie (CTA). CTP is vergelijkbaar met CTA, in beide wordt het contrastmiddel wordt gemeten, maar CTP geeft informatie over de doorbloeding op weefselniveau terwijl CTA de bloedvaten (en indirect de bloedprop) zelf afbeeldt. Meting of kwantificering van het contrastmiddel in een CT is beeld is theoretisch eenvoudig omdat het jodiumhoudend contrastmiddel een lokale toename van de rontgen absorptie ofwel verzwakking van de doorgelaten röntgenstralen veroorzaakt, die lineair evenredig is met de lokale concentratie van het contrastmiddel. Aldus, door het meten van de veranderingen in verzwakking (in Hounsfield eenheden, HU) gedurende een bepaalde tijd te meten, verkrijgt men een schatting de in- en uitstroom van contrastmiddel (en dus bloed) binnen een volume-element (voxel). Hieruit kan informatie over de doorbloeding ter plaatse van het voxel afgeleid worden.

Het principe van CTP is op zich eenvoudig, maar in de praktijk zijn er vele elementen die een negatieve invloed hebben op de bruikbaarheid en de nauwkeurigheid van de resulterende beelden. In het kader van dit werk is het van belang de onderliggende complexiteit van CTP beeldvorming te illustreren. Dit doe ik in hoofdstuk 1 door het beschrijven van de verschillende stappen in een typische beeldvormingsprocedure bij acute beroerte. Op deze manier kunnen zowel een aantal van de belangrijke technische aspecten bekeken worden alsmede hoe ze de invloed hebben op en beïnvloedt worden door de klinische eisen en beperkingen.

DOEL VAN HET PROEFSCHRIFT

Hoewel CTP een snelle techniek is, op grotere schaal beschikbaar, en goedkoper in vergelijking met andere beeldvormende technieken zoals MRI en PET, is er nog geen brede klinische consensus over de rol van CTP in het selecteren van patiënten voor rtPA. Bepaalde infarctgroottes en locaties kunnen leiden tot zeer verschillende CTP uitkomsten, ten gevolge van de grote en variërende invloed van technische en biologische factoren op deze meting. Er is daarom behoefte aan een praktisch en breed gedragen protocol zodat CTP op een betrouwbare en consistente manier gebruikt kan worden door artsen en leveranciers. Omdat er echter ook geen standaard manier is om de invloed van deze factoren op CTP te evalueren, is het lastig om een consensus te bereiken over wat het beste acquisitie protocol en analysemethode is. Dit proefschrift beschrijft daarom methoden, waaronder de ontwikkeling van digitaal fantoom, om de impact van de technische parameters en (niet-klinische) patiënt specifieke informatie op het CTP resultaat in kaart te brengen. Dit kan enerzijds helpen bij het ontwikkelen van een standaard protocol en daarnaast het optimaliseren van CTP studies, waardoor de klinische impact vergroot kan worden.

In hoofdstuk 2 wordt een digitaal CTP hoofd fantoom beschreven, met als doel om met dit fantoom CTP protocollen te evalueren. Het voordeel van een fantoom is dat de ideale uitkomst van de CTP analyse vooraf bekend is. De eerste eis van de digitale CTP fantoom was dat het zich zou gedragen als een realistisch klinische CTP studie in alle relevante aspecten. Dit werd bereikt door de verspreiding van het contrast middel in het brein te modelleren met behulp van de zogenaamde indicator-verdunnings theorie[1,2], door het gebruik van anatomisch correcte structuur afgeleid

van een hoog resoluut MRI beeld en door het verwerken van echte CT eigenschappen zoals ruis, beperkte beeld resolutie en typische CT artefacten. Na een klinische validatie, tonen we aan hoe het fantoom gebruikt kan worden om het verschil in resultaten van verscheidende CTP software pakketten in kaart te brengen, en hoe gevoelig deze software is voor het variëren van de beeld ruis. Dit eerste onderzoek demonstreert dat we met het fantoom een nuttig instrument in handen hebben om CTP protocollen te evalueren en vervolgens te optimaliseren, wat in de volgende hoofdstukken beschreven is.

In het derde hoofdstuk wordt gebruik gemaakt van de flexibiliteit en specifieke kenmerken van het fantoom om een groot aantal CTP protocollen te vergelijken, waarvan een aantal nooit eerder onderzocht waren. Het doel van dit hoofdstuk was tweeledig; om de betrouwbaarheid van CTP metingen te verbeteren door het optimaliseren van acquisitie protocollen en beeld verwerking en daarnaast het nut van het digitale fantoom verder aan te tonen als een instrument voor de optimalisatie en kalibratie van de CTP methode. Als resultaat worden een aantal protocollen voorgesteld die, met toepassing van het zogenaamde TIPS filter en geoptimaliseerde software instellingen, een sterk verbeterde diagnostische kwaliteit bieden met daarnaast nauwkeurigere waarden met aanzienlijk minder CT dosis, in vergelijking met de huidige klinisch gebruikte protocol.

In hoofdstuk 4 wordt het digitale fantoom gebruikt om het effect van hoofdbewegingen te bepalen op CTP resultaten. Het is belangrijk te weten hoeveel een patiënt mag bewegen voordat dat de CTP meting als onbetrouwbaar beschouwd moet worden en hoe effectief eventuele correctiemethoden zijn. Alhoewel dit onderzoek eventueel ook met klinische beelden uitgevoerd kan worden, heeft het voordelen een fantoom te gebruiken waarbij elke beweging gesimuleerd kan worden en de ideale uitkomst ook vaststaat. In de toekomst zal verdergaand onderzoek plaatsvinden naar meer geavanceerde manieren om voor beweging te corrigeren en ook de invloed van het protocol (bv plakdikte) hierop in kaart te brengen met het fantoom.

In hoofdstuk vijf wordt het onderwerp verlegt naar het zogenaamde partial volume effect, welke de nadelige invloed beschrijft van de beperkte resolutie van de CTP beelden op de metingen aan kleine structuren zoals bloedvaten. Het grootste

probleem met PVE in CTP imaging is dat het signaal van een bloedvat gemiddeld wordt met het signaal van het omliggende weefsel. Uit de metingen blijkt dat de diameters van belangrijkste arteriën in de hersenen (MCA en ACA), zo klein zijn dat zij snel worden beïnvloed door het PVE. Dit zorgt er uiteindelijk voor dat het bloedvolume en de perfusie foutief ingeschat worden. Door het meten van de bloedsignaal in een groot veneus vat (sagittale sinus) zou hiervoor gecorrigeerd kunnen worden, zoals in het algemeen wordt aangenomen (veneuze PVE correctie). In dit hoofdstuk worden zowel het digitale fantoom als klinisch verkregen beelden gebruikt om de effecten van PVE op bepaling van de signaal curve in een arterie (van belang voor CTP analyse) nauwkeurig te meten in verschillende situaties, en stelt vervolgens een hoog resolutie protocol voor dat geen veneuze correctie meer vereist[6].

Omdat uit hoofdstuk 5 aanwijzingen kwamen dat de veneuze PVE correctie op onjuiste aannames gebaseerd is, wordt hierop in hoofdstuk zes nader ingegaan. De arteriële en veneuze signalen en curves worden in 52 patiënten gemeten en vergeleken. De resultaten bevestigen de vermoedens uit hoofdstuk 5 dat er meer contrast door de grote arteriën de hersenen in lijkt te stromen dan door de venen de hersenen verlaat. Waar blijft het ontbrekende contrastmiddel?

Een scenario dat dit zou kunnen verklaren is het verschil in hematocriet waarden in de arteriën en venen. Omdat beide vaten vergelijkbaar in diameter zijn, namen we eerder altijd aan dat er geen verschil zou zijn. Als dit onjuist is, bijvoorbeeld onder invloed van de aanwezigheid van het contrastmiddel, zou dit een verklaring kunnen zijn voor het gesuggereerde "ontbrekende" contrastmiddel. We erkennen dat we geen goede verklaring voor het, in dit hoofdstuk waargenomen effect, hebben en zijn ons bewust van de implicatie dat deze bevinding kan hebben. Wij zijn echter overtuigd dat de waarneming van het effect niet te wijten is aan meetfouten, wat mogelijke gevolgen heeft voor de berekening van de perfusie wanneer de veneuze PVE correctie wordt gebruikt. Er zullen zeker vervolgstudies nodig zijn om onze bevindingen te bevestigen. In de tussentijd moeten de veneuze PVE correctie methode op zijn minste als twijfelachtig worden beschouwd, en zal er gekeken moeten worden naar alternatieven voor deze methode.

ALGEMENE CONCLUSIES

Een gebrek aan consensus en standaardisatie heeft een grote variatie in de CTP resultaten van verschillende leveranciers en onderzoeksgroepen tot gevolg. Hoewel er een aantal initiatieven zijn geweest om te komen tot standaardisatie, volgen de technische ontwikkelingen op het gebied van CTP elkaar in zo'n hoog tempo op dat dit doel lastig te bereiken is. Dit heeft een negatieve invloed op de geloofwaardigheid van CTP als een kwantitatieve meting van de perfusie. Een meer praktische reden voor ontbreken van standaardisatie van CTP is het gebrek aan een gouden standaard om methoden te valideren en te vergeleken en nieuwe ideeën en technieken te beoordelen. Een breed gebruik van een digitale hoofd fantoom zou kunnen leiden tot een gestandaardiseerde 'toolbox' voor het testen en ontwikkelen van nieuwe technieken in CTP en zou de weg kunnen vereffenen voor een uniforme CTP methodiek. Dit kan uiteindelijk de klinische impact van de CTP vergroten en daarmee de toepassing en acceptatie bevorde

LIST OF PUBLICATIONS AND ARTICLES UNDER REVIEW/SUBMITTED

PUBLISHED:

Riordan AJ, Prokop M, Viergever MA, Dankbaar JW, Smit EJ, de Jong HW. Validation of CT brain perfusion methods using a realistic dynamic head phantom. Medical physics. Jun 2011;38(6):3212-3221.

Mendrik AM, Vonken EJ, van Ginneken B, de Jong HWAM, Riordan AJ, van Seeters T, Smit EJ, Viergever MA. TIPS bilateral noise reduction in 4D CT perfusion scans produces high-quality cerebral blood flow maps. Physics in medicine and biology. Jul 7 2011;56(13):3857-3872.

Riordan AJ, Bennink E, Viergever MA, Velthuis BK, Dankbaar JW, de Jong HW. CT brain perfusion protocol to eliminate the need for selecting a venous output function. AJNR. American journal of neuroradiology. Jul 2013;34(7):1353-1358.

Niesten JM, van der Schaaf IC, Riordan AJ, de Jong HW, Mali WP, Velthuis BK. Optimisation of vascular input and output functions in CT-perfusion imaging using 256(or more)-slice multidetector CT. European radiology. May 2013;23(5):1242-1249.

Fahmi F, Beenen LF, Streekstra GJ, Janssen NY, de Jong HWAM, Riordan A, Roos YB, Majoie CB, Van Bavel E, Marquering HA. Head movement during CT brain perfusion acquisition of patients with suspected acute ischemic stroke. European journal of radiology. Dec 2013;82(12):2334-2341.

Bennink E, Riordan AJ, Horsch AD, Dankbaar JW, Velthuis BK, de Jong HW. A fast nonlinear regression method for estimating permeability in CT perfusion imaging. Journal of cerebral blood flow and metabolism : official journal of the International Society of Cerebral Blood Flow and Metabolism. Nov 2013;33(11):1743-1751.

Riordan AJ, Bennink E, Dankbaar JW, Viergever MA, Velthuis BK, Smit EJ, de Jong HW. Comparison of Partial Volume Effects in Arterial and Venous Contrast Curves in CT Brain Perfusion Imaging. PloS one. 2014;9(5):e97586.

Niesten JM, van der Schaaf IC, Riordan AJ, de Jong HWAM, Horsch AD, Eijspaart D, Smit EJ, Mali WP, Velthuis BK. Radiation dose reduction in cerebral CT perfusion imaging using iterative reconstruction. European radiology. Feb 2014;24(2):484-493.

Fahmi F, Riordan A, Beenen LF, Streekstra GJ, Janssen NY, de Jong HWAM, Majoie CB, van Bavel E, Marquering HA. The effect of head movement on CT perfusion summary maps: simulations with CT hybrid phantom data. Medical & biological engineering & computing. Feb 2014;52(2):141-147.

SUBMITTED FOR PUBLICATION:

Vos PC, Riordan AJ, Smit EJ, et al. *Computed Tomography Perfusion Evaluation after Extracranial-Intracranial Bypass Surgery.*

Borst J, Dankbaar JW, Beenen LF et al. *Effect of extended CT Perfusion acquisition time on ischemic core estimation in patients with acute ischemic stroke*.

ACKNOWLEGMENTS

This PhD thesis would not have been possible without the help and contributions of so many friends, colleagues, and mentors.

First and foremost, my parents, Marie and Derry. This PhD is the culmination of a long path which would not have been possible but the love and unconditional support given throughout my education and lifetime.

My co-promoter, dr. ir Hugo de Jong. Dear Hugo, I have never, nor do I ever expect to meet a PhD supervisor who dedicates so much time and effort to his students both professionally and personally. Your expertise and experience in the field brought me through my PhD, but your warm character and personality made it enjoyable and fun.

My first promoter prof. dr. ir. Max Viergever. I am privileged to be one of your graduates. Your confidence in my abilities helped me through the inevitable darker days of my PhD and your expertise and reputation have branded me with a mark of excellence I will carry with me throughout my academic career.

To my second promoter prof. dr. Mathias Prokop, although greener pastures took you to Nijmegen, the impact you made in those first years with your expertise, insights and enthusiasm defined the trajectory of my PhD.

I would like thank the members of my reading committee, Prof.dr. G.J.E. Rinkel, Prof.dr.ir. J.J.W. Lagendijk, Prof.dr. B. van Ginniken, Prof.dr. C.B.L.M. Majoie and Prof.dr. T. Leiner for taking the time to read my thesis.

During my years of research at UMC I met many fantastic people who made my time there a pleasure and made my work easier. Dr. ir. Mattijs Elschot and I began our PhD's together under Hugo's supervision (he beat me too it by a considerable margin). Mattijs, we had some great times together, I couldn't have asked for a better roommate. Someday we will have to go to Green St., Champaign, IL and find that bar, I'll navigate this time.

Dr. Jan Willem Dankbaar I consider myself very fortunate to have a clinical expert so willing to guide me in the opinions and needs of the physicians who have the tough job of interpreting the result of CTP analysis. Your help was invaluable, and it was a pleasure working with you on so many publications. Dr. Birgetta Velthuis for your leadership of the CTP group in UMC, and granting me access to the wealth of data within the DUST study.

Edwin Bennink joined our group in my third year. Edwin, it was refreshing to have a fellow PhD working on the same subject who I could hammer out the various facets of CTP with, I have no doubt your work will have a big impact on the field. Casper Beijst, another ideal roommate, the best of luck with your PhD, you are on the edge of your field and have it tougher than most. I hope to hear your Huapango music someday too.

The clinical physicists; Arnold Schilham, Bart Vermolen, Rob van Rooij, and Tim de Wit who drove my interest in the field by showing me the practical applications their expertise as well as instilling me with a pavlovian response to the question: *Coffee*?. Arnold in particular, whom I shared an office with for over a year, you are one of the most helpful, genuine gentleman I have had the pleasure to meet.

The members CTP/DUST group of UMC: Ewoud Smit, Tom van Seeters, Joris Niesten, Irene van der Schaaf, Adriënne Mendrik and Peter Vos, I hope that we together have made an impact on the field and it was great to work with such a group of dedicated knowledgeable clinicians and scientists. Also a big thanks to my co-authors at AMC, Fahmi Fahmi and Henk Marquering for such a fruitful and smooth collaboration, it was a pleasure working with you.

My *paranimfen* Femke and Cyriel who have put so much effort into the organisation of my defence. Femke in particular for your tolerance, patience and support during the writing of my thesis, Cyriel for your friendship and *moral* guidance during the years of my PhD.

CURRICULUM VITAE

Alan Riordan was born on January 5th 1983 in Cork City in the south of Ireland. After completing his secondary education at St. Colman's college in Fermoy he began studying a Bachelor of Science in University College Cork. Majoring in Physics, he graduated in 2005. Exploring the field of optics, he began a post-graduate diploma in applied physics working to characterise integrated 3R optical regenerators at the photonics systems research group at the Tyndall national institute. After completion of this study Alan stayed at the photonics systems group for two more years to work on his (research) Masters of Science under the supervision of Dr. Robert J. Manning and Dr. Rod Webb. During this time he developed a system for real-time sampling and measurement of the gain, phase, and alpha factor dynamics of semi-conductor optical amplifiers on a picosecond time-scale. He graduated with honours in 2008.

In late 2008 he moved to Utrecht in the Netherlands, beginning his PhD studies there in early 2009. Moving to live in the Netherlands was not the only major change made in this period, as his new field of study was now medical imaging. His PhD work was done at the department of Radiology at University Medical Centre Utrecht under the supervision of Dr. Hugo de Jong and his promoters; Prof. Max Viergever and Prof. Mathias Prokop. This thesis is the fruit of this work.

In 2013 Alan moved to live in Amsterdam and began work as post-doctoral researcher at the Bio-medical Engineering and Physics department of the Academic Medical Centre in Amsterdam.